JOURNAL OF MATHEMATICAL SCIENCES AND MODELLING

ISSN: 2636-8692

VOLUME VIII
ISSUE IV

VOLUME VIII ISSUE IV
ISSN 2636-8692

December 2025
https://dergipark.org.tr/en/pub/jmsm

JOURNAL OF MATHEMATICAL SCIENCES AND MODELLING

Language Editor

Technical Editor

Indexing and Abstracting

Contents

Research Article

J. Math. Sci. Model., 8(4) (2025) 167-174 https://doi.org/10.33187/jmsm.1742985

Journal of Mathematical Sciences and Modelling

ISSN (Online) 2636-8692
https://dergipark.org.tr/en/pub/jmsm

Research Article

Pursuit-Evasion in Minimal Time with Varying Observation Constraints

Özkan Değer

Department of Mathematics, Faculty of Science, Istanbul University, Istanbul, Türkiye

Article Info

Keywords: *Differential games, Pursuit-Evasion, Time-Dependent observer, Time-Optimal control*
2020 MSC: *49K15, 49N70, 49N75*
Received: *15 July 2025*
Accepted: *15 September 2025*
Available online: *2 October 2025*

Abstract

Optimal control problems under incomplete information, particularly in pursuit-evasion scenarios, present significant mathematical challenges. This study extends a basic time-optimal pursuit-evasion game by introducing a time-dependent observer parameter, $\lambda(t)$, which enhances the model's realism without altering the fundamental control strategy. We derive an optimal control law for the pursuer, based on current observations, and explicitly calculate the minimum capture time for a piecewise constant $\lambda(t)$. This work provides an analytical framework for managing uncertainty in dynamic environments, with direct applications in robotics, autonomous navigation, and search-and-rescue operations.

1. Introduction

Optimal control problems involving incomplete information frequently lead to intricate mathematical formulations, making their resolution highly challenging. A practical approach to addressing these complexities is to examine specific instances that reveal fundamental principles and have real-world applicability. One such instance is the pursuit-evasion differential game, where a pursuer aims to capture an evader while possessing only limited information about the evader's precise location. In this context, the evader's possible location is constrained within a defined set, which shrinks as the pursuer approaches. This paper extends this fundamental problem by introducing a time-dependent observer parameter, $\lambda(t)$. This generalization enhances the model's realism and complexity, allowing for scenarios where observation quality varies over time, without altering the core analytical solution strategy. Our primary contribution is the derivation of an optimal control strategy that guarantees capture under this dynamic information constraint, and the explicit calculation of the minimum capture time for a piecewise constant $\lambda(t)$.

The pursuit-evasion problem remains an area of significant theoretical and practical interest, yet it lacks a fully comprehensive solution, particularly when synthesizing optimal control strategies based on state-dependent rather than purely time-dependent variables. Such requirements inherently complicate the problem, making its resolution non-trivial. These challenges are relevant to various real-world applications, including robotics, autonomous navigation, military strategy, and search-and-rescue operations, where agents must operate effectively despite imperfect and evolving information about their targets.

Many studies have addressed differential games, with pursuit-evasion serving as a key case. The foundational work of Isaacs [1] provides a wealth of examples that illustrate core theoretical challenges and solution strategies within this domain. Additional contributions from Pontryagin et al. [2], Krasovskii and Subbotin [3], and Friedman [4] have further expanded the understanding of pursuit-evasion dynamics, particularly under constraints imposed by incomplete information. The analytical framework of this paper is heavily inspired by foundational studies on pursuit-evasion under incomplete information, particularly the pivotal works by Pshenichnyi and Ostapenko [5], Kuntsevich and Pshenichnyi [6], and Pshenichnyi [7]. Moreover, recent studies have explored multi-agent pursuit strategies, as seen in the works of Huang et al. [8] and Garcia et al. [9], while Kurzhanski [10] investigated coordinated control of a flock of systems performing joint motion under collision avoidance constraints. Expanding on these foundational studies, Samatov [11] has examined pursuit-evasion problems where pursuer controls are subject to both integral and geometric constraints, developing a parallel pursuit strategy and extending the work of Isaacs and other researchers. Beyond these, complex differential game formulations, such as those involving feedback control of constrained

Email address: ozdeger@istanbul.edu.tr
Cite as: Ö. Değer, *Pursuit-evasion in minimal time with varying observation constraints*, J. Math. Sci. Model., 8(4) (2025), 167-174.

parabolic systems under uncertainty, have also been explored, notably by Mordukhovich and Seidman [12], who formalized these as minimax problems reduced to asymmetric games. Similarly, related stabilization problems have been addressed for nonlinear systems with discrete controls under disturbance conditions by Shchelchkov [13]. These advancements have contributed to both the theoretical refinement and practical applicability of pursuit-evasion games.

This paper aims to establish a mathematical framework for a basic pursuit-evasion game under time-varying incomplete information. By examining how the pursuer's knowledge of the evader's position evolves with a dynamic observer parameter, we seek to derive an optimal control strategy that effectively manages uncertainty and provides a clear, calculable capture time.

2. Problem Statement

In what follows we will work in the Euclidean space $\mathbb{R}^n$. Given $x = (x_1, x_2, \ldots, x_n) \in \mathbb{R}^n$ and $y = (y_1, y_2, \ldots, y_n) \in \mathbb{R}^n$, the inner product of x and y is defined by

$$\langle x, y \rangle = \sum_{i=1}^{n} x_i y_i,$$

the Euclidean norm of $x = (x_1, x_2, \ldots, x_n) \in \mathbb{R}^n$, denoted by $\|x\|$, is the standard norm in Euclidean space and is given by

$$\|x\| = \sqrt{\langle x, x \rangle} = \sqrt{x_1^2 + x_2^2 + \cdots + x_n^2}.$$

We begin by examining a basic pursuit-evasion scenario described as follows. Let $x \in \mathbb{R}^n$ denote the state of the pursuer P, whose motion is governed by the differential equation given below.

$$\dot{x} = u, \quad \|u\| \leq 1,$$

where the dot represents the time derivative, and u is the control input that governs the motion of the pursuer P. The evader E with coordinates $y \in \mathbb{R}^n$ is at an unknown but fixed position. At each moment in time t, the pursuer P receives an observation w rather than the exact coordinates of the evader E. This observation satisfies the following inequality

$$\|y - w(t)\| \leq \lambda(t)\|x(t) - y\|, \quad 0 < \lambda(t) < 1, \tag{2.1}$$

where y represents the position of the evader E, $x(t)$ is the position of the pursuer P, and the observer parameter $\lambda(t)$ is a piecewise continuous function of time t such that $0 < \lambda(t) < 1$ for all $t \geq 0$.

We aim to construct a control law $u(t)$ for the pursuer P, relying solely on its current position and past observations, that drives the system to the terminal condition $x(T) = y$ in the least possible time. Thus, the optimization problem can be formulated as follows

$$\min_{u(\cdot)} T$$

subject to the constraints

$$\begin{gathered} \dot{x}(t) = u(t), \quad \|u(t)\| \leq 1, \quad t \geq 0 \\ \|y - w(t)\| \leq \lambda(t)\|x(t) - y\|, \quad 0 < \lambda(t) < 1 \\ x(0) = x_0 \\ x(T) = y \quad \text{for some } T > 0, \end{gathered}$$

where $x(t)$ and y represent the positions of the pursuer P and the evader E, respectively, $u(t)$ is the control input for P and satisfies the constraint $\|u(t)\| \leq 1$, $w(t)$ represents the observation made by P, with an error bound given by $\lambda(t)$. The objective is to minimize the capture time T, i.e., to find the smallest T such that $x(T) = y$. In the following, we use $x(t)$, y, $w(t)$ to represent the current positions of P and E, and the observation at time t, respectively.

For the purpose of this extended problem, we propose a piecewise constant form for $\lambda(t)$

$$\lambda(t) = \begin{cases} \lambda_1 & \text{if } 0 \leq t < t_s \\ \lambda_2 & \text{if } t \geq t_s, \end{cases} \tag{2.2}$$

where λ_1, λ_2 are constant values satisfying $0 < \lambda_1 < 1$ and $0 < \lambda_2 < 1$, and $t_s > 0$ is a specific switching time. This switching time t_s can represent various practical events, such as a change in the pursuer's sensor mode, a shift in environmental conditions (e.g., entering a high-interference zone), or the activation of an alternative observation system. It allows the model to capture dynamic changes in information quality over time. This piecewise constant form is chosen as it provides an analytically tractable model that effectively captures scenarios involving sudden shifts in observation quality, serving as a foundational case for more complex, continuously varying functions.

3. Main Results

In this section, we present the core results of our analysis. We begin by examining the observer relationship, which plays a central role in linking observed data to actual positions in the system. In particular, we derive and interpret key inequalities that quantify the uncertainty and provide bounds on the evader's true position based on observations. These results, together with the functions introduced below, serve as essential tools for characterizing the system's dynamics, operational constraints, and optimization objectives.
We begin by analyzing the observer relationship given in equation (2.1). Applying the triangle inequality and the properties of norms, we obtain

$$\|y-w\| \leq \lambda(t)\|x-y\| = \lambda(t)\|(x-w)+(w-y)\| \leq \lambda(t)\|x-w\| + \lambda(t)\|w-y\|.$$

Rearranging the terms, this leads to the following upper bound

$$\|y-w\| \leq \frac{\lambda(t)}{1-\lambda(t)}\|x-w\|. \tag{3.1}$$

This inequality indicates that the discrepancy between the evader's true position y and the observed position w is upper-bounded by a scaled measure of the distance between the pursuer x and w. This formulation provides a means to quantify the uncertainty associated with y relative to both w and x.

Using norm properties,

$$\lambda(t)\|x-y\| \geq \|w-y\| = \|(w-x)-(y-x)\| \geq \|w-x\| - \|y-x\|,$$

so that

$$\|y-x\| \geq \frac{1}{1+\lambda(t)}\|w-x\|. \tag{3.2}$$

This inequality establishes that the true distance between the pursuer x and the evader y is bounded below by a fixed fraction of the distance between x and the observed location w. This serves as a lower bound on the evader's proximity to the pursuer in the presence of observation uncertainty.

Let $u(t)$ be a control determined by the trajectory $x(t)$ and observation $w(t)$. Then for all $t \geq 0$, (3.1) yields:

$$\|y-w(t)\| \leq \frac{\lambda(t)}{1-\lambda(t)}\|x(t)-w(t)\|.$$

In order to precisely characterize the system's dynamics, the constraints under which it operates, and the objectives we aim to optimize, we define the following functions [6]. Let Ω denote any compact set in $\mathbb{R}^n$ and $x, y, z \in \mathbb{R}^n$.

$$\gamma_\Omega(x,z) = \frac{R_\Omega(z)}{\|z-x\|}, \quad R_\Omega(z) = \max_{y\in\Omega}\|y-z\|,$$

where $R_\Omega(z)$ is defined as the radius of the smallest enclosing ball centered at z that fully covers Ω.

Lemma 3.1. *Let Ω be any compact set in $\mathbb{R}^n$ and $x, z \in \mathbb{R}^n$. If $\gamma_\Omega(x,z) < 1$, the following inequality is satisfied for every $y \in \Omega$*

$$\langle \frac{y-x}{\|y-x\|}, \frac{z-x}{\|z-x\|} \rangle \geq \sqrt{1-\gamma_\Omega^2(x,z)}. \tag{3.3}$$

Proof. For any $x, z \in \mathbb{R}^n$ and $y \in \Omega$ we have the following identity

$$\|y-z\|^2 = \|(y-x)-(z-x)\|^2 = \|y-x\|^2 - 2\langle y-x, z-x\rangle + \|z-x\|^2.$$

Hence

$$\begin{aligned}
2\langle \frac{y-x}{\|y-x\|}, \frac{z-x}{\|z-x\|} \rangle &= \frac{\|y-x\|}{\|z-x\|} + \frac{\|z-x\|}{\|y-x\|} - \frac{\|y-z\|^2}{\|z-x\|\|y-x\|} \\
&= \frac{\|y-x\|}{\|z-x\|} + \frac{\|z-x\|}{\|y-x\|}\left(1 - \frac{\|y-z\|^2}{\|z-x\|^2}\right) \\
&\geq \frac{\|y-x\|}{\|z-x\|} + \frac{\|z-x\|}{\|y-x\|}\left(1 - \frac{(\max_{y\in\Omega}\|y-z\|)^2}{\|z-x\|^2}\right) \\
&= \frac{\|y-x\|}{\|z-x\|} + \frac{\|z-x\|}{\|y-x\|}\left(1 - \frac{(R_\Omega(z))^2}{\|z-x\|^2}\right).
\end{aligned}$$

Let us now define $\alpha = \frac{\|z-x\|}{\|y-x\|}$, then we have the following inequality,

$$2\langle \frac{y-x}{\|y-x\|}, \frac{z-x}{\|z-x\|} \rangle \geq \frac{1}{\alpha} + \alpha(1-\gamma_\Omega^2(x,z)). \tag{3.4}$$

We seek to minimize the right-hand side of inequality (3.4) over all $\alpha > 0$,

$$\frac{d}{d\alpha}\left(\frac{1}{\alpha}+\alpha(1-\gamma_\Omega^2(x,z))\right)=0,$$

$$-\frac{1}{\alpha^2}+1-\gamma_\Omega^2(x,z)=0.$$

Hence, taking into account that $\gamma_\Omega(x,z)<1$ is given in the lemma's statement, we have $\alpha=\frac{1}{\sqrt{1-\gamma_\Omega^2(x,z)}}$. So, we obtain

$$\min_{\alpha>0}\left(\frac{1}{\alpha}+\alpha(1-\gamma_\Omega^2(x,z))\right)=2\sqrt{1-\gamma_\Omega^2(x,z)}.$$

Therefore, we have the following inequality from (3.4)

$$2\langle\frac{y-x}{\|y-x\|},\frac{z-x}{\|z-x\|}\rangle\geq\frac{1}{\alpha}+\alpha(1-\gamma_\Omega^2(x,z))\geq 2\sqrt{1-\gamma_\Omega^2(x,z)}.$$

Thus, the desired inequality (3.3) has been demonstrated. □

It is important to observe that Lemma 3.1 provides a lower bound on the cosine of the angle between the vectors $(y-x)$ and $(z-x)$, where the bound is determined by the value of $\gamma_\Omega(x,z)$. The existence of a lower bound for the cosine indicates that the angle between the vectors $(y-x)$ and $(z-x)$ is within a specific range. In particular, this angle must be an acute angle (less than 90 degrees) because the cosine value is positive or close to zero. This implies that the points y and z are "close" to each other relative to point x. In other words, when viewed from point x, points y and z are located close to each other. This situation helps us understand how the distance between y and z changes depending on x. Specifically, it allows us to analyze the relationship and distance between y and z as point x changes.

Theorem 3.2. *If the observer parameter $\lambda(t)$ in equation (2.1) satisfies the condition*

$$0<\lambda(t)<1 \quad \textit{for all } t\geq 0,$$

then the control based on the current observation, given by

$$u(t)=\frac{w(t)-x(t)}{\|w(t)-x(t)\|}, \tag{3.5}$$

guarantees the capture of the evader. The capture is ensured by a time $T\leq T_0$, where T_0 represents a guaranteed upper bound on the capture time for the proposed control strategy, and is implicitly defined as the smallest positive time satisfying the integral equation

$$\int_0^{T_0}\sqrt{1-\lambda(t)^2}dt=\|x(0)-y\|.$$

Proof. Let us calculate the following derivative, which is critical in determining how to choose $u(t)$ to ensure pursuer P catches evader E as quickly as possible

$$\begin{aligned}\frac{d}{dt}\|y-x(t)\|&=\frac{\langle y-x(t),\frac{d}{dt}(y-x(t))\rangle}{\|y-x(t)\|}\\&=\frac{\langle y-x(t),-\dot{x}(t)\rangle}{\|y-x(t)\|}\\&=-\langle\frac{y-x(t)}{\|y-x(t)\|},u(t)\rangle.\end{aligned} \tag{3.6}$$

To prove the theorem, it suffices to show that the controls from (3.5) satisfy

$$\langle\frac{y-x(t)}{\|y-x(t)\|},u(t)\rangle\geq\sqrt{1-\lambda(t)^2}$$

for all admissible y, where (3.5) depends only on observations at time t. By Lemma 3.1, if $u(t)$ is chosen to point in the direction of some $z\in\Omega$ such that

$$\gamma_\Omega(x(t),z)=\frac{R_\Omega(z)}{\|x(t)-z\|}<1,$$

then we have, for all $y\in\Omega$,

$$\langle\frac{y-x(t)}{\|y-x(t)\|},\frac{z-x(t)}{\|z-x(t)\|}\rangle\geq\sqrt{1-\gamma_\Omega(x(t),z)^2}.$$

Thus, taking $u(t)=\frac{z-x(t)}{\|z-x(t)\|}$ ensures the required inequality.

Now, let us transform the initial observation inequality (2.1) as shown in [5]. The inequality $\|w-y\|\leq\lambda(t)\|y-x\|$ is equivalent to the inequality $\|y-a\|\leq R$, where

$$a=x+\frac{w-x}{1-\lambda(t)^2} \quad \text{and} \quad R=\frac{\lambda(t)}{1-\lambda(t)^2}\|w-x\|. \tag{3.7}$$

This transformation defines a ball centered at a with radius R that contains the evader's true position y. Let's define the set Ω as this ball $\Omega = \{y : \|y-a\| \leq R\}$. Now, we apply Lemma 3.1 by setting x in Lemma 3.1 to $x(t)$ (the pursuer's current position), z in Lemma 3.1 to $a(t)$ (the center of the uncertainty ball at time t) and Ω in Lemma 3.1 to the ball defined by (3.7).

We begin by computing $R_\Omega(a(t))$, defined as the radius of the smallest enclosing ball centered at $a(t)$ containing the set Ω. Since Ω itself is a ball centered at $a(t)$ with radius $R(t)$, we have $R_\Omega(a(t)) = R(t)$.

Next, we calculate $\gamma_\Omega(x(t), a(t))$

$$\gamma_\Omega(x(t),a(t)) = \frac{R_\Omega(a(t))}{\|x(t)-a(t)\|} = \frac{R(t)}{\|x(t)-\left(x(t)+\frac{w(t)-x(t)}{1-\lambda(t)^2}\right)\|} = \frac{\frac{\lambda(t)}{1-\lambda(t)^2}\|w(t)-x(t)\|}{\left\|-\frac{w(t)-x(t)}{1-\lambda(t)^2}\right\|}$$
$$= \frac{\frac{\lambda(t)}{1-\lambda(t)^2}\|w(t)-x(t)\|}{\frac{1}{1-\lambda(t)^2}\|w(t)-x(t)\|} = \lambda(t).$$

Since the condition for Lemma 3.1 is $\gamma_\Omega(x,z) < 1$, and we have derived $\gamma_\Omega(x(t),a(t)) = \lambda(t)$, the condition for the theorem becomes $\lambda(t) < 1$, which is given in the problem statement (2.1).

Now, applying Lemma 3.1 with $z = a(t)$ and $\gamma_\Omega(x(t),a(t)) = \lambda(t)$

$$\langle \frac{y-x(t)}{\|y-x(t)\|}, \frac{a(t)-x(t)}{\|a(t)-x(t)\|} \rangle \geq \sqrt{1-\lambda(t)^2}.$$

From the definition of $a(t)$ in (3.7), we have $a(t)-x(t) = \frac{w(t)-x(t)}{1-\lambda(t)^2}$. Since $1-\lambda(t)^2 > 0$, the vector $\frac{a(t)-x(t)}{\|a(t)-x(t)\|}$ is in the same direction as $\frac{w(t)-x(t)}{\|w(t)-x(t)\|}$. Therefore, the control strategy $u(t) = \frac{w(t)-x(t)}{\|w(t)-x(t)\|}$ is equivalent to $u(t) = \frac{a(t)-x(t)}{\|a(t)-x(t)\|}$. Substituting this into the inequality from Lemma 3.1

$$\langle \frac{y-x(t)}{\|y-x(t)\|}, u(t) \rangle \geq \sqrt{1-\lambda(t)^2}.$$

This inequality shows that the rate of change of the distance between the pursuer and evader, as given by (3.6), is bounded

$$\frac{d}{dt}\|y-x(t)\| = -\langle \frac{y-x(t)}{\|y-x(t)\|}, u(t) \rangle \leq -\sqrt{1-\lambda(t)^2}.$$

Since $\lambda(t) < 1$, $\sqrt{1-\lambda(t)^2}$ is a positive value. This implies that the distance $\|y-x(t)\|$ decreases at a rate of at least $\sqrt{1-\lambda(t)^2}$. Integrating this inequality, we find that the distance will reach zero in a time T such that

$$\int_0^T \frac{d}{dt}\|y-x(t)\|dt \leq \int_0^T -\sqrt{1-\lambda(t)^2}dt$$
$$\|y-x(T)\| - \|y-x(0)\| \leq -\int_0^T \sqrt{1-\lambda(t)^2}dt.$$

In order to achieve capture, it is required that $\|y-x(T)\| = 0$. Thus

$$0 - \|y-x(0)\| \leq -\int_0^T \sqrt{1-\lambda(t)^2}dt$$
$$-\|y-x(0)\| \leq -\int_0^T \sqrt{1-\lambda(t)^2}dt$$

which implies

$$\|y-x(0)\| \geq \int_0^T \sqrt{1-\lambda(t)^2}dt.$$

The minimum capture time T_0 is implicitly defined as the smallest value of T for which the corresponding inequality holds with equality. We now proceed to compute T_0 explicitly, based on the piecewise constant function $\lambda(t)$ introduced in (2.2). The evaluation of the integral $\int_0^{T_0} \sqrt{1-\lambda(t)^2}\,dt$ depends on whether T_0 is less than or greater than t_s.

Case 1: The capture occurs at or before t_s ($T_0 \leq t_s$)

In this case, $\lambda(t) = \lambda_1$ for all t. The integral becomes

$$\int_0^{T_0} \sqrt{1-\lambda(t)^2}dt = \int_0^{T_0} \sqrt{1-\lambda_1^2}dt = \sqrt{1-\lambda_1^2}T_0.$$

Setting this equal to $\|x(0)-y\|$

$$\sqrt{1-\lambda_1^2}\,T_0 = \|x(0)-y\|.$$

Thus, the capture time T_0 is given by

$$T_0 = \frac{\|x(0) - y\|}{\sqrt{1 - \lambda_1^2}}.$$

This solution is valid if the calculated $T_0 \leq t_s$.

Case 2: Capture occurs after t_s ($T_0 > t_s$)
In this case, the integral must be split into two parts

$$\begin{aligned}\int_0^{T_0} \sqrt{1 - \lambda(t)^2}\, dt &= \int_0^{t_s} \sqrt{1 - \lambda_1^2}\, dt + \int_{t_s}^{T_0} \sqrt{1 - \lambda_2^2}\, dt \\ &= \sqrt{1 - \lambda_1^2}\, t_s + \sqrt{1 - \lambda_2^2}\, (T_0 - t_s).\end{aligned}$$

Setting this equal to $\|x(0) - y\|$

$$\|x(0) - y\| = \sqrt{1 - \lambda_1^2}\, t_s + \sqrt{1 - \lambda_2^2}\, (T_0 - t_s).$$

Solving for T_0

$$\|x(0) - y\| - \sqrt{1 - \lambda_1^2}\, t_s = \sqrt{1 - \lambda_2^2}\, (T_0 - t_s)$$

$$T_0 - t_s = \frac{\|x(0) - y\| - \sqrt{1 - \lambda_1^2}\, t_s}{\sqrt{1 - \lambda_2^2}}$$

$$T_0 = t_s + \frac{\|x(0) - y\| - \sqrt{1 - \lambda_1^2}\, t_s}{\sqrt{1 - \lambda_2^2}}.$$

This solution is valid if the calculated $T_0 > t_s$.

The actual capture time T_0 will be the minimum of these two possibilities, depending on the initial distance $\|x(0) - y\|$ and the switching time t_s. □

4. Illustrative Example: Planar Visualization

To provide a clearer understanding of the problem's geometry and the interaction dynamics, we present a numerical example in a two-dimensional plane ($n = 2$). This example is designed to illustrate the application of the proposed methodology and to analyze the sensitivity of the optimal solution to key parameters.

Example 4.1. *The evader is assumed to maintain a fixed position at* $(5,3)$. *The pursuer begins its trajectory from an initial position of* $(0,0)$. *The control constraints and game dynamics are influenced by the observer parameters*

$$\lambda(t) = \begin{cases} 0.3 & \text{if } 0 \leq t < 5 \\ 0.8 & \text{if } t \geq 5, \end{cases}$$

where the switching time t_s is set to 5 seconds, and the capture tolerance, defining the proximity required for successful capture, is 0.1 *units. Numerical simulations are conducted with a time step* $dt = 0.01$ *seconds.*

The results of the simulation for the defined problem setup are visualized in Figure 4.1 below. The capture occurred in $T_0 = 5.86$ seconds, with the final position of the pursuer being $(4.93, 2.93)$. Figure 4.1 was generated using Python.
The parameter $\lambda(t)$ plays a significant role in the problem formulation by influencing the optimal time T_0. Table 4.1, generated using Python, demonstrates how the value of T_0 changes in response to variations in the parameters λ_1, λ_2, and the switching time t_s, providing insights into the sensitivity of the optimal solution to these critical factors.

Index	λ_1	λ_2	t_s	Capture Time (s)
0	0.3	0.5	2.0	5.88
1	0.3	0.5	5.0	5.81
2	0.3	0.8	2.0	6.11
3	0.3	0.8	5.0	5.86
4	0.6	0.5	2.0	5.97
5	0.6	0.5	5.0	5.99
6	0.6	0.8	2.0	6.16
7	0.6	0.8	5.0	6.06

Table 4.1: Capture times for various combinations of λ_1, λ_2, and t_s

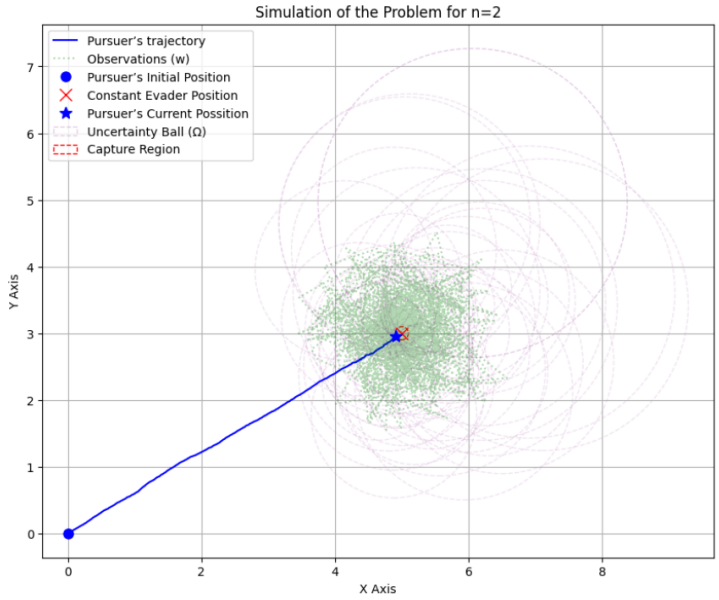

Figure 4.1: Simulation of the Problem for $n = 2$

As observed from Table 4.1, the capture time T_0 is sensitive to the variations in λ_1, λ_2, and t_s. Specifically, an increase in either λ_1 or λ_2 generally leads to an increase in the capture time T_0. For instance, comparing Index 0 ($\lambda_1 = 0.3, \lambda_2 = 0.5, t_s = 2.0, T_0 = 5.88$) with Index 2 ($\lambda_1 = 0.3, \lambda_2 = 0.8, t_s = 2.0, T_0 = 6.11$), an increase in λ_2 results in a longer capture time. Similarly, comparing Index 0 with Index 4 ($\lambda_1 = 0.6, \lambda_2 = 0.5, t_s = 2.0, T_0 = 5.97$), an increase in λ_1 also leads to a slightly longer T_0.

Regarding the switching time t_s, its effect on T_0 is not consistently monotonic and appears to depend on the specific values of λ_1 and λ_2. For example, when comparing Index 2 ($\lambda_1 = 0.3, \lambda_2 = 0.8, t_s = 2.0, T_0 = 6.11$) with Index 3 ($\lambda_1 = 0.3, \lambda_2 = 0.8, t_s = 5.0, T_0 = 5.86$), a longer t_s significantly reduces T_0. However, in contrast, comparing Index 4 ($\lambda_1 = 0.6, \lambda_2 = 0.5, t_s = 2.0, T_0 = 5.97$) with Index 5 ($\lambda_1 = 0.6, \lambda_2 = 0.5, t_s = 5.0, T_0 = 5.99$), an increase in t_s leads to a slight increase in T_0. These observations highlight the complex interplay between the control parameters and the game's outcome, underscoring the importance of their careful selection in optimizing pursuit strategies.

5. Materials and Methods

This section details the theoretical foundations and computational approaches employed in this study to analyze and solve the time-optimal pursuit-evasion game with a time-dependent observer parameter.

5.1. Theoretical framework

The core of our methodology is grounded in the principles of optimal control theory and differential games. The problem is formulated as a time-optimal control task, with the primary objective of minimizing the capture time T_0.

Our analysis begins with a rigorous examination of the observer relationship expressed in inequality (2.1). By employing the triangle inequality and properties of norms, we derive both upper and lower bounds on the evader's true position relative to the observed data and the pursuer's location, as shown in equations (3.1) and (3.2). This treatment follows the methodology established by Pshenichnyi and Ostapenko [5]. Complementing this, Lemma 3.1 provides a key geometric characterization by establishing a lower bound on the cosine of the angle between pertinent vectors, which plays a vital role in quantifying uncertainty and understanding the spatial relationship between the agents. Finally, Theorem 3.2 delivers the derivation of the optimal control law for the pursuer, which is based on the current observation and guarantees capture. This theorem explicitly calculates the minimum capture time T_0 by integrating the rate at which the distance decreases, taking into account the piecewise constant behavior of the observer parameter $\lambda(t)$ as defined in (2.2).

5.2. Computational methods and simulation setup

Numerical simulations were conducted to illustrate the theoretical findings and to analyze the sensitivity of the capture time to various parameters. All simulations and data visualizations were performed using Python, ensuring reproducibility and clarity of results.

The specific parameters for the numerical example in a two-dimensional plane ($n = 2$) are as follows: the evader's fixed position is set at $(5,3)$, while the pursuer starts from the initial position $(0,0)$. The observer parameters are chosen as $\lambda_1 = 0.3$ and $\lambda_2 = 0.8$ for the illustrative example discussed in Section 4, with various combinations considered for the sensitivity analysis presented in Table 4.1. The switching time t_s is set to 5 seconds in the example, while different values (2.0 s and 5.0 s) are used during the sensitivity analysis. A capture tolerance of 0.1 units defines the maximum allowable distance for a successful capture, and a time step of $dt = 0.01$ seconds is employed for the numerical integration of trajectories. It should be noted that while the theoretical framework assumes capture when the distance is exactly zero, this

numerical tolerance is a practical necessity for simulation. This may result in a measured capture time that is marginally shorter than the theoretical T_0, but it does not materially affect the validation of the control strategy's performance.

The simulation process involves defining the relative motion dynamics of the pursuer and the evader, implementing the derived optimal control law for the pursuer based on the current observation and the time-dependent parameter $\lambda(t)$, and numerically integrating the differential equations governing the pursuer's motion. Throughout the simulation, the distance between the pursuer and the evader is continuously monitored to determine the capture time T_0, which is identified when this distance falls within the specified capture tolerance.

6. Conclusion

This study extended a basic time-optimal pursuit-evasion game by incorporating a time-dependent observer parameter, $\lambda(t)$, which enhances the model's realism in scenarios where information quality varies over time. Our primary contribution lies in the derivation of an optimal control law for the pursuer, based solely on current observations, and the explicit calculation of the minimum capture time T_0 for a piecewise constant $\lambda(t)$. This analytical framework provides a robust method for managing uncertainty in dynamic environments.

The numerical illustrations, particularly the planar visualization in Figure 4.1, effectively demonstrate the geometric aspects of the problem and the interaction dynamics between the pursuer and the evader. The sensitivity analysis presented in Table 4.1 provides crucial insights into how the capture time T_0 is influenced by the observer parameters λ_1, λ_2, and the switching time t_s. We observed that increasing λ_1 or λ_2 generally leads to a longer capture time, reflecting the increased uncertainty. Furthermore, the effect of the switching time t_s on T_0 was found to be non-monotonic, indicating a complex interplay with the λ parameters and highlighting the need for careful parameter selection in optimizing pursuit strategies. This non-monotonic relationship has a significant practical implication: for mission planning, simply extending the duration of high-quality observation does not uniformly guarantee a faster capture; the optimal switching time is critically dependent on the relative qualities of the two observation periods.

This work offers a rigorous analytical foundation for addressing pursuit-evasion problems under dynamic incomplete information, with direct applicability in fields such as robotics, autonomous navigation, and search-and-rescue operations. The ability to explicitly calculate capture times under varying observation conditions is invaluable for mission planning and real-time decision-making in uncertain environments.

Future research directions include extending the model to scenarios in which the evader possesses its own dynamics and maneuvering capabilities, thereby allowing for the analysis of more sophisticated evasion strategies. Another avenue for exploration involves generalizing the time-dependent observer parameter $\lambda(t)$ to encompass continuously varying or stochastically evolving functions. Furthermore, a particularly important direction for future work, as suggested by our reviewers, is the explicit extension of the derived optimal control law to the setting of discrete-time control strategies [13]. This would involve the discretization of the system dynamics and a rigorous analysis of convergence and stability in a discrete-time framework, making the results more directly applicable to digital control systems used in modern robotics and autonomous navigation. In addition, incorporating practical constraints—such as fuel limitations for the pursuer or state-dependent restrictions on both agents—would enhance the model's applicability. Finally, the framework can be extended to multi-agent pursuit-evasion settings, where coordination and information sharing among multiple pursuers or evaders play a critical role.

Article Information

Artificial Intelligence Statement: No AI tools or technologies were used in the preparation of this manuscript. All content was created solely by the author.

Conflict of Interest Disclosure: No potential conflict of interest was declared by the author.

Plagiarism Statement: This article was scanned by the plagiarism program.

References

[1] R. Isaacs, *Differential Games: A Mathematical Theory with Applications to Warfare and Pursuit, Control and Optimization*, Dover Publications, Mineola, 1999.
[2] L. S. Pontryagin, V. G. Boltyanskii, R. S. Gamkrelidze, E. F. Mishchenko, *The Mathematical Theory of Optimal Processes*, Interscience Publishers, New York, 1962.
[3] N. N. Krasovskii, A. I. Subbotin, *Game-Theoretical Control Problems*, Springer, New York, 1988.
[4] A. Friedman, *Differential Games*, Wiley-Interscience, New York, 1971.
[5] B. N. Pshenichnyi, V. V. Ostapenko, *Differential Games*, Naukova Dumka, Kiev, 1992.
[6] V. M. Kuntsevich, B. N. Pshenichnyi, *Solution of a class of pursuit and evasion problems under uncertainty*, Cybernet. Systems Anal., **31** (1995), 365–372. https://doi.org/10.1007/BF02366515
[7] B. N. Pshenichnyi, *Special pursuit-and-evasion problem with incomplete information*, Cybernet. Systems Anal., **31** (1995), 246–251. https://doi.org/10.1007/BF02366924
[8] H. Huang, W. Zhang, J. Ding, D. M. Stipanović, C. J. Tomlin, *Guaranteed decentralized pursuit-evasion in the plane with multiple pursuers*, Proceedings of the 50th IEEE Conference on Decision and Control and European Control Conference, (2011), 4835–4840. https://doi.org/10.1109/CDC.2011.6161237
[9] E. Garcia, D. W. Casbeer, A. Von Moll, M. Pachter, *Multiple pursuer multiple evader differential games*, IEEE Trans. Autom. Control, **66**(5) (2021), 2345–2350. https://doi.org/10.1109/TAC.2020.3003840
[10] A. B. Kurzhanski, *Problem of collision avoidance for a team motion with obstacles*, Proc. Steklov Inst. Math., **293**(1) (2016), 120–136. https://doi.org/10.1134/S0081543816050114
[11] B. T. Samatov, *The pursuit-evasion problem under integral-geometric constraints on pursuer controls*, Autom. Remote Control, **74** (2013), 1072–1081. https://doi.org/10.1134/S0005117913070023
[12] B. S. Mordukhovich, T. I. Seidman, Feedback control of constrained parabolic systems in uncertainty conditions via asymmetric games, In: *Applied Analysis and Differential Equations*, 2007, 237–254. https://doi.org/10.1142/9789812708229_0020
[13] K. Shchelchkov, *Discrete control of nonlinear system with uncertain information under disturbance conditions*. Vestn. Udmurt. Univ. Mat. Mekh. Komp'yut. Nauki, **35**(1) (2025), 155–166. https://doi.org/10.35634/vm250110

J. Math. Sci. Model., 8(4) (2025) 175-184 https://doi.org/10.33187/jmsm.1760600

Journal of Mathematical Sciences and Modelling

ISSN (Online) 2636-8692
https://dergipark.org.tr/en/pub/jmsm

Research Article

Optimality Conditions for the Second-Order Semilinear Differential Inclusions of the Bolza Problem

Gülseren Çiçek[1]* **and Gülşah Bozcu Yüksek**[2]

[1]*Department of Mathematics, Faculty of Science, Istanbul University, Istanbul, Türkiye*
[2]*Department of Mathematics, Faculty of Engineering and Natural Sciences, Bahçeşehir University, Istanbul, Türkiye*
**Corresponding author*

Article Info

Keywords: *Boundary conditions, Discrete and differential inclusions, Euler-Lagrange inclusion, Locally adjoint mapping*
2020 MSC: *34A60, 49J53,49K21*
Received: *7 August 2025*
Accepted: *23 September 2025*
Available online: *2 October 2025*

Abstract

In this paper, optimality conditions for the Bolza problem with second-order semilinear differential inclusions (SDFIs) and initial conditions are derived. Despite its use in applications, there are few publications on this subject, and we hope to contribute to the literature. Locally adjoint mapping (LAM) is used to establish the adjoint discrete inclusion. Using the equivalence relations, necessary and sufficient conditions for the discrete approximation problem are formulated. By passing to the limit, sufficient optimality conditions are established for the optimal problem described by second-order SDFIs. Similar results for the non-convex problem are obtained by using the local tents. We provide an example of a semi-linear problem with initial conditions for which our results can be applied.

1. Introduction

Optimization problems involving ordinary [1–8] and partial [4,7] differential inclusions (DFIs) have been studied in several ways of approach, especially high-order differential inclusions have been included in many studies in recent years. [5] obtains optimality conditions for the Cauchy problem with higher order discrete and differential inclusions. Paper [2] derives conditions for second-order DFIs of the Mayer problem.

Semilinear differential inclusions (SDFI) [6,9–12] are used to obtain models for set-valued systems that are not linear and contain uncertainty. In particular, control problems encountered in the sciences of biology, engineering, and the environment may be represented in this way. SDFIs are suitable for modeling systems with uncertainty, multivalence, and complex dynamics, so they can be encountered in any field where optimization and control problems occur.

In the present paper, we obtain optimality conditions for the following second-order SDFIs problem:

$$\text{minimize} \quad J[x(\cdot)] = \int_0^1 g(x(t),t)\mathrm{d}t + \varphi(x(1)) \tag{1.1}$$

$$x''(t) \in Ax(t) + Bx'(t) + F(x(t),x'(t)), \quad t \in [0,1] \tag{1.2}$$

$$x(0) = \alpha_0,\ x'(0) = \alpha_1, \tag{1.3}$$

where $F : \mathbb{R}^{2n} \rightrightarrows \mathbb{R}^n$ is a convex multivalued mapping, $g(\cdot,t) : \mathbb{R}^n \times [0,1] \to \mathbb{R}$, continuous on x a proper convex function, α_0 and α_1 are constant vectors, $A,B \in \mathbb{R}^{n\times n}$ matrices that $rank\{A\} = n, rank\{B\} = n$. The problem is to derive optimality conditions for the trajectory $\tilde{x}(t)$ that minimizes the Bolza functional $J[x(\cdot)]$, satisfies the second-order SDFI (1.2) in $[0,1]$ and initial conditions (1.3). When the multi-valued mapping and the function in the problem are non-convex, we call problem (1.1)-(1.3) a non-convex problem.

During the last decades, problems of the semilinear form have received a great deal of attention and are more concerned with the existence results such as [11, 12].

Email addresses: cicekgul@istanbul.edu.tr, gulsah.bozcu@bau.edu.tr
Cite as: G. Çiçek, G. Bozcu Yüksek, *Optimality conditions for the second-order semilinear differential inclusions of the Bolza problem*, J. Math. Sci. Model., 8(4) (2025), 175-184.

The paper [9], on the other hand, studies an optimal control problem with higher-order semilinear delay differential inclusions (DFI) and obtains a sufficient optimality condition for higher-order DFIs in terms of Euler-Lagrange type adjoint DFIs and the Hamiltonian.
The paper is organized as follows. Section 2 gives the fundamental concepts such as the cone of tangent directions, local tent, locally adjoint mapping and Hamiltonian function. In Section 3 we formulate discrete- approximation problem, give equivalence relation between locally adjoint mappings and obtain optimality conditions for the discrete-approximate convex and non-convex problems. Finally,in Section 4, passing to the limit, sufficient optimality conditions are established for the optimal problem described by second-order SDFIs. Similar results for the non-convex problem are obtained by using the local tents. The results of the study will be evaluated in this section.

2. Notations and Needed Facts

The basic concepts and definitions are given below, and we recommend the book [4] for those interested in more details. Let $\langle x,y\rangle$ be an inner product of elements $x,y\in\mathbb{R}^n$, and (x,y) be a pair of x,y. The interior of subset A is denoted by $intA$ and the relative interior of A is denoted by riA, and consists of interior points of A with respect to its affine hull Aff$A$. The convex cone $K_A(z_0)$ is a cone of tangent directions of the set A at a point $z_0\in A$ if it consists of points $\bar{z}$ that there exists a function $\kappa(\lambda)$ satisfying the inclusion $z+\lambda\bar{z}+\kappa(\lambda)\in A$ for sufficiently small $\lambda>0$ and $\lambda^{-1}+\kappa(\lambda)\to 0$, as $\lambda\downarrow 0$.
K^* is said to be the dual cone to the convex cone K if $K^*=\{x^*\in\mathbb{R}^n:\ \langle x,x^*\rangle\geq 0,\forall x\in K\}$. It is not hard to see that a dual cone is convex.

Definition 2.1. *[4] If the cone of tangent directions $K_A(x_0)$ to a set A at the point $x_0\in A$, satisfies the following conditions*

i) $\bar{x}_0\in riK, LinK=LinK_A(x_0)$,

ii) $\psi(\bar{x})=\bar{x}+r(\bar{x}),\ \frac{r(\bar{x})}{\|\bar{x}\|}\to 0,\ as\ \bar{x}\to 0$,

iii) *there exists such ε that for $\bar{x}\in K\cap(\varepsilon B)$, the inclusion $x_0+\psi(\bar{x})\in A$, where B is the unit ball,*
such that for each point $\bar{x}\in riK_A(x_0)$ there exist a convex cone $K\subseteq K_A(x_0)$ and continuous function ψ, defined in the neighborhood of the origin, then $K_A(x_0)$ is said to be a local tent.

A function $g=g(x)$ is proper [13] if $g(x)<+\infty$ for at least one x and $g(x)>-\infty$ for each x. g is convex if its epigraph epi $g=\{(\mu,x):\mu\geq g(x)\}$ is a convex set in $\mathbb{R}\times\mathbb{R}^n$. The subdifferential [4, 7, 13] of the function g at the point x_0 is the subset of $\mathbb{R}^n$ and is defined by

$$\partial g(x_0)=\{x^*: g(x)-g(x_0)\geq\langle x^*,x-x_0\rangle,\forall x\}.$$

The Convex Upper Approximation (CUA) of a given function $g:\mathbb{R}^n\to\mathbb{R}\cup\{\pm\infty\}$ at any point x of its efficient domain $domg=\{x\in\mathbb{R}^n: |g(x)|<+\infty\}$ is a function $h(\bar{x},x)$ that

1. $h(\bar{x},x)\geq\Phi(\bar{x},x)$ for all $\bar{x}\neq 0$;
2. $h(\bar{x},x)$ is a closed (lower semicontinuous) positively homogeneous convex function,

where $\Phi(\bar{x},x)=sup_{r(\cdot)}limsup_{\lambda\downarrow 0}\frac{g(x+\lambda\bar{x}+r(\lambda))-g(x)}{\lambda}$.
It is clear that the function g has many CUA functions.
The multivalued mapping $F:\mathbb{R}^{2n}\rightrightarrows\mathbb{R}^n$ is convex if its graph is a convex subset of $\mathbb{R}^{3n}$ and is convex closed if its graph is a convex closed set in $\mathbb{R}^{3n}$, where its graph is $gphF=\{(x,u,v):\ v\in F(x,u)\}$. The Hamiltonian function and the argmaximum set for the multivalued mapping F

$$H_F(x,u,v^*)=\sup_v\{\langle v^*,v\rangle: v\in F(x,u)\},\ v^*\in\mathbb{R}^n,$$

$$F(x,u;v^*)=\{v\in F(x,u):\langle v^*,v\rangle=H_F(x,u,v^*)\},$$

are defined respectively.
When $F(x,u)=\emptyset$ for convex F we set $H_F(x,u,v^*)=-\infty$.
For a convex mapping F

$$K_{gphF}(x,u,v)=\{(\bar{x},\bar{u},\bar{v}):\bar{x}=\lambda(x_1-x),\bar{u}=\lambda(u_1-u),\bar{v}=\lambda(v_1-v)\},$$

for any $(x_1,u_1,v_1)\in gphF$ is a cone of tangent directions of $gphF$ at the point (x,u,v).

Definition 2.2. *[4] Let F be a convex multi-valued mapping, then multi-valued mapping $F^*:Y^*\longrightarrow X^*$ is defined by*

$$F^*(v^*;(x,u,v))=\left\{(x^*,u^*):(x^*,u^*,-v^*)\in K^*_{gphF}(x,u,v)\right\}$$

is called a locally adjoint mapping (LAM) of F at the point $(x,u,v)\in gphF$. Here, $K^*_{gphF}(x,u,v)$ is the dual of the cone of tangent directions $K_{gphF}(x,u,v)$.

The multi-valued mapping

$$F^*\left(v^*;(x,u,v)\right)=\left\{(x^*,u^*):H_F(x_1,u_1,v^*)-H_F(x,u,v^*)\leq\langle x^*,x_1-x\rangle+\langle u^*,u_1-u\rangle,\forall(x_1,u_1,v)\in gphF\right\},v\in F(x,u;v^*)$$

is said to be the LAM to a non-convex mapping F at the point $(x,u,v)\in gphF$. For the convex mapping F, $H(\cdot,\cdot,v^*)$ is concave, and the latter definition of LAM coincides with the previous definition of LAM. Mordukhovich [7] gave a definition similar to LAM and it is called the coderivative of a multi-valued mapping at a point.
Let us formulate the following discrete problem, briefly denoted by $(\mathscr{P}_D)$:

$$\text{minimize}\quad\sum_{t=2}^{T-1}g(x_t,t)\tag{2.1}$$

$$x_{t+2} \in Q(x_t, x_{t+1}), \quad t = 0, \dots, T-2 \tag{2.2}$$

$$x_0 = \alpha_0, \quad x_1 = \beta_1, \tag{2.3}$$

where $x_t \in \mathbb{R}^n$, $Q : \mathbb{R}^{2n} \rightrightarrows \mathbb{R}^n$ is multivalued convex mapping, $g(\cdot,t)$ are real-valued proper convex functions, that $g(\cdot,t) : \mathbb{R}^n \times [0,1] \to \mathbb{R}$, T is natural number and β_0, β_1 are constant vectors in $\mathbb{R}^n$. Let trajectory $\{x_t\}_{t=0}^T = \{x_t : t = 0, 1, \cdots, T\}$ be a feasible solution for problem $(\mathscr{P}_D)$. If the functions and multivalued mapping in the problem $(\mathscr{P}_D)$ are convex, then it is called a convex problem.

Definition 2.3. *The regularity condition is satisfied for the convex problem $(\mathscr{P}_D)$ if for the points $x_t^0 \in \mathbb{R}^n$ one of the following cases holds:*
1) $(x_t^0, x_{t+1}^0, x_{t+2}^0) \in ri\, gph(Q)$, $x_t^0 \in ri\,(dom g(\cdot,t))$,
or
2) $(x_t^0, x_{t+1}^0, x_{t+2}^0) \in int\, gph(Q)$, $t = 0, \cdots, T-2$,
where $g(\cdot,t)$ is continuous at the point x_t^0.

Condition 2.1. *Suppose $\{\tilde{x}_t\}_{t=0}^T$ is a feasible trajectory for problem $(\mathscr{P}_D)$ and the cone of tangent directions $K_{gphQ}(\tilde{x}_t, \tilde{x}_{t+1}, \tilde{x}_{t+2})$ to the mapping Q is a local tent. Let also functions $h_t(\bar{x}, \tilde{x}_t)$, continuous on $\bar{x}$ be CUA to functions $g(\cdot,t)$ at points $\tilde{x}_t$, $t = 0, \dots, T$. Therefore, $\partial g(\tilde{x}_t, t) = \partial h_t(0, \tilde{x}_t)$ holds.*

The following theorem is studied in [1, 5].

Theorem 2.4. *Let discrete problem (2.1)-(2.3) be convex, then for the feasible trajectory $\{\tilde{x}_t\}_{t=0}^T$ to be optimal it is necessary that there exist $\lambda \in \{0,1\}$ and not all equal to zero vectors x_t^*, x_T^*, η_t^*, $t = 0, \cdots, T-1$ that satisfy the Euler-Lagrange inclusion*

$$(x_t^* - \eta_t^*, \eta_{t+1}^*) \in Q^*\left(x_{t+2}^*; (\tilde{x}_t, \tilde{x}_{t+1}, \tilde{x}_{t+2})\right) - \left(\lambda \partial g(\tilde{x}_t, t) \times \{0\}\right),$$

$$t = 0, \dots, T-2,$$

$$\partial g(\tilde{x}_0, 0) = \partial g(\tilde{x}_1, 1) = 0$$

and transversality conditions

$$\eta_{T-1}^* - x_{T-1}^* \in \partial g(\tilde{x}_{T-1}, T-1), \quad x_T^* = 0,$$

respectively. Moreover, if the regularity condition (see Definition 2.3) is satisfied, then these conditions are also sufficient for the optimality of the trajectory $\{\tilde{x}_t\}_{t=0}^T$.

3. Conditions for the Discrete-Approximation Problem

Let h be a grid function on the t-axis then the first and second step operators are given,

$$\Delta x(t) = \frac{x(t+h) - x(t)}{h} \text{ and } \Delta^2 x(t) = \frac{\Delta x(t+h) - \Delta x(t)}{h} = \frac{x(t+2h) - 2x(t+h) + x(t)}{h^2}$$

respectively.
In order to obtain sufficient conditions for the optimality of the problem (1.1)-(1.3) we now give the Discrete-Approximation problem:

$$minimum\, J_h[x(\cdot)] = \sum_{t=0,h,2h,\dots,1-2h} hg(x(t),t) + \varphi(x(1-h)) \tag{3.1}$$

$$\Delta^2 x(t) \in Ax(t) + B\Delta x(t) + F\left(x(t), \Delta x(t)\right), \tag{3.2}$$

$$t = 0, h, 2h, \cdots, 1-2h,$$

$$x(0) = \alpha_0, \quad \Delta x(0) = \alpha_1. \tag{3.3}$$

By inclusion (3.2) we have

$$x(t+2h) - 2x(t+h) + x(t) \in h^2 Ax(t) + h^2 B\left(\frac{x(t+h) - x(t)}{h}\right) + h^2 F\left(x(t), \frac{x(t+h) - x(t)}{h}\right)$$

or

$$x(t+2h) \in -x(t) + h^2 Ax(t) - hBx(t) + 2x(t+h) + hBx(t+h) + h^2 F\left(x(t), \frac{x(t+h) - x(t)}{h}\right)$$

in other words we obtain

$$x(t+2h) \in (h^2 A - hB - I)x(t) + (hB + 2I)x(t+h) + h^2 F\left(x(t), \frac{x(t+h) - x(t)}{h}\right), \tag{3.4}$$

where I denotes the identity matrix. If we denote the right side of the inclusion (3.4) by $Q(x(t),x(t+h))$, then we rewrite (3.4) as follows

$$x(t+2h) \in Q\big(x(t),x(t+h)\big).$$

Putting $x(t)=x_1$, $x(t+h)=x_2$, $x(t+2h)=y$, we have $y \in Q\big(x_1,x_2\big)$, where

$$Q(x_1,x_2) = (h^2A-hB-I)x_1+(hB+2I)x_2+h^2F\Big(x_1,\frac{x_2-x_1}{h}\Big). \tag{3.5}$$

Then the Discrete-Approximation problem (3.1)-(3.3) is stated as follows

$$\textit{minimum } J_h[x(\cdot)] = \sum_{t=0,h,2h,\ldots,1-2h} hg(x(t),t)+\varphi\big(x(1-h)\big), \tag{3.6}$$

$$x(t+2h) \in Q\big(x(t),x(t+h)\big), \quad t=0,h,2h,\cdots,1-2h, \tag{3.7}$$

$$x(0)=\alpha_0, \quad x(h)=\alpha_0+h\alpha_1=\beta_1. \tag{3.8}$$

Therefore using Theorem 2.4, for the optimality of the trajectory $\{\tilde{x}(t)\}$ in problem (3.6)-(3.8) it is necessary that there exist vectors $x_t^*(t),\eta_t^*(t)$, a number $\lambda=\lambda_h\in\{0,1\}$ that are not all equal to zero and satisfy the inclusions

$$\big(x^*(t)-\eta^*(t),\eta^*(t+h)\big) \in Q^*\big(x^*(t+2h);\big(\tilde{x}(t),\tilde{x}(t+h),\tilde{x}(t+2h)\big)\big)-\big(\lambda h\partial g(\tilde{x}(t),t)\times\{0\}\big), \tag{3.9}$$

$$t=2h,\cdots,1-2h,$$

$$\eta^*(1-h)-x^*(1-h) \in \lambda h\partial\varphi\big(\tilde{x}(1-h)\big), \quad x^*(1)=0. \tag{3.10}$$

Under the regularity condition (see Definition 2.3) these conditions are also sufficient for the trajectory $\{\tilde{x}(t)\}$.
Now, let us give the relation between the locally adjoint mappings Q^* and F^*.

Theorem 3.1. *Let $F:\mathbb{R}^{2n}\rightrightarrows\mathbb{R}^n$ be a multi-valued mapping and let multi-valued mapping Q be defined by the relation (3.5). If the cones of tangent directions $K_{gphQ}(x_1,x_2,y)$, $y\in Q(x_1,x_2)$ is a local tent, then $K_{gphF}\big(x_1,\frac{x_2-x_1}{h},\frac{y-(h^2A-hB-I)x_1-(hB+2I)x_2}{h^2}\big)$ is also a local tent and the following inclusions are equivalent:*

i) $(x_1^*,x_2^*)\in Q^*\big(y^*;(x_1,x_2,y)\big), \quad y\in Q(x_1,x_2;y^*),$

ii) $\Big(\frac{x_1^*+x_2^*-y^*}{h^2}-A^*y^*,\frac{x_2^*-2y^*}{h}-B^*y^*\Big)\in F^*\Big(y^*;\big(x_1,\frac{x_2-x_1}{h},\frac{y-(h^2A-hB-I)x_1-(hB+2I)x_2}{h^2}\big)\Big),\frac{x_1+x_2-y}{h^2}\in F\big(x_1,\frac{x_2-x_1}{h};y^*\big),y^*\in\mathbb{R}^n.$

Here, the argmaximum set of Q is defined by $Q(x_1,x_2;y^*)=\{y\in Q(x_1,x_2):\langle y,y^*\rangle=H_Q(x_1,x_2,y^*)\}$.

Proof. Let us start by obtaining the equivalence relation between the cones of tangent directions of $gphF$ and $gphQ$. Since $K_{gphQ}(x_1,x_2,y)$, $y\in Q(x_1,x_2)$, is a local tent then the cone of tangent directions $K_{gphF}\left(x_1,\frac{x_2-x_1}{h},\frac{y-(h^2A-hB-I)x_1-(hB+2I)x_2}{h^2}\right)$, is a local tent and the following relations are equivalent:

$$(\bar{x}_1,\bar{x}_2,\bar{y})\in K_{gphQ}(x_1,x_2,y) \tag{3.11}$$

and

$$\left(\bar{x}_1,\frac{\bar{x}_2-\bar{x}_1}{h},\frac{\bar{y}-(h^2A-hB-I)\bar{x}_1-(hB+2I)\bar{x}_2}{h^2}\right)\in K_{gphF}\left(x_1,\frac{x_2-x_1}{h},\frac{y-(h^2A-hB-I)x_1-(hB+2I)x_2}{h^2}\right), \tag{3.12}$$

where $\frac{y-(h^2A-hB-I)x_1-(hB+2I)x_2}{h^2}\in F\big(x_1,\frac{x_2-x_1}{h}\big)$.
Suppose $(\bar{x}_1,\bar{x}_2,\bar{y})\in K_{gphQ}(x_1,x_2,y)$ is arbitrary. Since $K_{gphQ}(x_1,x_2,y)$ is a local tent then by Definition 2.1 there exist functions $r_i(\bar{z}),i=0,1,2$ of $\bar{z}=(\bar{x}_1,\bar{x}_2,\bar{y})$ such that $\frac{r_i(\bar{z})}{\|\bar{z}\|}\to 0, i=0,1,2$ as $\bar{z}\to 0$ and there exists a convex cone $K\subseteq ri\,K_{gphQ}(z)$, for small $\bar{z}\in ri\,K_{gphQ}$. Therefore we have

$$y+\bar{y}+r_0(\bar{z})\in Q(x_1+\bar{x}_1+r_1(\bar{z}),x_2+\bar{x}_2+r_2(\bar{z}))$$

and by the definition of function Q, (3.5), the following inclusion

$$y+\bar{y}+r_0(\bar{z}) \quad \in (h^2A-hB-I)\big(x_1+\bar{x}_1+r_1(\bar{z})\big)+(hB+2I)\big(x_2+\bar{x}_2+r_2(\bar{z})\big)+h^2F\left(x_1+\bar{x}_1+r_1(\bar{z}),\frac{x_2+\bar{x}_2+r_2(\bar{z})-x_1-\bar{x}_1-r_1(\bar{z})}{h}\right)$$

holds. Hence, we derive

$$y+\bar{y}+r_0(\bar{z})-(h^2A-hB-I)\big(x_1+\bar{x}_1+r_1(\bar{z})\big)-(hB+2I)\big(x_2+\bar{x}_2+r_2(\bar{z})\big)\in h^2F\left(x_1+\bar{x}_1+r_1(\bar{z}),\frac{x_2-x_1}{h}+\frac{\bar{x}_2-\bar{x}_1}{h}+\frac{r_2(\bar{z})-r_1(\bar{z})}{h}\right)$$

or, in other words,

$$\Big(y-(h^2A-hB-I)x_1-(hB+2I)x_2\Big)+\Big(\bar{y}-(h^2A-hB-I)\bar{x}_1-(hB+2I)\bar{x}_2\Big)+\Big(r_0(\bar{z})-(h^2A-hB-I)r_1(\bar{z})-(hB+2I)r_2(\bar{z})\Big)$$
$$\in h^2F\left(x_1+\bar{x}_1+r_1(\bar{z}),\frac{x_2-x_1}{h}+\frac{\bar{x}_2-\bar{x}_1}{h}+\frac{r_2(\bar{z})-r_1(\bar{z})}{h}\right). \tag{3.13}$$

If we denote $w=\left(x_1,\frac{x_2-x_1}{h},\frac{y-(h^2A-hB-I)x_1-(hB+2I)x_2}{h^2}\right)$ and $\bar{w}=\left(\bar{x}_1,\frac{\bar{x}_2-\bar{x}_1}{h},\frac{\bar{y}-(h^2A-hB-I)\bar{x}_1-(hB+2I)\bar{x}_2}{h^2}\right)$ then there exist such functions $\varphi_i(\bar{w}), i=0,1,2$ that $\frac{\varphi_i(\bar{w})}{\|\bar{w}\|}\to 0, i=0,1,2$ as $\bar{w}\to 0$ and $K\subseteq ri\,K_{gphF}(w)$ and, by (3.13) we have $\bar{w}\in K_{gphF}(w)$. So, we obtain the relation (3.12) and see that $K_{gphF}(w)$ is a local tent for $gphF$. Conversely, (3.12) implies that (3.11) holds.
Therefore, it follows that inclusions (3.11) and (3.12) are equivalent.
Now, let us indicate the equivalence between inclusions **i)** and **ii)**.
Let $(x_1^*,x_2^*)\in Q^*\left(y^*;(x_1,x_2,y)\right), y\in Q(x_1,x_2;y^*)$ be given. Then by the definition of LAM we have $(x_1^*,x_2^*,-y^*)\in K^*_{gphQ}(x_1,x_2,y)$ and so

$$\langle\bar{x}_1,x_1^*\rangle+\langle\bar{x}_2,x_2^*\rangle-\langle\bar{y},y^*\rangle\geq 0,\quad (\bar{x}_1,\bar{x}_2,\bar{y})\in K_{gphQ}(x_1,x_2,y) \tag{3.14}$$

hold. Let $\gamma_1^*,\gamma_2^*,\gamma^*$ be such that

$$(\gamma_1^*,\gamma_2^*,-\gamma^*)\in K^*_{gphF}\left(x_1,\frac{x_2-x_1}{h},\frac{y-(h^2A-hB-I)x_1-(hB+2I)x_2}{h^2}\right),$$

where K^*_{gphF} is the dual cone to the cone of tangent directions K_{gphF} and the inclusion (3.12) be provided. Using the definition of dual cones, the above inclusion reduces to the inequality

$$\left\langle\bar{x}_1,\gamma_1^*\right\rangle+\left\langle\frac{\bar{x}_2-\bar{x}_1}{h},\gamma_2^*\right\rangle-\left\langle\frac{\bar{y}-(h^2A-hB-I)\bar{x}_1-(hB+2I)\bar{x}_2}{h^2},\gamma^*\right\rangle\geq 0.$$

If we rearrange the last inequality, then we obtain

$$\left\langle\bar{x}_1,h^2\gamma_1^*-h\gamma_2^*\right\rangle+\left\langle\bar{x}_2,h\gamma_2^*\right\rangle-\left\langle\bar{y},\gamma^*\right\rangle+\left\langle(h^2A-hB-I)\bar{x}_1,\gamma^*\right\rangle+\left\langle(hB+2I)\bar{x}_2,\gamma^*\right\rangle\geq 0$$

and, as a result, we get

$$\langle\bar{x}_1,h^2\gamma_1^*-h\gamma_2^*+h^2A^*\gamma^*-hB^*\gamma^*-\gamma^*\rangle+\langle\bar{x}_2,h\gamma_2^*+hB^*\gamma^*+2\gamma^*\rangle-\langle\bar{y},\gamma^*\rangle\geq 0. \tag{3.15}$$

Using the equivalence between (3.11) and (3.12), we compare relation between inequalities (3.14) and (3.15)

$$\begin{aligned}
x_1^* &= h^2\gamma_1^*-h\gamma_2^*+h^2A^*\gamma^*-hB^*\gamma^*-\gamma^*,\\
x_2^* &= h\gamma_2^*+hB^*\gamma^*+2\gamma^*,\\
y^* &= \gamma^*
\end{aligned}$$

and then we obtain the following equalities

$$\begin{aligned}
\gamma_1^* &= \frac{x_1^*+x_2^*-y^*}{h^2}-A^*y^*,\\
\gamma_2^* &= \frac{x_2^*-2y^*}{h}-B^*y^*,\\
\gamma^* &= y^*.
\end{aligned} \tag{3.16}$$

Consequently, taking into account Definition 2.2 and by the equations (3.16) we have

$$\left(\frac{x_1^*+x_2^*-y^*}{h^2}-A^*y^*,\frac{x_2^*-2y^*}{h}-B^*y^*\right)\in F^*\left(y^*;\left(x_1,\frac{x_2-x_1}{h},\frac{y-(h^2A-hB-I)x_1-(hB+2I)x_2}{h^2}\right)\right)$$

if and only if $(x_1^*,x_2^*)\in Q^*\left(y^*;(x_1,x_2,y)\right)$. Then the desired result is obtained.
Note that the inclusions $y\in Q(x_1,x_2;y^*)$ and $\frac{y-(h^2A-hB-I)x_1-(hB+2I)x_2}{h^2}\in F\left(x_1,\frac{x_2-x_1}{h};y^*\right)$ ensure that LAMs $Q^*(y^*;(x_1,x_2,y))\neq\emptyset$ and $F^*\left(y^*;\left(x_1,\frac{x_2-x_1}{h},\frac{y-(h^2A-hB-I)x_1-(hB+2I)x_2}{h^2}\right)\right)\neq\emptyset$ are nonempty, respectively. □

The following corollary, written for convex functions, is proved similarly.

Corollary 3.2. *Let $F:\mathbb{R}^{2n}\rightrightarrows\mathbb{R}^n$ be a convex multi-valued mapping and let the multi-valued mapping Q be defined by the relation (3.5), then the inclusions i) and ii) are equivalent.*

Theorem 3.3. *Let F be a multi-valued convex mapping and g be a convex continuous function on a feasible trajectory $\{\tilde{x}(t)\}, t=0,h,\cdots,1$, which is proper on x. Then necessary conditions for the optimality of the trajectory $\{\tilde{x}(t)\}$ of discrete-approximation problem (3.1)-(3.3) are that there exist not all zero vectors $\{x^*(t),\eta^*(t)\}$ and number $\lambda=\lambda_h\in\{0,1\}$ satisfying Euler-Lagrange inclusion and transversality conditions*

$$\begin{aligned}
&\left(\Delta^2x^*(t)+\Delta v^*(t)-A^*x^*(t+2h),v^*(t+h)-B^*x^*(t+2h)\right)\\
&\in F^*\left(x^*(t+2h);\left(\tilde{x}(t),\Delta\tilde{x}(t),\Delta^2\tilde{x}(t)-B\Delta\tilde{x}(t)-A\tilde{x}(t)\right)\right)-\left(\lambda\partial g(\tilde{x}(t),t)\times\{0\}\right),
\end{aligned} \tag{3.17}$$

$$t=2h,\cdots,1-2h,$$

$$v^*(1-h)+\Delta x^*(1-h)\in\lambda h\partial\varphi(\tilde{x}(1-h)),\ x^*(1)=0, \tag{3.18}$$

respectively.
Moreover, under the regularity condition (see Definition 2.3) the above conditions are also sufficient for the optimality of the trajectory $\{\tilde{x}(t)\}$.

Proof. Using the equivalence relations in Corollary 3.2 and writing $x_1^* = x(t)^* - \eta^*(t)$, $x_2^* = \eta^*(t+h)$ under the condition **ii)** of Theorem 3.1, the inclusions (3.9) and (3.10) are converted to inclusions

$$\left(\frac{x^*(t)-\eta^*(t)+\eta^*(t+h)-x^*(t+2h)}{h^2} - A^*x^*(t+2h), \frac{\eta^*(t+h)-2x^*(t+2h)}{h} - B^*x^*(t+2h)\right)$$
$$\in F^*\Big(x^*(t+2h); \big(\tilde{x}(t), \Delta\tilde{x}(t), \Delta^2\tilde{x}(t) - B\Delta\tilde{x}(t) - A\tilde{x}(t)\big)\Big) - \big(\lambda\partial g(\tilde{x}(t),t)\times\{0\}\big), \tag{3.19}$$
$$t = 2h, \cdots, 1-2h,$$
$$\eta^*(1-h) - x^*(1-h) \in \lambda h\partial\varphi(\tilde{x}(1-h)),\ x^*(1) = 0, \tag{3.20}$$

respectively.
If we put $v^*(t) = \frac{\eta^*(t)-2x^*(t+h)}{h}$, then condition (3.19) is formed as follows

$$\begin{aligned}
&\frac{x^*(t) - \eta^*(t) + \eta^*(t+h) - x^*(t+2h)}{h^2} - A^*x^*(t+2h)\\
&= \frac{x^*(t) - hv^*(t) - 2x^*(t+h) + hv^*(t+h) + x^*(t+2h)}{h^2} - A^*x^*(t+2h)\\
&= \frac{x^*(t+2h) - 2x^*(t+h) + x^*(t)}{h^2} + \frac{v^*(t+h) - v^*(t)}{h} - A^*x^*(t+2h)\\
&= \Delta^2x^*(t) + \Delta v^*(t) - A^*x^*(t+2h),
\end{aligned}$$

where $v^*(t+h) = \frac{\eta^*(t+h)-2x^*(t+2h)}{h}$. Then we obtain the condition (3.17) of the theorem.
On the other hand, by constructing condition (3.20) according to $x^*(1) = 0$ we get

$$\frac{hv^*(1-h) + x^*(1) + x^*(1) - x^*(1-h)}{h} \in \lambda\partial\varphi\big(\tilde{x}(1-h)\big)$$

and so,

$$v^*(1-h) + \Delta x^*(1-h) \in \lambda\partial\varphi(\tilde{x}(1-h)),$$

where $v^*(1-h) = \frac{\eta^*(1-h)-2x^*(1)}{h}$. Therefore, condition (3.18) holds and the desired results are achieved. □

The following theorem is obtained similarly.

Theorem 3.4. *Suppose that Condition 2.1 is satisfied for the non-convex problem (3.1)-(3.3), then $\{\tilde{x}(t)\}$ is an optimal trajectory for this problem if there exists a number $\lambda = \lambda_h \in \{0,1\}$ and vectors $\{x^*(t), \eta^*(t)\}$, simultaneously not all equal to zero, satisfying conditions (3.17) and (3.18) for the non-convex case.*

4. Conditions for the Main Problem

Now, let us obtain sufficient conditions for the optimality of the continuous problem (1.1)-(1.3) by applying conditions (3.17)-(3.18) in Theorem 3.3. Under the conditions of Theorem 3.3, letting $\lambda = 1$ and passing the limit as $h \to 0$, we obtain the Euler-Lagrange differential inclusion

a) $\left(\frac{d^2x^*(t)}{dt^2} + \frac{dv^*(t)}{dt} - A^*x^*(t), v^*(t) - B^*x^*(t)\right) \in F^*\Big(x^*(t); \big(\tilde{x}(t), \tilde{x}'(t), \tilde{x}''(t) - B\tilde{x}'(t) - A\tilde{x}(t)\big)\Big) - \big(\lambda\partial g(\tilde{x}(t),t)\times\{0\}\big)$, $t \in [0,1]$

and the transversality condition

b) $v^*(1) + \frac{dx^*(1)}{dt} \in \partial\varphi(\tilde{x}(1))$, $x^*(1) = 0$.

Furthermore, the condition that ensures that the LAM F^* is not empty at a given point follows

c) $\frac{d^2\tilde{x}(t)}{dt^2} - B\frac{d\tilde{x}(t)}{dt} - A\tilde{x}(t) \in F\big(\tilde{x}(t), \tilde{x}'(t); x^*(t)\big)$, $t \in [0,1]$,

where $F(x,u;v^*) = \{v \in F(x,u) : \langle v, v^*\rangle = H(x,u,v^*)\}$ is the argmaximum set of multivalued mapping F. Then conditions **a)**-**c)** are sufficient for optimality, and we express the following theorem.

Theorem 4.1. *Let $g(\cdot,t) : \mathbb{R}^n \times [0,1] \to \mathbb{R}$ and $\varphi : \mathbb{R}^n \to \mathbb{R}$ be continuous convex functions, and F be a convex multi-valued mapping. Then there exist absolutely continuous functions $\{x^*(t), v^*(t)\}$, $t \in [0,1]$, satisfying conditions **a), b), c)** and among the feasible solutions of the problem (1.1)-(1.3), these conditions are sufficient for the optimality of the trajectory $\tilde{x}(t)$.*

Proof. Since $F^*\big(v^*; (x,u,v)\big) = \partial_{(x,u)}H(x,u,v^*)$, $v \in F(x,u;v^*)$, then Moreau-Rockafellar Theorem [13] and $-\partial g(\cdot,t) = \partial(-g(\cdot,t))$ imply in condition **a)**:

$$\Big(\frac{d^2x^*(t)}{dt^2} + \frac{dv^*(t)}{dt} - A^*x^*(t), v^*(t) - B^*x^*(t)\Big) \in \partial_{(x,u)}\big[H(\tilde{x}(t), \tilde{x}'(t), x^*(t)) - g(\tilde{x}(t),t)\big]. \tag{4.1}$$

If we denote $y(t) = x''(t) - Bx'(t) - Ax(t)$, then the argmaximum set of the multi-valued mapping F and its Hamiltonian function are as follows:

$$F\big(\tilde{x}(t), \tilde{x}'(t); x^*(t)\big) = \big\{y(t) \in F\big(\tilde{x}(t), \tilde{x}'(t)\big) : \big\langle y(t), x^*(t)\big\rangle = H\big(\tilde{x}(t), \tilde{x}'(t), x^*(t)\big)\big\},$$
$$H\big(\tilde{x}(t), \tilde{x}'(t), x^*(t)\big) = \sup_y\big\{\big\langle y(t), x^*(t)\big\rangle : y(t) \in F\big(\tilde{x}(t), \tilde{x}'(t); x^*(t)\big)\big\},$$

respectively. Inclusion (4.1) and subdifferential definition give

$$H_F(x(t),x'(t),x^*(t)) - H_F(\tilde{x}(t),\tilde{x}'(t),x^*(t)) - g(x(t),t) + g(\tilde{x}(t),t)$$
$$\leq \Big\langle \frac{\mathrm{d}^2x^*(t)}{\mathrm{d}t^2} + \frac{\mathrm{d}v^*(t)}{\mathrm{d}t} - A^*x^*(t), x(t) - \tilde{x}(t)\Big\rangle + \big\langle v^*(t) - B^*x^*(t), x'(t) - \tilde{x}'(t)\big\rangle.$$

Using the Hamiltonian function definition, we rearrange the above inequality and derive

$$\Big\langle \frac{\mathrm{d}^2x(t)}{\mathrm{d}t^2} - B\frac{\mathrm{d}x(t)}{\mathrm{d}t} - Ax(t), x^*(t)\Big\rangle - \Big\langle \frac{\mathrm{d}^2\tilde{x}(t)}{\mathrm{d}t^2} - B\frac{\mathrm{d}\tilde{x}(t)}{\mathrm{d}t} - A\tilde{x}(t), x^*(t)\Big\rangle - g(x(t),t) + g(\tilde{x}(t),t)$$
$$\leq \Big\langle \frac{\mathrm{d}^2x^*(t)}{\mathrm{d}t^2} + \frac{\mathrm{d}v^*(t)}{\mathrm{d}t} - A^*x^*(t), x(t) - \tilde{x}(t)\Big\rangle + \big\langle v^*(t) - B^*x^*(t), x'(t) - \tilde{x}'(t)\big\rangle,$$

and finally,

$$g(x(t),t) - g(\tilde{x}(t),t) \geq \Big\langle \frac{\mathrm{d}^2\big(x(t) - \tilde{x}(t)\big)}{\mathrm{d}t^2}, x^*(t)\Big\rangle - \Big\langle B\frac{\mathrm{d}\big(x(t) - \tilde{x}(t)\big)}{\mathrm{d}t}, x^*(t)\Big\rangle - \big\langle A(x(t) - \tilde{x}(t)), x^*(t)\big\rangle$$
$$-\Big\langle \frac{\mathrm{d}^2x^*(t)}{\mathrm{d}t^2}, x(t) - \tilde{x}(t)\Big\rangle - \frac{\mathrm{d}}{\mathrm{d}t}\big\langle v^*(t), x(t) - \tilde{x}(t)\big\rangle + \big\langle A^*x^*(t), x(t) - \tilde{x}(t)\big\rangle + \big\langle B^*x^*(t), x'(t) - \tilde{x}'(t)\big\rangle. \tag{4.2}$$

On the other hand, by the properties of the inner product, we have

$$\big\langle A(x(t) - \tilde{x}(t)), x^*(t)\big\rangle = \big\langle x(t) - \tilde{x}(t), A^*x^*(t)\big\rangle$$

and

$$\Big\langle B\frac{\mathrm{d}\big(x(t) - \tilde{x}(t)\big)}{\mathrm{d}t}, x^*(t)\Big\rangle = \big\langle x'(t) - \tilde{x}'(t), B^*x^*(t)\big\rangle,$$

respectively. Thus, writing the equalities above in the inequality (4.2) and arranging (4.2) we achieve

$$g(x(t),t) - g(\tilde{x}(t),t) \geq \frac{\mathrm{d}}{\mathrm{d}t}\Big\langle \frac{\mathrm{d}\big(x(t) - \tilde{x}(t)\big)}{\mathrm{d}t}, x^*(t)\Big\rangle - \frac{\mathrm{d}}{\mathrm{d}t}\Big\langle \frac{\mathrm{d}x^*(t)}{\mathrm{d}t}, x(t) - \tilde{x}(t)\Big\rangle - \frac{\mathrm{d}}{\mathrm{d}t}\big\langle v^*(t), x(t) - \tilde{x}(t)\big\rangle.$$

Therefore, integrating on $[0,1]$ both sides of the last inequality obtained, we have

$$\int_0^1 \big[g(x(t),t) - g(\tilde{x}(t),t)\big]\mathrm{d}t \geq \int_0^1 \Big[\frac{\mathrm{d}}{\mathrm{d}t}\Big\langle \frac{\mathrm{d}(x(t) - \tilde{x}(t))}{\mathrm{d}t}, x^*(t)\Big\rangle - \frac{\mathrm{d}}{\mathrm{d}t}\Big\langle \frac{\mathrm{d}x^*(t)}{\mathrm{d}t}, x(t) - \tilde{x}(t)\Big\rangle\Big]\mathrm{d}t - \big\langle v^*(1), x(1) - \tilde{x}(1)\big\rangle + \big\langle v^*(0), x(0) - \tilde{x}(0)\big\rangle.$$

If we evaluate the integrals on the right side of the inequality, then we get

$$\int_0^1 \big[g(x(t),t) - g(\tilde{x}(t),t)\big]\mathrm{d}t \geq \Big\langle \frac{\mathrm{d}(x(1) - \tilde{x}(1))}{\mathrm{d}t}, x^*(1)\Big\rangle - \Big\langle \frac{\mathrm{d}(x(0) - \tilde{x}(0))}{\mathrm{d}t}, x^*(0)\Big\rangle$$
$$-\Big\langle \frac{\mathrm{d}x^*(1)}{\mathrm{d}t}, x(1) - \tilde{x}(1)\Big\rangle + \Big\langle \frac{\mathrm{d}x^*(0)}{\mathrm{d}t}, x(0) - \tilde{x}(0)\Big\rangle - \big\langle v^*(1), x(1) - \tilde{x}(1)\big\rangle + \big\langle v^*(0), x(0) - \tilde{x}(0)\big\rangle.$$

Taking into account that $x(\cdot), \tilde{x}(\cdot)$ are feasible and $x(0) = \tilde{x}(0) = \alpha_0$, $x'(0) = \tilde{x}'(0) = \alpha_1$, we have

$$\Big\langle \frac{\mathrm{d}(x(1) - \tilde{x}(1))}{\mathrm{d}t}, x^*(1)\Big\rangle = 0, \ \Big\langle \frac{\mathrm{d}(x(0) - \tilde{x}(0))}{\mathrm{d}t}, x^*(0)\Big\rangle = 0$$

and

$$\Big\langle \frac{\mathrm{d}x^*(0)}{\mathrm{d}t}, x(0) - \tilde{x}(0)\Big\rangle = 0, \ \big\langle v^*(0), x(0) - \tilde{x}(0)\big\rangle = 0.$$

Therefore, the inequality

$$\int_0^1 \big[g(x(t),t) - g(\tilde{x}(t),t)\big]\mathrm{d}t \geq -\Big\langle \frac{\mathrm{d}x^*(1)}{dt}, x(1) - \tilde{x}(1)\Big\rangle - \big\langle v^*(1), x(1) - \tilde{x}(1)\big\rangle \tag{4.3}$$

is obtained.

Now, by the definition of subdifferential, for all feasible trajectories $x(t), t \in [0,1]$, condition **b)** in Theorem 4.1 gives us

$$\varphi(x(1)) - \varphi(\tilde{x}(1)) \geq \Big\langle v^*(1) + \frac{\mathrm{d}x^*(1)}{\mathrm{d}t}, x(1) - \tilde{x}(1)\Big\rangle. \tag{4.4}$$

Collecting inequalities (4.3) and (4.4) side by side, we obtain

$$\int_0^1 \big[g(x(t),t) - g(\tilde{x}(t),t)\big]\mathrm{d}t + \varphi(x(1)) - \varphi(\tilde{x}(1)) \geq 0,$$

which means that for each feasible $x(t), t \in [0,1]$, the inequality $J[x(\cdot)] \geq J[\tilde{x}(\cdot)]$ holds. As a result, the trajectory $\tilde{x}(t), t \in [0,1]$, is optimal. This completes the proof. □

Consider now the non-convex second-order SDIs problem (1.1)-(1.3) and obtain sufficient conditions for optimality.

Theorem 4.2. *Suppose problem (1.1)-(1.3) is non-convex, that is, functions $g(\cdot,t):\mathbb{R}^n\times[0,1]\to\mathbb{R}$ and $\varphi:\mathbb{R}^n\to\mathbb{R}$ are non-convex with respect to x, multi-valued mapping F is non-convex. Then for the optimality of trajectory $\tilde{x}(t)$, among all feasible solutions of the non-convex problem (1.1)-(1.3) it is sufficient that there exists a pair of absolutely continuous functions $\{x^*(t),v^*(t)\}$, $t\in[0,1]$, that satisfies the following conditions*

i) $\Big(\frac{\mathrm{d}^2x^*(t)}{\mathrm{d}t^2}+\frac{\mathrm{d}v^*(t)}{\mathrm{d}t}-A^*x^*(t)+x^*(t),v^*(t)-B^*x^*(t)\Big)\in F^*\Big(x^*(t);\big(\tilde{x}(t),\tilde{x}'(t),\tilde{x}''(t)-B\tilde{x}'(t)-A\tilde{x}(t)\big)\Big)$, $t\in[0,1]$,

ii) $g(x,t)-g(\tilde{x}(t),t)\geq\big\langle x^*(t),x-\tilde{x}(t)\big\rangle$, $\forall x\in\mathbb{R}^n$,

iii) $\varphi(x)-\varphi(\tilde{x}(1))\geq\big\langle v^*(1)+\frac{\mathrm{d}x^*(1)}{\mathrm{d}t},x-\tilde{x}(1)\big\rangle$, $\forall x\in\mathbb{R}^n$, $x^*(1)=0$,

iv) $\big\langle\frac{\mathrm{d}^2\tilde{x}(t)}{\mathrm{d}t^2}-B\frac{\mathrm{d}\tilde{x}(t)}{\mathrm{d}t}-A\tilde{x}(t),x^*(t)\big\rangle=H_F\big(\tilde{x}(t),\tilde{x}'(t),x^*(t)\big)$, $t\in[0,1]$.

Proof. Using the definition of LAM for nonconvex mapping F and condition **i)** of the theorem, we have

$$H_F(x(t),x'(t),x^*(t))-H_F(\tilde{x}(t),\tilde{x}'(t),x^*(t))\leq\big\langle\frac{\mathrm{d}^2x^*(t)}{\mathrm{d}t^2}+\frac{\mathrm{d}v^*(t)}{\mathrm{d}t}-A^*x^*(t)+x^*(t),x(t)-\tilde{x}(t)\big\rangle+\big\langle v^*(t)-B^*x^*(t),x'(t)-\tilde{x}'(t)\big\rangle.$$

If we arrange the above inequality, taking into account **iv)** then we obtain

$$\begin{aligned}&\big\langle\frac{\mathrm{d}^2x(t)}{\mathrm{d}t^2}-B\frac{\mathrm{d}x(t)}{\mathrm{d}t}-Ax(t),x^*(t)\big\rangle-\big\langle\frac{\mathrm{d}^2\tilde{x}(t)}{\mathrm{d}t^2}-B\frac{\mathrm{d}\tilde{x}(t)}{\mathrm{d}t}-A\tilde{x}(t),x^*(t)\big\rangle\\&\leq\big\langle\frac{\mathrm{d}^2x^*(t)}{\mathrm{d}t^2}+\frac{\mathrm{d}v^*(t)}{\mathrm{d}t}-A^*x^*(t)+x^*(t),x(t)-\tilde{x}(t)\big\rangle+\big\langle v^*(t)-B^*x^*(t),x'(t)-\tilde{x}'(t)\big\rangle.\end{aligned}$$

Performing the necessary operations, we write the inequality

$$\begin{aligned}0\geq&\big\langle\frac{\mathrm{d}^2\big(x(t)-\tilde{x}(t)\big)}{\mathrm{d}t^2},x^*(t)\big\rangle-\big\langle A(x(t)-\tilde{x}(t)),x^*(t)\big\rangle-\big\langle B\frac{\mathrm{d}\big(x(t)-\tilde{x}(t)\big)}{\mathrm{d}t},x^*(t)\big\rangle-\big\langle\frac{\mathrm{d}^2x^*(t)}{\mathrm{d}t^2},x(t)-\tilde{x}(t)\big\rangle\\&-\frac{\mathrm{d}}{\mathrm{d}t}\big\langle v^*(t),x(t)-\tilde{x}(t)\big\rangle+\big\langle A^*x^*(t),x(t)-\tilde{x}(t)\big\rangle+\big\langle B^*x^*(t),x'(t)-\tilde{x}'(t)\big\rangle-\big\langle x^*(t),x(t)-\tilde{x}(t)\big\rangle\end{aligned}$$

and then we obtain

$$0\geq\frac{\mathrm{d}}{\mathrm{d}t}\big\langle\frac{\mathrm{d}\big(x(t)-\tilde{x}(t)\big)}{\mathrm{d}t},x^*(t)\big\rangle-\frac{\mathrm{d}}{\mathrm{d}t}\big\langle\frac{\mathrm{d}x^*(t)}{\mathrm{d}t},x(t)-\tilde{x}(t)\big\rangle-\frac{\mathrm{d}}{\mathrm{d}t}\big\langle v^*(t),x(t)-\tilde{x}(t)\big\rangle-\big\langle x^*(t),x(t)-\tilde{x}(t)\big\rangle,\tag{4.5}$$

since

$$\big\langle A(x(t)-\tilde{x}(t)),x^*(t)\big\rangle=\big\langle x(t)-\tilde{x}(t),A^*x^*(t)\big\rangle$$

and

$$\big\langle B\frac{\mathrm{d}\big(x(t)-\tilde{x}(t)\big)}{\mathrm{d}t},x^*(t)\big\rangle=\big\langle\frac{\mathrm{d}x(t)}{\mathrm{d}t}-\frac{\mathrm{d}\tilde{x}(t)}{\mathrm{d}t},B^*x^*(t)\big\rangle.$$

If we add the inequality (4.5) side by side to condition **ii)** of the theorem

$$g(x(t),t)-g(\tilde{x}(t),t)\geq\big\langle x^*(t),x(t)-\tilde{x}(t)\big\rangle,$$

then we have

$$g(x(t),t)-g(\tilde{x}(t),t)\geq\frac{\mathrm{d}}{\mathrm{d}t}\big\langle\frac{\mathrm{d}\big(x(t)-\tilde{x}(t)\big)}{\mathrm{d}t},x^*(t)\big\rangle-\frac{\mathrm{d}}{\mathrm{d}t}\big\langle\frac{\mathrm{d}x^*(t)}{\mathrm{d}t},x(t)-\tilde{x}(t)\big\rangle-\frac{\mathrm{d}}{\mathrm{d}t}\big\langle v^*(t),x(t)-\tilde{x}(t)\big\rangle.\tag{4.6}$$

Integrating both sides of (4.6) over $[0,1]$, we write

$$\int_0^1\big[g(x(t),t)-g(\tilde{x}(t),t)\big]\mathrm{d}t\geq\int_0^1\Big[\frac{\mathrm{d}}{\mathrm{d}t}\big\langle\frac{\mathrm{d}\big(x(t)-\tilde{x}(t)\big)}{\mathrm{d}t},x^*(t)\big\rangle-\frac{\mathrm{d}}{\mathrm{d}t}\big\langle\frac{\mathrm{d}x^*(t)}{\mathrm{d}t},x(t)-\tilde{x}(t)\big\rangle\Big]\mathrm{d}t-\big\langle v^*(1),x(1)-\tilde{x}(1)\big\rangle+\big\langle v^*(0),x(0)-\tilde{x}(0)\big\rangle$$

or, equivalently

$$\begin{aligned}\int_0^1\big[g(x(t),t)-g(\tilde{x}(t),t)\big]\mathrm{d}t\geq&\big\langle\frac{\mathrm{d}\big(x(1)-\tilde{x}(1)\big)}{\mathrm{d}t},x^*(1)\big\rangle-\big\langle\frac{\mathrm{d}\big(x(0)-\tilde{x}(0)\big)}{\mathrm{d}t},x^*(0)\big\rangle-\big\langle\frac{\mathrm{d}x^*(1)}{\mathrm{d}t},x(1)-\tilde{x}(1)\big\rangle\\&+\big\langle\frac{\mathrm{d}x^*(0)}{\mathrm{d}t},x(0)-\tilde{x}(0)\big\rangle-\big\langle v^*(1),x(1)-\tilde{x}(1)\big\rangle+\big\langle v^*(0),x(0)-\tilde{x}(0)\big\rangle.\end{aligned}$$

Taking into account that $x(\cdot),\tilde{x}(\cdot)$ are feasible and $x(0)=\tilde{x}(0)=\alpha_0$, $x'(0)=\tilde{x}'(0)=\alpha_1$, we have

$$\big\langle\frac{\mathrm{d}(x(1)-\tilde{x}(1))}{\mathrm{d}t},x^*(1)\big\rangle=0,\ \big\langle\frac{\mathrm{d}(x(0)-\tilde{x}(0))}{\mathrm{d}t},x^*(0)\big\rangle=0,$$

$$\Big\langle \frac{\mathrm{d}x^*(0)}{\mathrm{d}t}, x(0)-\tilde{x}(0)\Big\rangle = 0,\ \big\langle v^*(0), x(0)-\tilde{x}(0)\big\rangle = 0$$

and then deduce that

$$\int_0^1 \big[g(x(t),t)-g(\tilde{x}(t),t)\big]\mathrm{d}t \geq -\Big\langle \frac{\mathrm{d}x^*(1)}{\mathrm{d}t}, x(1)-\tilde{x}(1)\Big\rangle - \big\langle v^*(1), x(1)-\tilde{x}(1)\big\rangle. \tag{4.7}$$

Now, adding side by side inequality (4.7) and condition **iii)** of the theorem,

$$\varphi(x(1))-\varphi(\tilde{x}(1)) \geq \Big\langle v^*(1)+\frac{\mathrm{d}x^*(1)}{\mathrm{d}t}, x(1)-\tilde{x}(1)\Big\rangle,$$

satisfied for each $x(t)$, $t\in[0,1]$, we conclude that

$$\int_0^1 \big[g(x(t),t)-g(\tilde{x}(t),t)\big]\mathrm{d}t + \varphi(x(1))-\varphi(\tilde{x}(1)) \geq 0.$$

Thus for each feasible $x(t)$, $t\in[0,1]$, we have $J[x(t)]\geq J[\tilde{x}(t)]$. Therefore $\tilde{x}(t)$, $t\in[0,1]$, is optimal for the non-convex problem (1.1)-(1.3). □

Example 4.3. *Let consider the problem with semilinear differential equation (1.1)-(1.3), where*

$$x''(t) = Ax(t)+Bx'(t)+Cu(t), u(t)\in U, \tag{4.8}$$

and A,B are $n\times n$ matrices, C is an $n\times r$ matrix, and $U\subset\mathbb{R}^r$ is a convex set.
Let us replace (4.8) with the second-order semilinear differential inclusion

$$x''(t) \in Ax(t)+Bx'(t)+CU. \tag{4.9}$$

Since we have

$$H_F(x(t),x'(t),x^*(t)) = \sup_{u\in U}\langle u, C^*x^*(t)\rangle$$

then

$$F^*\big(x^*(t);\big(x(t),x'(t),x''(t)\big)\big) = \begin{cases} 0, & -C^*x^*(t)\in K_U^*(\tilde{u}),\\ \emptyset, & -C^*x^*(t)\notin K_U^*(\tilde{u}),\end{cases}$$

where C^* is the adjoint(transpose) matrix of C.
Then by Theorem 4.2 we have

$$\frac{d^2x^*(t)}{dt^2}+\frac{dv^*(t)}{dt} = A^*x^*(t)-x^*(t),$$

$$v^*(t) = B^*x^*(t),\ t\in[0,1],$$

so

$$\frac{d^2x^*(t)}{dt^2} = A^*x^*(t)-B^*\frac{dx^*(t)}{dt}-x^*(t),\ t\in[0,1].$$

On the other hand, by condition iv) of Theorem 4.2 and by condition $-C^*x^*(t)\in K_U^*(\tilde{u})$ we obtain $\langle x^*(t),C\tilde{u}(t)\rangle = \sup_{u\in U}\langle x^*(t),Cu(t)\rangle$, where $\tilde{u}(\cdot)$ is a controlling parameter corresponding to $\tilde{x}(\cdot)$.

5. Conclusion

In this article, we obtain optimality conditions for the Bolza problem with second-order SDFIs and initial conditions. If we replace the boundary conditions in the problem then the problem turns into a completely different optimization problem, and this problem can be examined under different boundary conditions. In addition, when the problem is formed for non-constant intervals, the necessary and sufficient conditions for optimality can be explored.
Using the methods described in this paper, similar results can be obtained for optimal control problems for any higher-order semi-linear differential inclusions.

Article Information

Acknowledgements: The authors would like to express their sincere thanks to the editor and the anonymous reviewers for their helpful comments and suggestions. The first author was funded by the Scientific Research Projects Coordination Unit of Istanbul University, Project number: FBA-2023-38876.

Author's Contributions: The first author introduced the study topic and defined the scope of the article. The first author formulates the discrete-approximation problem. The second author obtained an equivalence relation of LAMs and proved the theorem of optimality conditions for the discrete-approximation problem. The first author obtained optimality conditions for the main problem and proved theorems for convex and non-convex cases. The article was written and thoroughly reviewed by both authors. All authors read and approved the final manuscript.

Artificial Intelligence Statement: No Artificial Intelligence (AI) tools were used in the preparation of this manuscript.

Conflict of Interest Disclosure: The authors declare there are no conflicts of interest.

Plagiarism Statement: This article was scanned by the plagiarism program.

References

[1] G. Çiçek, E. N. Mahmudov, *Optimization of Mayer functional in problems with discrete and differential inclusions and viability constraints*, Turk. J. Math., **45**(5) (2021), 2084-2102. https://doi.org/10.3906/mat-2103-102
[2] G. Çiçek, E. N. Mahmudov, *The problem of Mayer for discrete and differential inclusions with initial boundary constraints*, Appl. Math. and Inf. Sciences, **10**(5)(2016), 1719-1728. http://dx.doi.org/10.18576/amis/100510
[3] S. Demir Sağlam, E. N. Mahmudov, *Convex optimization of nonlinear inequality with higher order derivatives*, Appl. Anal., **102**(5) (2023), 1473-1489. https://doi.org/10.1080/00036811.2021.1988578
[4] E. N. Mahmudov, *Approximation and Optimization of Discrete and Differential Inclusions*, Elsevier, Boston, 2011.
[5] E. N. Mahmudov, *Approximation and optimization of higher order discrete and differential inclusions*, Nonlinear Differ. Equ. Appl., **21**(1) (2014), 1-26. https://doi.org/10.1007/s00030-013-0234-1
[6] G. Bozcu, *İkinci mertebeden diferansiyel içermeli optimizasyon problemleri*, Master Thesis, Istanbul University, 2016.
[7] B. S. Mordukhovich, *Variational Analysis and Generalized Differentiation, I: Basic Theory; II. Applications*, Grundlehren Series (Fundamental Principles of Mathematical Sciences), Vol. 330 and 331, Springer, 2006.
[8] B. N. Pshenichnyi, *Convex Analysis and Extremal Problems*, Nauka, Moscow, 1980.
[9] E.N. Mahmudov, D. I. Mastaliyeva, *Optimization of semilinear higher-order delay differential inclusions*, Appl. Anal., (2025), 1–17. https://doi.org/10.1080/00036811.2025.2501273
[10] L. Li, L. Lu, M. Sofonea, *Generalized penalty method for semilinear differential variational inequalities*, Applicable Analysis, **101**(2) (2020), 437–453. https://doi.org/10.1080/00036811.2020.1745780
[11] Y. Luo, *Existence for semilinear impulsive differential inclusions without compactness*, J. Dyn. Control Syst., **26** (2020), 663–672. https://doi.org/10.1007/s10883-019-09473-2
[12] N. Abada, M. Benchohra, H. Hammouche, *Existence results for semilinear differential evolution equations with impulses and delay*, Cubo: A Mathematical Journal, **12**(2) (2010), 1-17. https://doi.org/10.4067/S0719-06462010000200001
[13] R.T. Rockafellar, *Convex Analysis*, Princeton University Press, New Jersey, 1972.

J. Math. Sci. Model., 8(4) (2025) 185-194 https://doi.org/10.33187/jmsm.1749478

Journal of Mathematical Sciences and Modelling

ISSN (Online) 2636-8692
https://dergipark.org.tr/en/pub/jmsm

Research Article

A Fractional-Order Chemical System: Numerical Analysis with Distinct Variable-Order Derivatives

Ughur Budag[1] **and Emrullah Yaşar**[1]*

[1] *Department of Mathematics, Faculty of Arts and Sciences, Bursa Uludag University, 16059 Bursa, Türkiye*
* *Corresponding author*

Article Info

Keywords: *Chemical system, Fractional calculus, Fractional derivative, Lagrange interpolation, Newton interpolation*
2020 MSC: *26A33, 34A08, 65H10*
Received: *23 July 2025*
Accepted: *29 September 2025*
Available online: *21 October 2025*

Abstract

Fractional calculus models complicated systems that exhibit memory effects, showing much greater potential than classical integer-order derivatives in modeling chaotic systems. In this study, we investigate the application of two numerical interpolation methods, Newton and Lagrange polynomials, for solving a fractional-order Lorenz-type chemical model based on various fractional derivatives. The Lorenz-type model is modified, as it is known for its chaotic behavior, and augmented to allow for modeling chemical reactions, with variable-order fractional derivatives to reflect reality. We utilize numerical schemes for the Caputo-Liouville, Caputo-Fabrizio, and Atangana-Baleanu-Caputo fractional derivatives, and we assess the performance of the Newton and the Lagrange numerical approximations.

1. Introduction

The concept of fractional differentials were originally proposed in the mid-17th century by a query of L'Hôpital to Leibniz. In 1819, S. F. Lacroix first used the term arbitrary order in his work. He formulated the general nth-order derivative using Legendre's Γ symbol. Subsequently, some eminent mathematicians like Leibniz, Euler, Laplace, and Fourier interpreted and progressed the idea of derivatives of any order. Niels Abel applied fractional calculus to the solution of the isochrome problem [1]. Liouville proved that a function with arbitrary-order derivatives could be calculated using a series expansion. As a result of numerous studies, fractional derivatives have been categorized based on the existence of their singular kernels [2, 3]. Among them, using singular kernels, the popular Caputo derivative and Riemann-Liouville derivative are prominent. On the other hand, the Caputo-Fabrizio derivative (CF) and the Atangana–Baleanu (ABC) derivative are comprised of generalized non-local function kernels [4–6].

For a long period of time, the real-world problems were solved with the aid of differential equations. In addition, the applicability of fractional-order differential equations (FODEs) and their ability to handle complex modelling have been demonstrated in diverse studies [7–9]. These studies demonstrate to us that the mnemonic effect of a fractional-order derivative is an appropriate method for modelling complex, real-world phenomena. The variable-order fractional differential equations (VOFDEs) are preferred to constant-order fractional derivatives due to the necessity that allows the order of differentiation to change dynamically. The greater flexibility of VOFDEs allows them to more suitably model natural observations, where the effects of memory or path dependence on system behavior are not fixed. The combination of mnemonic effect and variable-order fractional derivatives leads us to capture chemical species behaviour over time. Overall, more realistic models will be achieved [10–12].

In recent decades, applied research has increasingly required the use of VOFDE. It is required to investigate the development of more complex chaotic systems with multi-scroll or multi-wing attractors, both theoretically and experimentally, for engineering applications. The Lorenz system is one such example indicating that dissipative systems can lead to chaotic behavior, in which even a slight difference in initial state can lead to very varied results. Chaotic dynamics in the Lorenz chemical system can be used to regulate energy dissipation and entropy change. The generalized Lorenz system is quite versatile and can lead to a wide range of chaotic systems, including the classical Lorenz system [13], Chen system [14], and Lü system [15].

Since the exact solution of differential equations cannot be obtained in general, various numerical techniques have been introduced over time. The Adams-Bashforth method is widely used by researchers because it is an effective numerical technique for solving nonlinear

Email addresses: ughurbudag@gmail.com, eyasar@uludag.edu.tr
Cite as: ***A Fractional-order chemical system: Numerical analysis with distinct variable-order derivatives*****, J. Math. Sci. Model., 8(4) (2025), 185-194.**

equations. However, its weakness in solving fractional differential equations with non-local and non-singular kernels has triggered research into new methods [16, 17]. Therefore, a new numerical approach to nonlinear fractional differentiation is required. In the past few years, new techniques have been developed that mix the two-step Newton method and two-step Lagrange interpolation with the fundamental theorem of calculus. These two techniques have been well investigated in [18–22].

The chemical Lorenz system is very responsive to its parameters and derivative order. The main motivation of the study stems from the application of the variable-order derivative to the chaotic system can offer better accuracy in simulating particle transfer in various chemical processes, and better prediction in modelling, compared to the integer-order derivative. In addition, the emerging system solved with two different interpolation methods: Newton and Lagrange. While there are some research studies on this system with various methods, as far as current knowledge, they have not been solved by these specific interpolation methods. Moreover, we investigated the impact of these two interpolation methods on fractional operators and illustrated the differences graphically. The idea of comparing the interpolations has been done [23–26]. It is possible to calculate the error analysis of an equation with an exact solution using several techniques [27, 28].

The organization of the paper is as follows. Section 2 presents notations and descriptions of VOFDEs. In Section 3, the classical Lorenz dynamical system with parameters and initial conditions has been presented. We also presented a general outline of the behavior of Lorenz-based chemical systems. Section 4 provides significant details of two different numerical interpolation methods and their applications to fractional derivatives. In Section 5, we have shown numerical simulations obtained by both methods to illustrate the results. Physical interpretations and concluding discussions are provided in the last section.

2. Variable Order Fractional Derivatives

This section will present the fundamentals of the Caputo-Liouville (CL), Caputo-Fabrizio (FC), and Atangana-Baleanu (ABC) equations. The variable-order CL derivative that we will consider is defined as follows [5]:

$$ {}_{0}^{CL}D_{s}^{\zeta(s)}\Psi(s) = \frac{1}{\Gamma(1-\zeta(s))}\int_{0}^{s}(s-\rho)^{-\zeta(s)}\Psi'(\rho)\,d\rho, \quad 0<\zeta(s)\leq 1. $$

The variable-order CF derivative that we will deal with is expressed as follows [2]:

$$ {}_{0}^{CF}D_{s}^{\zeta(s)}\Psi(s) = \frac{(2-\zeta(s))M(\zeta(s))}{2(1-\zeta(s))}\int_{0}^{s}\exp\left[-\zeta(s)\frac{(s-\rho)}{1-\zeta(s)}\right]\Psi'(\rho)d\rho, \quad 0<\zeta(s)<1, $$

where $M(\zeta(s)) = \frac{2}{2-\zeta(s)}$.

The variable-order ABC derivative that we will examined is given as follows [4]:

$$ {}_{0}^{ABC}\mathscr{D}_{s}^{\zeta(s)}\Psi(s) = \frac{B(\zeta(s))}{1-\zeta(s)}\int_{0}^{s}E_{\zeta(s)}\left[-\zeta(s)\frac{(s-\rho)^{\zeta(s)}}{1-\zeta(s)}\right]\Psi(\rho)\,d\rho, \quad 0<\zeta(s)<1, $$

where $B(\zeta(s)) = 1-\zeta(s)+\frac{\zeta(s)}{\Gamma(\zeta(s))}$.

3. Lorenz-Based Chemical System

The generalized Lorenz system first introduced in [13] and then extended and investigated in [29–34]. The logical meaning of the Lorenz system represents fluid motion under the external pressure, and it is an appropriate model for chaos in low-dimensional manifolds [35, 36]. It is given by

$$ \begin{aligned} \frac{d\bar{x}}{ds} &= a(\bar{y}-\bar{x}),\\ \frac{d\bar{y}}{ds} &= b\bar{x}-\bar{y}-\bar{x}\,\bar{z},\\ \frac{d\bar{z}}{ds} &= \bar{x}\,\bar{y}-c\bar{z}, \end{aligned} $$

where $\bar{x}$, $\bar{y}$, and $\bar{z}$ in the system represent the reactions of: intensity of spontaneous flow, variance of the temperature between higher and lower altitude flow, and aberration from the linear of the lateral flow. Such physical phenomena are investigated due to the chaotic behaviours in the equation, and the memory effect is a crucial nuance in the appearance of chaotic behaviour. The constant a is a property of the fluid [37, 38]. The b term in the system represents natural spontaneous flow, and a constant c defines the system's geometry [39].

For a more extensive understanding, we define the generalized Lorenz system as follows [40]:

$$ \begin{aligned} \frac{d\bar{x}}{ds} &= \left(10+\tfrac{25}{29}\mu\right)(\bar{y}-\bar{x}),\\ \frac{d\bar{y}}{ds} &= \left(28-\tfrac{35}{29}\mu\right)\bar{x}+(\mu-1)\bar{y}-\bar{x}\,\bar{z},\\ \frac{d\bar{z}}{ds} &= \bar{x}\,\bar{y}-\left(\tfrac{8}{3}+\tfrac{1}{87}\mu\right)\bar{z}, \end{aligned} $$

where μ is a system parameter and the system exhibits chaotic behavior when $0\leq\mu\leq 29$. For the parameter $\mu = 0$, the system is simplified to the classic Lorenz system, which is defined as follows:

$$\begin{aligned}\frac{d\bar{x}}{ds} &= 10(\bar{y}-\bar{x}),\\ \frac{d\bar{y}}{ds} &= 28\bar{x}-\bar{y}-\bar{x}\,\bar{z},\\ \frac{d\bar{z}}{ds} &= \bar{x}\,\bar{y}-\tfrac{8}{3}\bar{z}.\end{aligned} \tag{3.1}$$

Since it represents a chemical model, the $\bar{x}$ and $\bar{y}$ values cannot be negative [30]. For convenience, the $\bar{x}$ and $\bar{y}$ axes are shifted by an equal distance (for $\eta = 30$)

$$\bar{x} = x-\eta, \quad \bar{y} = y-\eta, \quad \bar{z} = z.$$

The new equation system is defined as given below:

$$\begin{aligned}\frac{dx}{ds} &= 10(y-x),\\ \frac{dy}{ds} &= 28x-y-xz-27\eta+z\eta,\\ \frac{dz}{ds} &= xy-\tfrac{8}{3}z-x\eta-y\eta+\eta^2.\end{aligned} \tag{3.2}$$

One of the challenges in formulating a reaction pathway that leads to equations of the form given in (3.1) is due to the presence of a nonlinear component for $\frac{dz}{ds}$. This term suggests a reaction of the type $x+y \to z$. However, if this is the correct mechanistic interpretation, then by mass-action kinetics, the equations for $\frac{dx}{ds}$ and $\frac{dy}{ds}$ must also include a corresponding $-xy$ term. The xz term is another compelling part of (3.2).

Here, we assume x, y, and z variables as reactive species and include four reaction classes: irreversible source (S), cooperative catalysis (C), external reservoir (R), and chemical species sink (E). The reaction C is a passive species of constant concentration, and R denotes an external reservoir. In addition, R can be considered as an irreversible source and sink. The equivalents of each chemical reaction are given in Table 3.1 (see in [29]).

Chemical Reaction Category	**Rate Expression (J)**
Source	$JS = \sigma_{12}$
Catalytic 1	$JC_1 = y\sigma_2$
Catalytic 2	$JC_2 = x\sigma_3$
Catalytic 3	$JC_3 = z\sigma_5$
Catalytic 4	$JC_4 = xy\sigma_{11}$
Reservoir 1	$JR_1 = xz\sigma_6$
Reservoir 2	$JR_2 = \sigma_7$
Reservoir 3	$JR_3 = x\sigma_8$
Reservoir 4	$JR_4 = y\sigma_9$
Sink 1	$JE_1 = x\sigma_1$
Sink 2	$JE_2 = y\sigma_4$
Sink 3	$JE_3 = z\sigma_{10}$

Table 3.1: Chemical reactions and their rates for the chaotic dynamic model

Where reaction currents (J) are defined by rate constants σ_i. Table 3.1 is equivalent to the following in differential form in terms of J [41]:

$$\begin{aligned}\frac{dx}{ds} &= JC_1 - JE_1,\\ \frac{dy}{ds} &= JC_2 - JE_2 + JC_3 - JR_1 + JR_2,\\ \frac{dz}{ds} &= -JR_3 - JR_4 - JE_3 + JC_4 + JS.\end{aligned}$$

Substituting each term in Table 3.1 into (3.3), we obtain:

$$\begin{aligned}\frac{dx}{ds} &= \sigma_2 y - \sigma_1 x,\\ \frac{dy}{ds} &= \sigma_3 x - \sigma_4 y + \sigma_5 z - \sigma_6 xz + \sigma_7,\\ \frac{dz}{ds} &= -\sigma_8 x - \sigma_9 y - \sigma_{10} z + \sigma_{11} xy + \sigma_{12}.\end{aligned} \tag{3.3}$$

For the reaction to satisfy (3.2), the σ_i values in (3.3) are set equal to the values in Table 3.2.

Initial Conditions	**Parameter Values**
$x_0 = 32$, $y_0 = 32$, $z_0 = 32$	$\sigma_1 = 10$, $\sigma_2 = 10$, $\sigma_3 = 28$, $\sigma_4 = 1$, $\sigma_5 = 30$, $\sigma_6 = 1$, $\sigma_7 = -810$, $\sigma_8 = 30$, $\sigma_9 = 35.5$, $\sigma_{10} = \frac{8}{3}$, $\sigma_{11} = 1$, $\sigma_{12} = 900$

Table 3.2: States and boundary settings for the chaotic dynamic

As mentioned in the introduction, fractional derivatives are an ideal instrument for precise modeling. Using the fractional derivative operator on system (3.3), we obtain the following three-dimensional variable-order Lorenz-based chemical system:

$$\begin{aligned} D_s^{\zeta(s)}\, x(s) &= \sigma_2 y - \sigma_1 x, \\ D_s^{\zeta(s)}\, y(s) &= \sigma_3 x - \sigma_4 y + \sigma_5 z - \sigma_6 xz + \sigma_7, \\ D_s^{\zeta(s)}\, z(s) &= -\sigma_8 x - \sigma_9 y - \sigma_{10} z + \sigma_{11} xy + \sigma_{12}. \end{aligned}$$

4. Numerical Methods

The variable-order Lorenz chemical system described in the previous section provides fundamental knowledge of chaos. There is always a need for a numerical approach to approximate fractional-order systems. To tackle such challenges and simulate effectively, we present a numerical framework for fractional derivatives of variable order. Toufik and Atangana developed an effective numerical approach based on Lagrange polynomial interpolation. It is known to be a suitable method for calculating fractional differential equations with non-local and non-singular functions [42]. Empirical findings also validate the very good accuracy of Newton polynomial interpolation for chaotic systems [19]. This approach has received general acceptance, proving itself to be effective and accurate as a strong numerical method for solving fractional ordinary differential equations as well as systems of fractional differential equations with various types of fractional integral operators.
The next section gives two numerical methods. Specifically, within each $[s_m, s_{m+1}]$ interval, the $\Psi(s, y(s))$ function is calculated using two-step Lagrange polynomial interpolation.

4.1. Caputo-Liouville fractional derivative with Newton interpolation

In this subsection, we will apply Newton's polynomial interpolation method to a variable-order Lorenz system with CL derivative.
The definition of VOFDE with the initial condition is given below:

$$ {}_0^{CL}D_s^{\zeta(s)}\, y(s) = \Psi(s, y(s)) \;\text{ with }\; y(0) = y_0. \tag{4.1}$$

Using the explanation of the CL integral, we obtain the following:

$$ y(s) - y(0) = \frac{1}{\Gamma(\zeta(s))} \int_0^s \psi(\rho, y(\rho))(s-\rho)^{\zeta(s)-1} d\rho. \tag{4.2}$$

This leads to the following relation $s_{m+1} = (m+1)h$, for $m \in \{0, 1, 2, \dots\}$

$$ y(s_{m+1}) - y(0) = \frac{1}{\Gamma(\zeta(s))} \int_{s_m}^{s_{m+1}} \psi(\rho, y(\rho))(s_{m+1}-\rho)^{\zeta(s)-1} d\rho. \tag{4.3}$$

Applying Newton's polynomial, we get [43], [44]:

$$\begin{aligned} y(s_{m+1}) - y(0) = \frac{1}{\Gamma(\zeta(\rho))} \sum_{k=2}^{m} \Bigg\{ \int_{s_{k-1}}^{s_k} \Bigg[& \psi(s_k, y(s_k)) + [\psi(s_{k-1}, y(s_{k-1})) - \psi(s_{k-2}, y(s_{k-2}))] \\ & + \frac{1}{2} \Big(\psi(s_k, y(s_k)) - 2\psi(s_{k-1}, y(s_{k-1})) \\ & + \psi(s_{k-2}, y(s_{k-2})) \Big) (\rho - s_{k-1}) \Bigg] \Bigg\} \\ & \times (\rho - s_{k-2})(\rho - s_{k-1})^{\zeta(s)-1} d\rho. \end{aligned} \tag{4.4}$$

By solving the integrals in (4.4) using fractional calculus knowledge, we yield

$$\begin{aligned} & y(s_{m+1}) - y(0) = \frac{h^{\zeta(s)}}{\Gamma(\zeta(s)+1)} \sum_{k=2}^{m} \psi(s_{k-2}, y(s_{k-2})) \Big[(m-k+1)^{\zeta(s)} - (m-k)^{\zeta(s)} \Big] \\ & + \frac{h^{\zeta(s)}}{\Gamma(\zeta(s)+2)} \sum_{k=2}^{m} [\psi(s_{k-1}, y(s_{k-1})) - \psi(s_{k-2}, y(s_{k-2}))] \times P_1 \\ & + \frac{h^{\zeta(s)}}{2\Gamma(\zeta(s)+3)} \sum_{k=2}^{m} [\psi(s_k, y(s_k)) - 2\psi(s_{k-1}, y(s_{k-1})) + \psi(s_{k-2}, y(s_{k-2}))] \times P_2, \end{aligned} \tag{4.5}$$

where

$$\begin{aligned} P_1 &= (m-k+1)^{\zeta(s)}(m-k+3+2\zeta(s)) - (m-k)^{\zeta(s)}(m-k+3+3\zeta(s)), \\ P_2 &= (m-k+1)^{\zeta(s)} \Big(2(m-k)^2 + (3\zeta(s)+10)(m-k) + 2\zeta(s)^2 + 9\zeta(s) + 12 \Big) \\ & - (m-k)^{\zeta(s)} \Big(2(m-k)^2 + (5\zeta(s)+10)(m-k) + 6\zeta(s)^2 + 18\zeta(s) + 12 \Big). \end{aligned} \tag{4.6}$$

4.2. Caputo-Fabrizio fractional derivative with Newton interpolation

In this subsection, we will apply Newton's polynomial interpolation method to variable-order Lorenz system with CF derivative. The definition of VOFDE with the initial condition is given below:

$$ {}_{0}^{CF}D_{s}^{\zeta(s)}y(s) = \Psi(s,y(s)) \text{ with } y(0) = y_0. \tag{4.7}$$

By employing the clarification of the CF integral, we get

$$ y(s) - y(0) = \frac{1-\zeta(s)}{M(\zeta(s))}\psi(s,y(s)) + \frac{\zeta(s)}{M(\zeta(s))}\int_0^s \psi(\rho,y(\rho))\,d\rho. \tag{4.8}$$

This leads to the relation $s_{m+1} = (m+1)h$, for $m \in \{0,1,2,\dots\}$

$$ y(s_{m+1}) - y(0) = \frac{1-\zeta(s)}{M(\zeta(s))}\psi(s_m,y(s_m)) + \frac{\zeta(s)}{M(\zeta(s))}\int_0^{s_{m+1}} \psi(\rho,y(\rho))\,d\rho. \tag{4.9}$$

For $s_m = mh$, we have

$$ y(s_{m+1}) - y(s_m) = \frac{1-\zeta(s)}{M(\zeta(s))}\left[\psi(s_m,y(s_m)) - \psi(s_{m-1},y(s_{m-1}))\right] + \frac{\zeta(s)}{M(\zeta(s))}\int_{s_m}^{s_{m+1}} \psi(\rho,y(\rho))d\rho. \tag{4.10}$$

By solving the integrals in (4.10) using fractional calculus knowledge, we obtain

$$\begin{aligned} y(s_{m+1}) - y(s_m) &= \frac{1-\zeta(s)}{M(\zeta(s))}\left[\psi(s_m,y(s_m)) - \psi(s_{m-1},y(s_{m-1}))\right] + \\ &\frac{\zeta(s)}{M(\zeta(s))}\left[\frac{\psi(s_{m-2},y(s_{m-2}))+\psi(s_{m-1},y(s_{m-1}))-\psi(s_{s-2},y(s_{m-2}))}{h}\int_{s_m}^{s_{m+1}}(\rho - s_{m-2})\,d\rho\right] \\ &+\frac{\zeta(s)}{M(\zeta(s))}\left(\frac{\psi(s_m,y(s_m))-2\psi(s_{m-1},y(s_{m-1}))+\psi(s_{m-2},y(s_{m-2}))}{2h^2}\int_{s_m}^{s_{m+1}}(\rho - s_{m-2})(\rho - s_{m-1})\,d\rho\right). \end{aligned}$$

Subsequently, the equation is rearranged to obtain the two-stage Newton approximation method as follows [44]:

$$ y(s_{m+1}) - y(s) = \frac{1-\zeta(s)}{M(\zeta(s))}\left[\psi(s_m,y(s_m)) - \psi(s_{m-1},y(s_{m-1}))\right] + \frac{\zeta(s)}{M(\zeta(s))}\left[\frac{23}{12}\psi(s_m,y(s_m))h - \frac{4}{3}\psi(s_{m-1},y(s_{m-1}))h + \frac{5}{12}\psi(s_{m-2},y(s_{m-2}))\right].$$

4.3. Atangana-Baleanu-Caputo fractional derivative with Newton interpolation

In this subsection, we will apply Newton's polynomial interpolation method to a variable-order Lorenz system with ABC derivative. The definition of VOFDE with the initial condition is given below:

$$ {}_{0}^{ABC}D_{s}^{\zeta(s)}\, y(s) = \Psi(s,y(s)) \text{ with } y(0) = y_0.$$

Using the ABC integral, we conclude the following result:

$$ y(s) - y(0) = \frac{1-\zeta(s)}{AB(\zeta(s))}\psi(s,y(s)) + \frac{\zeta(s)}{AB(\zeta(s))\Gamma(\zeta(s))}\int_0^s \psi(s,y(s))(s-\rho)^{\zeta(s)-1}d\rho,$$

[5] articulated as

$$ y(s_{m+1}) - y(0) = \frac{1-\zeta(s)}{AB(\zeta(s))}\psi(s_m,y(s_m)) + \frac{\zeta(s)}{AB(\zeta(s))\Gamma(\zeta(s))}\sum_{k=2}^{m}\int_{s_k}^{s_{k+1}} \psi(s,y(s))(s_{k+1}-\rho)^{\zeta(s)-1}d\rho. \tag{4.11}$$

The result of applying Newton's polynomial is as follows [44]:

$$\begin{aligned} y(s_{m+1}) - y(0) &= \frac{1-\zeta(s)}{AB(\zeta(s))}\psi(s_m,y(s_m)) \\ &+\frac{\zeta(s)}{AB(\zeta(s))\Gamma(\zeta(s))}\sum_{k=2}^{m}\psi(s_{k-2},y(s_{k-2}))\int_{s_k}^{s_{k+1}}(s_{k+1}-\rho)^{\zeta(s)-1}d\rho \\ &+\frac{\zeta(s)}{AB(\zeta(s))\Gamma(\zeta(s))}\sum_{k=2}^{m}\frac{\psi(s_{k-1},y(s_{k-1}))-\psi(s_{k-2},y(s_{k-2}))}{h}\int_{s_k}^{s_{k+1}}(\rho - s_{k-2})(s_{k+1}-\rho)^{\zeta(s)-1}d\rho \\ &+\frac{\zeta(s)}{AB(\zeta(s))\Gamma(\zeta(s))}\sum_{k=2}^{m}\left(\begin{array}{c}\frac{\psi(s_k,y(s_k))-2\psi(s_{k-1},y(s_{k-1}))+\psi(s_{k-2},y(s_{k-2}))}{2h^2} \\ \times\int_{s_k}^{s_{k+1}}(\rho - s_{k-2})(\rho - s_{k-1})(s_{k+1}-\rho)^{\zeta(s)-1}d\rho\end{array}\right). \end{aligned} \tag{4.12}$$

By solving the integrals in (4.12) using fractional calculus knowledge, we get

$$\begin{aligned} y(s_{m+1})-y(0) &= \tfrac{1-\zeta(s)}{AB(\zeta(s))}\psi(s_m,y(s_m)) + \tfrac{\zeta(s)h^{\zeta(s)}}{AB(\zeta(s))\Gamma(\zeta(s)+1)}\textstyle\sum_{k=2}^{m}\psi(s_{k-2},y(s_{k-2}))\left[(m-k+1)^{\zeta(s)}-(m-k)^{\zeta(s)}\right] \\ &+ \tfrac{\zeta(s)h^{\zeta(s)}}{AB(\zeta(s))\Gamma(\zeta(s)+2)}\textstyle\sum_{k=2}^{m}\left[\psi(s_{k-1},y(s_{k-1}))-\psi(s_{k-2},y(s_{k-2}))\right]\times P_1 \\ &+ \tfrac{\zeta(s)h^{\zeta(s)}}{AB(\zeta(s))\Gamma(\zeta(s)+3)}\textstyle\sum_{m=2}^{k}\left[\psi(s_k,y(s_k))-2\psi(s_{k-1},y(s_{k-1}))+\psi(s_{k-2},y(s_{k-2}))\right]\times P_2, \end{aligned}$$

where P_1 and P_2 considered same as (4.6).

4.4. Caputo-Liouville fractional derivative with Lagrange interpolation

In this subsection, we will apply Lagrange's polynomial interpolation method to a variable-order Lorenz system with CL derivative. The definition of VOFDE with the initial condition is given below:

$$ {}_0^{CL}D^{\zeta(s)}\, y(s) = \Psi(s,y(s)) \text{ with } y(0)=y_0. $$

The two-stage Lagrange polynomial provides an approximation of the $\Psi(\rho,y(\rho))$ over the interval $[s_m,s_{m+1}]$ by leveraging two discrete data points (s_m,ψ_m) and (s_{m+1},ψ_{m+1}).

$$ P_m(\theta) \simeq \tfrac{\psi(s_m,y(s_m))}{h}(\rho-s_{m-1}) - \tfrac{\psi(s_{m-1},y(s_{m-1}))}{h}(\rho-s_m). $$

Following same procedures through (4.1)–(4.5) based on Lagrange interpolation, we deduce [45]:

$$\begin{aligned} y(s_{m+1})-y(0) = \tfrac{1}{\Gamma(\zeta(s))}\textstyle\sum_{k=1}^{m}\Big(&\tfrac{\psi(s_k,y(s_k))}{h}\int_{s_k}^{s_{k+1}}(\rho-s_{k-1})(s_{k+1}-\rho)^{\zeta(s)-1}d\rho \\ &-\tfrac{\psi(s_{k-1},y(s_{k-1}))}{h}\int_{s_k}^{s_{k+1}}(\rho-s_k)(s_{k+1}-\rho)^{\zeta(s)-1}d\rho\Big). \end{aligned} \tag{4.13}$$

By solving the integrals in (4.13) using fractional calculus knowledge, we derive

$$\begin{aligned} y(s_{m+1})-y(0) = \tfrac{1}{\Gamma(\zeta(s))}\textstyle\sum_{k=1}^{m}\Bigg(&\tfrac{h^{\zeta(s)}\psi(s_k,y(s_k))}{\zeta(s)(\zeta(s)+1)}\Big((m+1-k)^{\zeta(s)} \\ &\times(m-k+2+\zeta(s))-(m-k)^{\zeta(s)}(m-k+2+2\zeta(s))\Big) \\ &-\tfrac{h^{\zeta(s)}\psi(s_{k-1},y(s_{k-1}))}{\zeta(s)(\zeta(s)+1)}\Big((m+1-k)^{\zeta(s)+1}-(m-k)^{\zeta(s)}(m-k+1+\zeta(s))\Big)\Bigg). \end{aligned}$$

4.5. Caputo-Fabrizio fractional derivative with Lagrange interpolation

In this subsection, we will apply Lagrange's polynomial interpolation method to a variable-order Lorenz system with CF derivative. The definition of VOFDE with the initial condition is given below:

$$ {}_0^{FC}D^{\zeta(s)}\, y(s) = \Psi(s,y(s)) \text{ with } y(0)=y_0. $$

We obtain (4.14) with follow same procedures through (4.7)–(4.9) based on Lagrange interpolation, we will obtain the following expression [45]:

$$ y(s_{m+1}) = y(s_m) + \tfrac{(2-\zeta(s))(1-\zeta(s))}{2}\left[\ \psi(s_m,y(s_m)) - \psi(s_{m-1},y(s_{m-1})) + \tfrac{\zeta(s)(2-\zeta(s))}{2}\textstyle\int_{s_m}^{s_{m+1}}\psi(s,y(s))\,ds\ \right], \tag{4.14} $$

where

$$ \textstyle\int_{s_m}^{s_{m+1}}\psi(s,y(s))\,ds = \tfrac{3h}{2}\psi(s_m,y(s_m)) - \tfrac{h}{2}\psi(s_{m-1},y(s_{m-1}))\,. $$

Then the numerical solution form is represented by the following expression:

$$ y(s_{m+1})-y(s_m) = \left[\tfrac{(2-\zeta(s))(1-\zeta(s))}{2} + \tfrac{3h}{4}\zeta(s)(2-\zeta(s))\right]\psi(s_m,y(s_m)) - \left[\tfrac{(2-\zeta(s))(1-\zeta(s))}{2} + \tfrac{h}{4}\zeta(s)(2-\zeta(s))\right]\psi(s_{m-1},y(s_{m-1})). $$

4.6. Atangana-Baleanu-Caputo fractional derivative with Lagrange interpolation

By applying the two-step Lagrange polynomial to (4.11), we get [45].

$$y(s_{m+1})-y(0)=\frac{\Gamma(\zeta(s))(1-\zeta(s))}{\Gamma(\zeta(s))(1-\zeta(s))+\zeta(s)}f(s_m,y(s_m))$$
$$+\frac{\zeta(s)}{\Gamma(\zeta(s))+\zeta(s)(1-\Gamma(\zeta(s)))}\sum_{k=1}^{m}\left(\frac{f(s_k,y_k)}{h}\int_{s_k}^{s_{k+1}}(\theta-s_{k-1})(s_{k+1}-\theta)^{\zeta(s)-1}d\theta-\frac{f(s_{k-1},y_{k-1})}{h}\int_{s_k}^{s_{k+1}}(\theta-s_k)(s_{k+1}-\theta)^{\zeta(s)-1}d\theta\right).$$

5. Numerical Approach

In this section, two different interpolation approaches are applied to fractional derivatives with constant and variable orders. Figures 5.1–5.5 demonstrate numerical approximation for the Lorenz-based chemical system. In each approximate solution, we considered $\zeta(s)=0.995$ for the constant order, which is considered as a variable order fractional case. The time interval $s=100$, step size $h=0.001$, and initial conditions are provided in Table 3.2. The Figure 5.1 describes the simple algorithm of MATLAB code, which is commonly used for numerical computation and plotting. The N is for calculating the number of time steps needed for the numerical simulation.

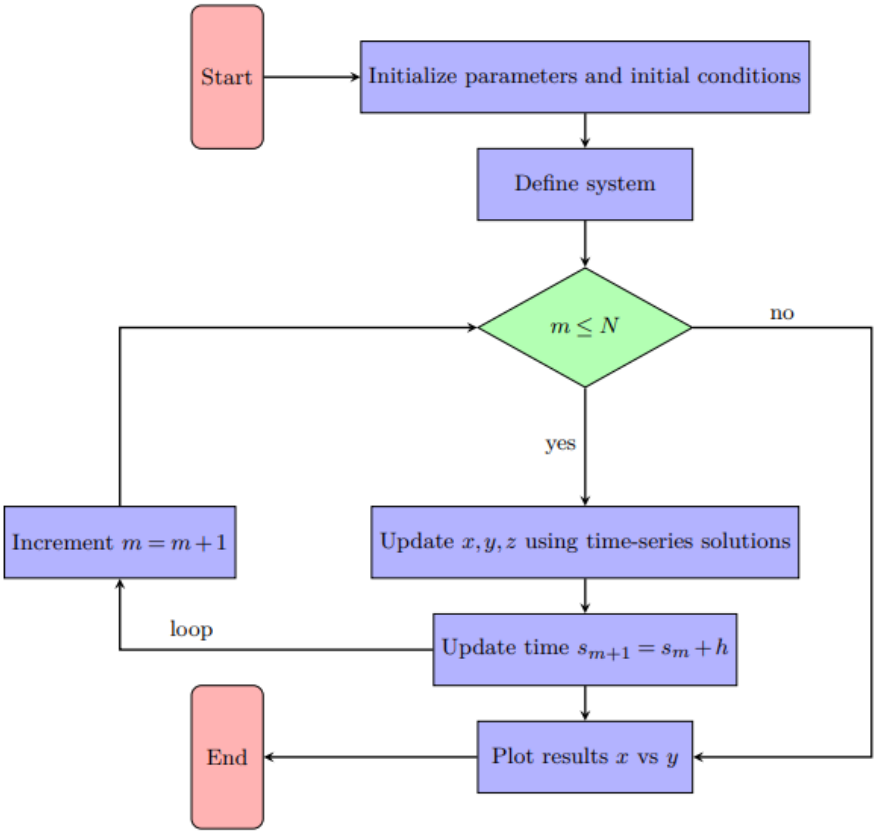

Figure 5.1: Flowchart of the fractional-order differential equation solver

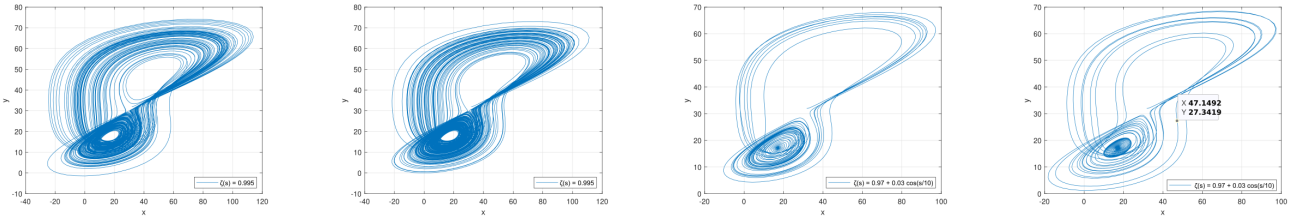

(a) Using the Lagrange interpolation approximation with the order of $\zeta(s)=0.995$

(b) Using the Newton interpolation approximation with the order of $\zeta(s)=0.995$

(c) Using the Lagrange interpolation approximation with the order of $\zeta(s)=0.97+0.03\cos(\frac{s}{10})$.

(d) Using the Newton interpolation approximation with the order of $\zeta(s)=0.97+0.03\cos(\frac{s}{10})$.

Figure 5.2: Numerical approach in Caputo-Liouville sense on a time domain $0\le s\le 100$ with a interval h=0.001.

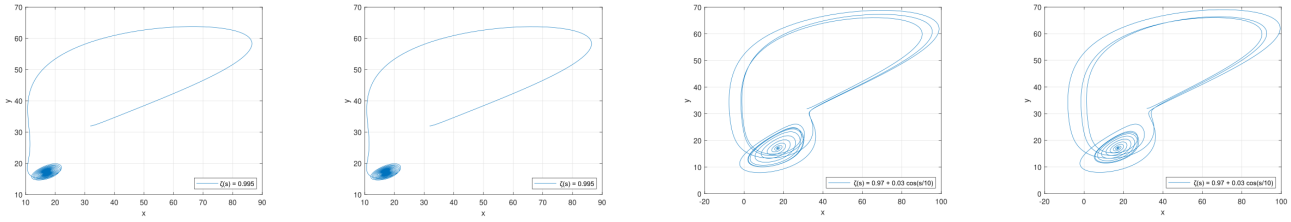

(a) Using the Lagrange interpolation approximation with the order of $\zeta(s) = 0.995$

(b) Using the Newton interpolation approximation with the order of $\zeta(s) = 0.995$

(c) Using the Lagrange interpolation approximation with the order of $\zeta(s) = 0.97 + 0.03\cos(\frac{s}{10})$.

(d) Using the Newton interpolation approximation with the order of $\zeta(s) = 0.97 + 0.03\cos(\frac{s}{10})$.

Figure 5.3: Numerical approach in Caputo-Fabrizio sense on a time domain $0 \leq s \leq 100$ with a interval h=0.001.

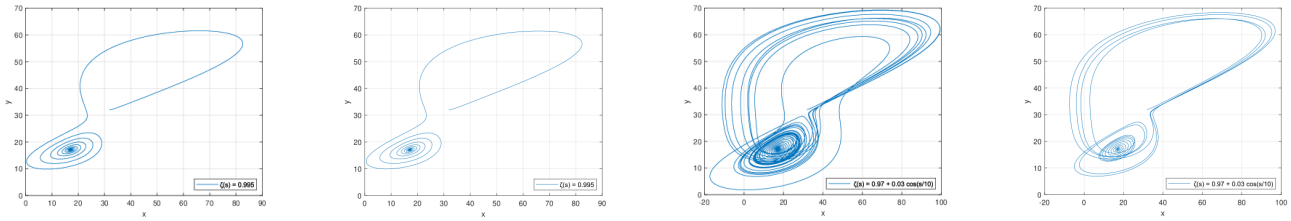

(a) Using the Lagrange interpolation approximation with the order of $\zeta(s) = 0.995$

(b) Using the Newton interpolation approximation with the order of $\zeta(s) = 0.995$

(c) Using the Lagrange interpolation approximation with the order of $\zeta(s) = 0.97 + 0.03\cos(\frac{s}{10})$.

(d) Using the Newton interpolation approximation with the order of $\zeta(s) = 0.97 + 0.03\cos(\frac{s}{10})$.

Figure 5.4: Numerical approach in Atangana–Baleanu sense on a time domain $0 \leq s \leq 100$ with a interval h=0.001.

To observe the different behaviours of the interpolation approaches we are considering, we employ different $\zeta(s)$ functions.

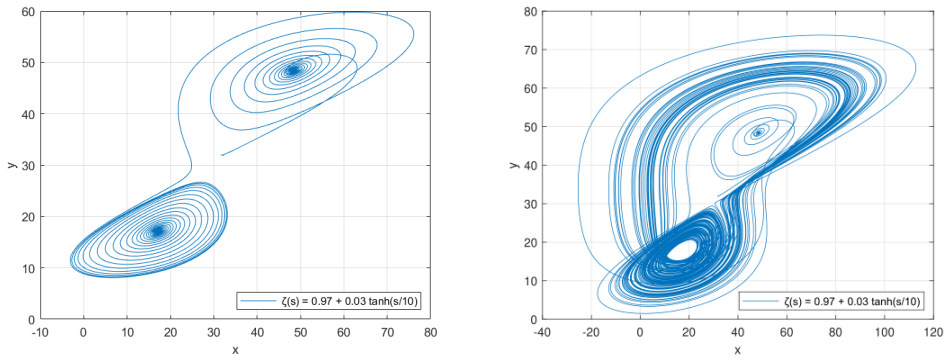

(a) Lagrange interpolation of Atangana-Baleanu.

(b) Newton interpolation of Atangana-Baleanu.

Figure 5.5: Investigation of interpolation methods in the Atangana–Baleanu sense on a time domain $0 \leq s \leq 100$ with a interval h=0.001 order of the s parameter function $\zeta(s) = 0.97 + 0.03\tanh(\frac{s}{10})$.

6. Conclusion

In this study, we examined the fractional order Lorenz-based chemical system with three different derivative operators. The obtained graphical results reveal distinct behavioral patterns under each operator. The ABC operator made chaotic attractors that were smoother and more structured in the phase portraits, essentially in the xy plane.

The differences between operators have captured the different chaotic behaviours of the chemical equation. One of the primary objectives of this study was the investigation of chaotic behaviours of the dynamic system with variable-order derivatives. In addition, we demonstrated that the different states of the $\zeta(s)$ function influence different chaotic attractors. Based on this, we concluded that it was useful to select a suitable $\zeta(s)$ function that allows us to determine the distinct chaotic attractors of the dynamic system. Both methods are precise, efficient, and comprehensive. A small separation step is not required, which saves time in the calculation.

The results show the complexity of chaotic attractors, mostly insectuous with its operators and their derivative orders. Additionally, we can capture a better chaotic attractor by choosing a suitable order for the interpolation method. Future research could look into adaptive order selection or hybrid operators to make predictions in chemical reaction networks even more accurate.

Article Information

Acknowledgements: The authors gratefully acknowledge the editor and anonymous reviewers for their insightful comments and constructive suggestions, which greatly contributed to improving the quality of this article.

Author's contributions: EY: Supervision, methodology, review, and editing. UB: Methodology, writing, review and editing.

Artificial Intelligence Statement: The artificial intelligence was not used in this article.

Conflict of Interest Disclosure: The authors declare that there is no potential conflict of interest.

Plagiarism Statement: This article was scanned by the plagiarism program.

References

[1] B. Ross, *The development of fractional calculus 1695–1900,* Hist. Math., **4**(1) (1977), 75-89. https://doi.org/10.1016/0315-0860(77)90039-8
[2] M. Caputo, M. Fabrizio, *A new definition of fractional derivative without singular kernel,* Prog. Fract. Differ. Appl., **1**(2) (2015), 73-85.
[3] M. Caputo, M. Fabrizio, *Applications of new time and spatial fractional derivatives with exponential kernels,* Prog. Fract. Differ. Appl., **2**(1) (2016), 1-11. https://doi.org/10.18576/pfda/020101
[4] A. Atangana, D. Baleanu, *New fractional derivatives with nonlocal and non-singular kernel: Theory and application to heat transfer model,* (2016), arXiv:1602.03408.
[5] B. P. Moghaddam, Sh. Yaghoobi, J. A. Tenreiro Machado, *An extended predictor–corrector algorithm for variable-order fractional delay differential equations,* J. Comput. Nonlinear Dynam., **11**(6) (2016), Article ID 061001. https://doi.org/10.1115/1.4032574
[6] D. Kumar, J. Singh, D. Baleanu, et al., *Analysis of regularized long-wave equation associated with a new fractional operator with Mittag-Leffler type kernel* Phys. A: Stat. Mech. Appl., **492** (2018), 155-167. https://doi.org/10.1016/j.physa.2017.10.002
[7] W. W. Mohammed, D. Blömker, *Fast-diffusion limit for reaction-diffusion equations with multiplicative noise,* J. Math. Analy. Appl., **496**(2) (2021), Article ID 124808. https://doi.org/10.1016/j.jmaa.2020.124808
[8] W. W. Mohammed, N. Iqbal, *Impact of the same degenerate additive noise on a coupled system of fractional space diffusion equations,* Fractals, **30**(01) (2022), Article ID 2240033. https://doi.org/10.1142/s0218348x22400333
[9] M. Chaudhary, M. K. Singh, *Anomalous transport for multispecies reactive system with first order decay: Time-fractional model,* Physica Scripta, **97**(7) (2022), Article ID 074001. https://doi.org/10.1088/1402-4896/ac71e0
[10] S. He, H. Wang, K. Sun, *Solutions and memory effect of fractional-order chaotic system: A review,* Chinese Phys. B, **31**(6) (2022), Article ID 060501. https://doi.org/10.1088/1674-1056/ac43ae
[11] C. Baishya, M. K. Naik, R. N. Premakumari, *Design and implementation of a sliding mode controller and adaptive sliding mode controller for a novel fractional chaotic class of equations,* Res. Control Optim., **14** (2024), Article ID 100338. https://doi.org/10.1016/j.rico.2023.100338
[12] H. G. Sun, A. Chang, Y. Zhang, et al., *A review on variable-order fractional differential equations: Mathematical foundations, physical models, numerical methods and applications,* Fract. Calc. Appl. Anal., **22**(1) (2019), 27-59. https://doi.org/10.1515/fca-2019-0003
[13] E. N. Lorenz, *Deterministic nonperiodic flow 1,* In Universality in Chaos, 2nd edition, 2017.
[14] G. Chen, T. Ueta, *Yet another chaotic attractor,* Int. J. Bifurc. Chaos., **9**(07) (1999), 1465-1466. https://doi.org/10.1142/s0218127499001024
[15] J. Lü, G. Chen, *A new chaotic attractor coined,* Int. J. Bifurc. Chaos., **12**(03) (2002), 659-661. https://doi.org/10.1142/s0218127402004620
[16] G. Dahlquist, *Convergence and stability in the numerical integration of ordinary differential equations*. Math. Scand., **4** (1956), 33-53. https://doi.org/10.7146/math.scand.a-10454
[17] W. E. Milne, *Numerical integration of ordinary differential equations,* Amer. Math. Monthly, **33**(9) (1926), 455-460. https://doi.org/10.1080/00029890.1926.11986619
[18] Z. Wang, Y. Sun, B. J. van Wyk, et al., *A 3-d four-wing attractor and its analysis,* Braz. J. Phys., **39**(3) (2009), 547-553. https://doi.org/10.1590/s0103-97332009000500007
[19] B. S. T. Alkahtani, *A new numerical scheme based on Newton polynomial with application to fractional nonlinear differential equations,* Alex. Eng. J., **59**(4) (2020), 1893-1907. https://doi.org/10.1016/j.aej.2019.11.008
[20] B. Babayar-Razlighi, *Newton-Taylor polynomial solutions of systems of nonlinear differential equations with variable coefficients,* Int. J. Nonlinear Anal. Appl., **12**(2) (2021), 237-248. https://doi.org/10.22075/ijnaa.2020.18371.2007
[21] M. H. Heydari, A. Atangana, Z. Avazzadeh, *Chebyshev polynomials for the numerical solution of fractal–fractional model of nonlinear Ginzburg–Landau equation,* Eng. Comput., **37** (2021), 1377-1388. https://doi.org/10.1007/s00366-019-00889-9
[22] A. Atangana, S. I. Araz, *New numerical scheme with Newton polynomial: Theory, methods, and applications,* Acad. Pr., 2021. https://doi.org/10.1016/b978-0-32-385448-1.00007-x
[23] W. Werner, *Polynomial interpolation: Lagrange versus Newton,* Math. Comp., **43** (1984), 205-217. https://doi.org/10.1090/s0025-5718-1984-0744931-0
[24] Y. Yang, S. P. Gordon, *Visualizing and understanding the components of Lagrange and Newton interpolation,* PRIMUS, **26**(1) (2016), 39-52. https://doi.org/10.1080/10511970.2015.1045053
[25] A. Atangana, S. Qureshi, *Modeling attractors of chaotic dynamical systems with fractal–fractional operators,* Chaos Soliton Fract., **123** (2019), 320-337. https://doi.org/10.1016/j.chaos.2019.04.020
[26] A. Vaněček, S. Čelikovský, *Control systems: From linear analysis to synthesis of chaos*, Prentice-Hall, New Jersey, 1996.
[27] L. Sadek, M. E. Samei, M. S. Hashemi, *The Galerkin Mittag-Leffler method for solving fractional optimal control problems with inequality constraints,* Math. Comput. Simul., **240** (2026), 191-207. https://doi.org/10.1016/j.matcom.2025.07.018
[28] M. S. Hashemi, M. Bayram, *Numerical treatment on fractional differential-algebraic equations by an optimization technique,* Int. J. Comput. Math., (2025), 1-13. https://doi.org/10.1080/00207160.2025.2528092
[29] D. Poland, *Cooperative catalysis and chemical chaos: A chemical model for the Lorenz equations*, Physica D: Nonlinear Phenomena, **65**(1-2) (1993), 86-99. https://doi.org/10.1016/0167-2789(93)90006-m
[30] N. Samardzija, L. D. Greller, E. Wasserman, *Nonlinear chemical kinetic schemes derived from mechanical and electrical dynamical systems,* J. Chem. Phys., **90** (1989), 2296-2304. https://doi.org/10.1063/1.455970
[31] I. Petráš, *The fractional-order Lorenz-type systems: A review*, Fract. Calc. Appl. Analy., **25** (2022), 362-377. https://doi.org/10.1007/s13540-022-00016-4
[32] S. Čelikovský, G. Chen, *On a generalized Lorenz canonical form of chaotic systems,* Int. J. Bifurc. Chaos, **12**(08) (2002), 1789-1812. https://doi.org/10.1142/s0218127402005467
[33] S. Čelikovský, G. Chen, *On the generalized Lorenz canonical form,* Chaos Soliton Fract., **26**(5) (2005), 1271-1276. https://doi.org/10.1016/j.chaos.2005.02.040
[34] G. Chen, J. Lü, *Dynamics of the Lorenz system family: Analysis, control and synchronization,* Sci. Press, Beijing, 2003.
[35] C. Sparrow, *The Lorenz equations: Bifurcations, chaos, and strange attractors,* Vol.41, Springer Sci. Bus. Med., 2012.
[36] Z. Galias, P. Zgliczyński, *Computer assisted proof of chaos in the Lorenz equations,* Phys. D: Nonlin. Phen., **115**(3-4) (1998), 165-188. https://doi.org/10.1016/s0167-2789(97)00233-9
[37] E. Bodenschatz, W.Pesch, G. Ahlers, *Recent developments in Rayleigh-Bénard convection,* Annu. Rev. Fluid Mech., **32** (2000), 709-778. https://doi.org/10.1146/annurev.fluid.32.1.709
[38] J. Lü, G. Chen, D. Cheng, *A new chaotic system and beyond: The generalized Lorenz-like system,* Int. J. Bifurc. Chaos, **14**(05) (2004), 1507-1537. https://doi.org/10.1142/s021812740401014x
[39] U. S. Thounaojam, *Stochastic chaos in chemical Lorenz system: Interplay of intrinsic noise and nonlinearity,* Chaos Soliton. Frac., **165** (2022), Article ID 112763. https://doi.org/10.1016/j.chaos.2022.112763
[40] Y. J. Sun, *A simple observer design of the generalized Lorenz chaotic systems,* Phys. Lett. A, **374**(7) (2010), 933-937. https://doi.org/10.1016/j.physleta.2009.12.019
[41] H. Nabil, H. Tayeb, *A fractional-order chaotic Lorenz-based chemical system: Dynamic investigation, complexity analysis, chaos synchronization, and its application to secure communication,* Chin. Phys. B, **33**(12) (2024), Article ID 120503. https://doi.org/10.1088/1674-1056/ad7fcf
[42] M. Toufik, A. Atangana, *New numerical approximation of fractional derivative with non-local and non-singular kernel: Application to chaotic models,* Eur. Phys. J. Plus, **132** (2017), Article ID 444. https://doi.org/10.1140/epjp/i2017-11717-0
[43] N. Almutairi, S. Saber, *Application of a time-fractal fractional derivative with a power-law kernel to the Burke-Shaw system based on Newton's interpolation polynomials,* MethodsX, **12** (2024), Article ID 102510. https://doi.org/10.1016/j.mex.2023.102510

[44] S. Naveen, V. Parthiban, *Application of Newton's polynomial interpolation scheme for variable order fractional derivative with power-law kernel,* Sci. Rep., **14** (2024), Article ID 16090. https://doi.org/10.1038/s41598-024-66494-z
[45] J. E. Solís-Pérez, J. F. Gómez-Aguilar, A. Atangana, *Novel numerical method for solving variable-order fractional differential equations with power, exponential and Mittag-Leffler laws,* Chaos Soliton Frac., **114** (2018), 175-185. https://doi.org/10.1016/j.chaos.2018.06.032

J. Math. Sci. Model., 8(4) (2025) 195-200 https://doi.org/10.33187/jmsm.1725741

Journal of Mathematical Sciences and Modelling

ISSN (Online) 2636-8692
https://dergipark.org.tr/en/pub/jmsm

Research Article

Analytic Five-Body Gerono Lemniscata Choreography

M. Fernández-Guasti

Lab. de Óptica Cuántica, Departamento de Física, Universidad Autónoma Metropolitana - Iztapalapa, 09340 Ciudad de México, Mexico

Article Info

Keywords: *Analytical solutions, Celestial mechanics, n-body problem, Periodic orbits*
2020 MSC: *37E15, 42B37, 70F10*
Received: *23 June 2025*
Accepted: *11 November 2025*
Available online: *27 November 2025*

Abstract

The trajectories and interaction forces of five bodies with equal masses are analytically described. The bodies follow a choreographic motion in a figure of eight, Gerono lemniscata periodic orbit without collisions. The forces are a linear combination of pairwise distances with either attractive or repulsive coefficients. The center of mass is fixed at the origin. The moment of inertia, as well as the kinetic and potential energies of the system, are constant. Notably, the angular momentum is zero just as in the Bernoulli Lemniscata parametrized by elliptic functions. The number of bodies in the choreography can be increased in a straightforward way. The orbit can be readily generalized to symmetric chains with an arbitrary number of loops.

1. Introduction

The figure of eight has become a celebrated orbit since the three body choreography with a Newtonian potential was shown to exist in this type of curve [1–3], although its analytic form is still unknown. However, an analytic solution has been obtained in a Bernoulli Lemniscata, in terms of elliptic functions under an inhomogeneous logarithmic and square potential [4]. A five body choreography in a Bernoulli Lemniscata, also parametrized with elliptic functions, has been recently reported [5]. The present results will be compared with these previous important landmarks. The Gerono lemniscata, also referred as Viviani's curve, is a quartic polynomial $y^2 = x^2\left(1-x^2\right)$, that can be generated in a variety of ways [6]. Three bodies in a Gerono lemniscata have been parametrized by trigonometric functions. The time average of each body angular momentum is zero, and consequently the average total angular momentum is zero. However, the total angular momentum is a non zero time dependent function equal to $L_z = -\frac{3}{2}\mu\omega\sin(3\omega t)$ [7]. Furthermore, four bodies in the Gerono lemniscata inevitably collide at the crossing point. These results deterred pursuing further possibilities of choreographic motion in this curve. Nonetheless, as we shall presently see, five bodies in the Gerono lemniscata parametrized by trigonometric functions, satisfy equations of motion with harmonic linear attractive and repulsive forces. The present result together with the five body choreography in a Bernoulli lemniscata are, to the best of our knowledge, the only two explicit analytical solutions known in the figure of eight trajectory.

2. Five Bodies in the Gerono Lemniscata

Recently, a four body choreography in a Pascal trisectrix limax plane curve was analytically described [8]. In a choreography, the bodies follow the same periodic orbit with a constant phase difference between them. In addition to a constant centre of mass, usually set at the origin, choreographies are required to exhibit a constant angular momentum and the motion be such that, for all times, no collisions between bodies occur.

Proposition 2.1. *Five bodies with equal masses, labeled 1 to 5, subject to linear forces dependent on the relative distance* $\mathbf{r}_{ij}$ *between the* i *and* j *bodies, with attractive/repulsive (upper/lower sign) force strengths* $-\mu\omega^2\frac{\pm3+\sqrt{5}}{2\sqrt{5}}$ *for* $i-j=1$ *and* $i-j=2$ *respectively, describe a choreographic trajectory with a fixed centre of mass, zero angular momentum and constant total energy in a Gerono type lemniscata plane curve without collisions.*

Proof. The equation of motion of body 1 is

$$\mu d_t^2\mathbf{r}_1 = \kappa_1\left(\mathbf{r}_{12}+\mathbf{r}_{15}\right)+\kappa_2\left(\mathbf{r}_{13}+\mathbf{r}_{14}\right), \tag{2.1}$$

Email address: mfg@xanum.uam.mx
Cite as: M. Fernández-Guasti, *Analytic five-body Gerono lemniscata choreography*, J. Math. Sci. Model., 8(4) (2025), 195-200.

where μ is the mass and the relative distance between bodies is $\mathbf{r}_{ij}=\mathbf{r}_i-\mathbf{r}_i$. The equations of motion for the other bodies, provided that a choreographic motion is attained, are obtained from the argument evaluation $\mathbf{r}_j(\omega t)=\mathbf{r}_1\left(\omega t+\frac{2\pi}{5}(j-1)\right)$. The proposed solution to the equation of motion is

$$\mathbf{r}_1=\sin\phi\,\hat{\mathbf{e}}_x+\sin(2\phi)\,\hat{\mathbf{e}}_y \tag{2.2a}$$

where $\phi=\omega t$. The positions of the remaining four bodies, imposing the choreographic condition $\mathbf{r}_2(\omega t)=\mathbf{r}_1\left(\omega t+\frac{2\pi}{5}\right)$, …; upon evaluation of the sum of angles, are

$$\begin{aligned}
\mathbf{r}_2 &= \left(c_1^-\sin\phi+c_2^+\cos\phi\right)\hat{\mathbf{e}}_x+\left(-c_1^+\sin(2\phi)+c_2^-\cos(2\phi)\right)\hat{\mathbf{e}}_y && (2.2b)\\
\mathbf{r}_3 &= \left(-c_1^+\sin\phi+c_2^-\cos\phi\right)\hat{\mathbf{e}}_x+\left(c_1^-\sin(2\phi)-c_2^+\cos(2\phi)\right)\hat{\mathbf{e}}_y && (2.2c)\\
\mathbf{r}_4 &= \left(-c_1^+\sin\phi-c_2^-\cos\phi\right)\hat{\mathbf{e}}_x+\left(c_1^-\sin(2\phi)+c_2^+\cos(2\phi)\right)\hat{\mathbf{e}}_y && (2.2d)\\
\mathbf{r}_5 &= \left(c_1^-\sin\phi-c_2^+\cos\phi\right)\hat{\mathbf{e}}_x+\left(-c_1^+\sin(2\phi)-c_2^-\cos(2\phi)\right)\hat{\mathbf{e}}_y && (2.2e)
\end{aligned}$$

where $c_1^\pm=\frac{1}{4}\left(\sqrt{5}\pm1\right)$, $c_2^\pm=\frac{1}{4}\sqrt{2\left(5\pm\sqrt{5}\right)}$. The centre of mass obtained from the sum of the bodies' positions is zero, $\frac{\mu}{5\mu}\sum_{j=1}^5\mathbf{r}_j=0$. The sum of relative distances for bodies with $\pm\frac{2\pi}{5}$ phase difference is

$$\mathbf{r}_{12}+\mathbf{r}_{15}=2\mathbf{r}_1-(\mathbf{r}_2+\mathbf{r}_5)=2\left(1-c_1^-\right)\sin\phi\,\hat{\mathbf{e}}_x+2\left(1+c_1^+\right)\sin(2\phi)\,\hat{\mathbf{e}}_y,$$

whereas for a $\pm\frac{4\pi}{5}$ difference,

$$\mathbf{r}_{13}+\mathbf{r}_{14}=2\left(1+c_1^+\right)\sin\phi\,\hat{\mathbf{e}}_x+2\left(1-c_1^-\right)\sin(2\phi)\,\hat{\mathbf{e}}_y.$$

Mass times acceleration for body 1 is $\mu\partial_t^2\mathbf{r}_1=-\mu\omega^2\sin\phi\,\hat{\mathbf{e}}_x-4\mu\omega^2\sin(2\phi)\,\hat{\mathbf{e}}_y$, where $\phi=\omega t$. The equation of motion (2.1) is evaluated by components and equal function arguments, since it should be fulfilled for all times. For $\hat{\mathbf{e}}_x$ (ϕ argument),

$$2\left(1-c_1^-\right)\kappa_1+2\left(1+c_1^+\right)\kappa_2=-\mu\omega^2$$

and for $\hat{\mathbf{e}}_y$ (2ϕ argument),

$$2\left(1+c_1^+\right)\kappa_1+2\left(1-c_1^-\right)\kappa_2=-4\mu\omega^2.$$

From these two equations, upon substitution of $c_1^\pm$,

$$\kappa_1=-\mu\omega^2\frac{3+\sqrt{5}}{2\sqrt{5}},\qquad \kappa_2=\mu\omega^2\frac{3-\sqrt{5}}{2\sqrt{5}}.$$

Thus a 5-body choreographic motion is satisfied. Since the forces are only position dependent, the system angular momentum must be constant. Explicit calculation of $\mathbf{r}_i\times\mathbf{p}_i$, where the momenta $\mathbf{p}_i=\mu d_t\mathbf{r}_i$ are obtained from the time derivative of (2.2a)-(2.2e), gives a zero total angular momentum $L_z=\sum_{i=1}^5\ell_i=\sum_{i=1}^5\mathbf{r}_i\times\mathbf{p}_i=0$. The kinetic energy of the system is constant, $T=\frac{1}{2}\mu\sum_{i=1}^5(d_t\mathbf{r}_i)^2=\frac{25}{4}\mu\omega^2$ (values for each body is discussed hereafter). The potential energy, separating terms with κ_1 and κ_2 coefficients is

$$V=-\frac{1}{2}\kappa_1\left(r_{12}^2+r_{15}^2+r_{23}^2+r_{34}^2+r_{45}^2\right)-\frac{1}{2}\kappa_2\left(r_{13}^2+r_{14}^2+r_{24}^2+r_{25}^2+r_{35}^2\right). \tag{2.3}$$

Each sum of square distances is separately conserved, $\left(r_{12}^2+r_{15}^2+r_{23}^2+r_{34}^2+r_{45}^2\right)=\left(r_{13}^2+r_{14}^2+r_{24}^2+r_{25}^2+r_{35}^2\right)=\frac{25}{2}$, and since $\kappa_1+\kappa_2=-\mu\omega^2$, $V=\frac{25}{4}\mu\omega^2$. The kinetic and potential terms are equal as expected from the Lagrange-Jacobi identity for a sum of harmonic potentials.

The implicit curve of the parametric representation $\mathbf{r}_1=\sin\phi\,\hat{\mathbf{e}}_x+\sin(2\phi)\,\hat{\mathbf{e}}_y=\sin\phi\,\hat{\mathbf{e}}_x+2\sin\phi\cos\phi\,\hat{\mathbf{e}}_y$ with $x=\sin\phi$ is $y=2x\sqrt{1-x^2}$. Upon squaring and scaling the ordinate by two $y\mapsto 2y$, the canonical $y^2=x^2\left(1-x^2\right)$ form of the Gerono/Huygens lemniscata is obtained. A collision occurs if two bodies are at the same position $\mathbf{r}_j(t_c)=\mathbf{r}_k(t_c)$, at a collision time t_c. In this case, there is no $1\le(k-j)<5$ such that $\sin(\omega t_c)=\sin\left(\omega t_c+\frac{2\pi}{5}(k-j)\right)$. □

The Gerono type lemniscata with five bodies at $t=0$ is depicted in Figure 2.1. Their positions at this initial time are centro-symmetric. In order to compare the five-body results with the analytic four body trisectrix limaçon [8] and trifolium rose [9] choreographies, individual body values are presented. The moment of inertia of each body and the system's constant moment of inertia are

$$\begin{aligned}
I_1 &= \frac{\mu}{2}\left(2-\cos(2\phi)-\cos(4\phi)\right),\\
I_{2,5} &= \frac{\mu}{2}\left(2\pm c_2^-\sin(2\phi)\mp c_2^+\sin(4\phi)+c_1^+\cos(2\phi)-c_1^-\cos(4\phi)\right),\\
I_{3,4} &= \frac{\mu}{2}\left(2\mp c_2^+\sin(2\phi)\mp c_2^-\sin(4\phi)-c_1^-\cos(2\phi)+c_1^+\cos(4\phi)\right),\\
I &= \mu\sum_{i=1}^5\mathbf{r}_i\cdot\mathbf{r}_i=5\mu,
\end{aligned}$$

where the upper/lower sign corresponds to the first/second subindex respectively. The sum of square distances between the five bodies, adding the two terms in the potential (2.3), is $\sum_{i<j}^5|\mathbf{r}_{ij}|^2=25$, consistent with $\sum_{i<j}^5|\mathbf{r}_{ij}|^2=\frac{5I}{\mu}$. If different scalings are not introduced in the

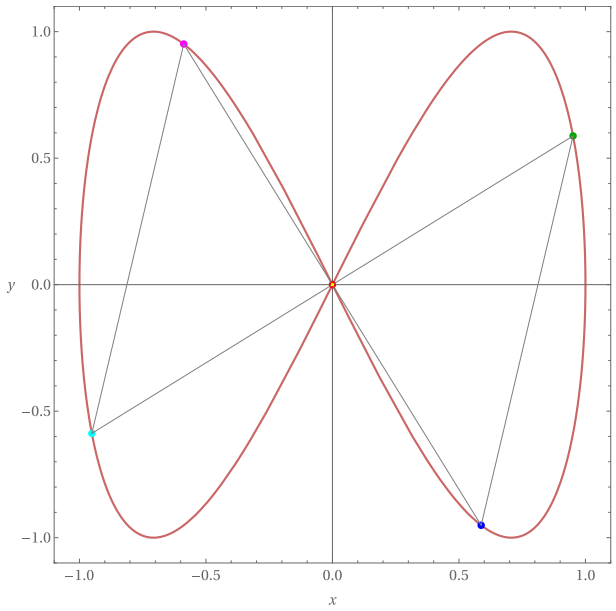

Figure 2.1: Initial positions and forces of five bodies in a plane. The centre of mass (yellow dot) is fixed at the origin.

limaçon and rose choreographies, the moment of inertia is conserved by pairs of bodies, i.e. $I_1^{(4)}+I_3^{(4)}=I_2^{(4)}+I_4^{(4)}=$ constant. The angular momenta $\ell_j=\left(\mathbf{r}_j\times\mathbf{p}_j\right)_z$ from (2.2a)-(2.2e) for each of the five bodies is

$$\begin{aligned}
\ell_1 &= \frac{\mu\omega}{2}\left(-3\sin\phi+\sin(3\phi)\right),\\
\ell_{2,5} &= \frac{\mu\omega}{2}\left(-3c_1^-\sin\phi-c_1^+\sin(3\phi)\mp 3c_2^+\cos\phi\mp c_2^-\cos(3\phi)\right),\\
\ell_{3,4} &= \frac{\mu\omega}{2}\left(3c_1^+\sin\phi+c_1^-\sin(3\phi)\mp 3c_2^-\cos\phi\pm c_2^+\cos(3\phi)\right),\\
L_z &= \sum_{i=1}^{5}\ell_i=0.
\end{aligned}$$

The sums of $\ell_2+\ell_5$ and $\ell_3+\ell_4$ cancel out the cosine terms. However, these sums are still time dependent and only the addition of all bodies angular momenta is constant.
The kinetic energies are

$$\begin{aligned}
T_1 &= \frac{\mu\omega^2}{4}\left(5+\cos(2\phi)+4\cos(4\phi)\right),\\
T_{2,5} &= \frac{\mu\omega^2}{4}\left(5\mp c_2^-\sin(2\phi)\pm\frac{1}{2}c_1^+c_2^-\sin(4\phi)-c_1^+\cos(2\phi)+4c_1^-\cos(4\phi)\right),\\
T_{3,4} &= \frac{\mu\omega^2}{4}\left(5\pm c_2^+\sin(2\phi)\pm\frac{1}{2}c_1^-c_2^+\sin(4\phi)+c_1^-\cos(2\phi)-4c_1^+\cos(4\phi)\right),\\
T &= \sum_{j=1}^{5}\mathscr{E}_{kj}=\frac{25}{4}\mu\omega^2.
\end{aligned}$$

The sums T_2+T_5 and T_3+T_4 cancel out the sine contributions but remain time dependent. It is only when these terms are added, since $c_1^--c_1^+=-\frac{1}{2}$, that all five terms add up to a constant. In contrast, pairs of four-body configurations in the limax or the rose have constant kinetic energies. These results suggest that choreographies with an n non prime number of bodies will exhibit extra symmetries not present in orbits with n prime.

3. Bernoulli and Gerono Lemniscatae Comparison

The three and five bodies trajectories in the Bernoulli lemniscata were parametrized using the Jacobi elliptic functions. Interestingly, a trigonometric parametrization of the Bernoulli lemnsicata does not yield a constant centre of mass [10]. In contrast, the three body trigonometric parametrization of the Gerono lemniscata preserves a constant centre of mass but fails to conserve angular momentum [7]. For three bodies, the elliptic modulus is $k^2=\frac{1}{4}\left(2+\sqrt{3}\right)$. For 5 bodies, two numerical solutions for the elliptic modulus have been found, $k_1^2=0.65\ldots$ and $k_2^2=0.99\ldots$ [10]. A guiding criterion to the difficult problem of finding a potential given a trajectory, is established in [5]. The potential is proposed to be a function of the momentum independent conserved quantities. If necessary, mappings of these quantities are evaluated such that pairwise interactions are described. A comparison of the Gerono and Bernoulli lemniscatae parameters is shown in Table 3.1. The sum of square distances between bodies with adjecent periods is conserved as well as those with alternate periods. In the Bernoulli lemniscata, the product of square distances is constant. The log function then provides a pairwise interaction, and thus a logarithmic potential is also required. In the Gerono lemniscata, the constant quantities involve the sums of squares but the products are not time independent. Thus, consistent with the López-Vieyra potential guiding criterion [5], no logarithmic function is required.

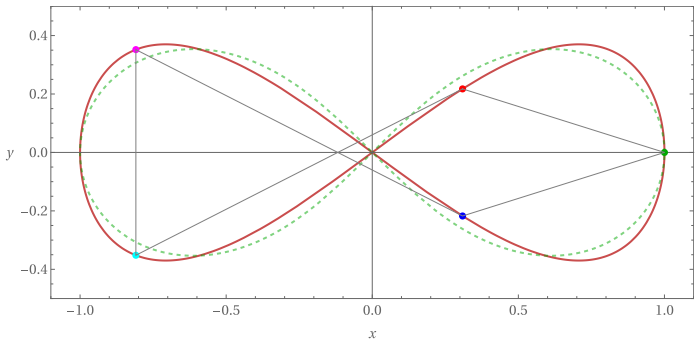

Figure 3.1: Lemniscatae of Gerono (red) and Bernoulli (dotted green) types. Five bodies at $\phi = \omega t = \frac{\pi}{10}$, are shown on the Gerono curve, with the $\hat{\mathbf{e}}_y$ parametric component scaled by $k_y = 0.37$.

		Gerono	Bernoulli	
			k_1^2	k_2^2
1	$\mathscr{E}_{\text{total}}$	$\frac{25}{2}\mu\omega^2$	0.54…	0.31…
2	$\mathscr{E}_k$	$\frac{25}{4}\mu\omega^2$	1.06…	0.35…
3	$\mathscr{E}_p$	$\frac{25}{4}\mu\omega^2$	$\mathscr{E}_{\text{total}} - \mathscr{E}_k$	$\mathscr{E}_{\text{total}} - \mathscr{E}_k$
4	I	5μ	11.99…	17.97…
5	$\sum r_{j,j\pm1}^2$	$\frac{25}{2}$	$I_{2a}^{(5)}$	$I_{2a}^{(5)}$
6	$\sum r_{j,j\pm2}^2$	$\frac{25}{2}$	$I_{2a}^{(5)}$	$I_{2a}^{(5)}$
7	$\prod r_{j,j\pm1}^2$	not constant	$I_1^{(5)}$	$I_1^{(5)}$
8	$\prod r_{j,j\pm2}^2$	not constant	$I_1^{(5)}$	$I_1^{(5)}$

Table 3.1: Five-body constants in the Gerono and Bernoulli Lemniscatae, centre of mass is constant and angular momentum is zero in all cases. Bernoulli data retrieved from [5].

4. n-bodies in the Gerono Lemniscata and Chains

Curves labeled as chains with m loops, the eight being a chain with 2 loops, have been numerically obtained for a Newtonian potential [11]. These chains, that may be symmetrical or not, allow for choreographic motion of different numbers of bodies. For the planar Newtonian n-body problem with equal masses, the existence and number of different main simple choreographies without collisions in linear chains has been recently proved [12]. Let us restrict here to an analytical description of symmetric chains under a harmonic potential with attractive and repulsive contributions. A curve of the form $\mathbf{r} = \sin\phi\,\hat{\mathbf{e}}_x + \sin(m\phi)\,\hat{\mathbf{e}}_y$ generates chains with m loops for even m. Unfortunately, for odd m, the curve retraces itself leaving end points where the motion reverses. However, a parametrization of the form $\mathbf{r} = \cos\phi\,\hat{\mathbf{e}}_x + k_y \sin(m\phi)\,\hat{\mathbf{e}}_y$, generates chains with m loops for all $m \in \mathbb{Z}$, where $m = 0$ gives a line and $m = 1$ an ellipse.

Lemma 4.1. *A chain parametrized by*

$$\mathbf{r} = \cos\phi\,\hat{\mathbf{e}}_x + k_y \sin(m\phi)\,\hat{\mathbf{e}}_y, \tag{4.1}$$

with $n > 3$ bodies evenly separated by a $\frac{2\pi}{n}$ phase difference, satisfies the equations of motion for a κ_1 linear force coefficient with their first neighbours and a κ_2 linear force coefficient with their second neighbours if $m \neq \beta n$ and $m \pm 1 \neq \beta n$, $\beta \in \mathbb{Z}$. If m, n are relative primes, no collisions occur.

Proof. Allow for n bodies in the m loops chain (4.1), the position of the j^{th} body is $\mathbf{r}_j(\phi) = \mathbf{r}\left(\phi + \frac{2\pi}{n}(j-1)\right)$. Consider that each body only has a non vanishing interaction with their first and second phase advanced/retarded neighbours. This condition simplifies the results here derived, but may be lifted to include interactions with all the remaining bodies. Let κ_1 and κ_2 be the first and second order attractive and repulsive coefficients respectively. The equation of motion for the j body is

$$\mu d_t^2 \mathbf{r}_j = \kappa_1 \left(\mathbf{r}_{j,j+1} + \mathbf{r}_{j,j-1}\right) + \kappa_2 \left(\mathbf{r}_{j,j+2} + \mathbf{r}_{j,j-2}\right),$$

where $\mathbf{r}_{j,k} = \mathbf{r}_j - \mathbf{r}_k$. The equation of motion evaluated by components, after a bit of algebra, for $\hat{\mathbf{e}}_x$ (ϕ argument) is

$$-\mu\omega^2 = 2\kappa_1\left(1 - \cos\left(\frac{2\pi}{n}\right)\right) + 4\kappa_2\left(1 - \cos^2\left(\frac{2\pi}{n}\right)\right),$$

and for $\hat{\mathbf{e}}_y$ ($m\phi$ argument),

$$-\frac{1}{2}\mu m^2\omega^2 = \kappa_1\left(1 - \cos\left(m\frac{2\pi}{n}\right)\right) + 2\kappa_2\left(1 - \cos^2\left(m\frac{2\pi}{n}\right)\right).$$

From these two algebraic equations, κ_1 and κ_2 are obtained. Unique solutions exist if the determinant

$$D = \left(1-\cos\left(\frac{2\pi}{n}\right)\right)2\left(1-\cos^2\left(m\frac{2\pi}{n}\right)\right)-2\left(1-\cos^2\left(\frac{2\pi}{n}\right)\right)\left(1-\cos\left(m\frac{2\pi}{n}\right)\right),$$

differs from zero. If $m=\beta n\pm 1$, $\beta\in\mathbb{Z}$, $\cos\left(m\frac{2\pi}{n}\right)=\cos\left((\beta n\pm 1)\frac{2\pi}{n}\right)=\cos\left(\frac{2\pi}{n}\right)$, the determinant two addends are equal and add up to zero. In these cases, the angular momentum is not conserved, as can be seen from direct evaluation. If $m=\beta n$, $\cos\left(m\frac{2\pi}{n}\right)=\cos(2\pi)=1$, the two addends in the determinant vanish. In this case, the centre of mass is not conserved. For other values of m, the equations of motion are satisfied.
Nonetheless, even if the equations of motion are satisfied, collisions may occur. The chain exhibits crossings at $\phi_c=\frac{\pi}{m}\beta$. There exists a collision at time t_c if $\mathbf{r}(\omega t_c)=\mathbf{r}_k(\omega t_c)=\mathbf{r}\left(\omega t_c+\frac{2\pi}{n}(k-1)\right)$. Equating the y components, there is a collision if $\frac{2\pi m}{n}(k-1)=\beta\pi$, $1\le k\le n$. If a common divisor λ exists, $\frac{m}{n}=\frac{\lambda m'}{\lambda n'}=\frac{m'}{n'}$, where $n'<n$. Then $k-1$ can be set equal to n', and the equality $\frac{2m'}{n'}(k-1)=2m'=\beta$ holds. Thus, the collision condition is satisfied if n,m have a common divisor other than one. Therefore, for the linear symmetric chain, $\frac{m}{n}$, $\frac{m\pm 1}{n}\notin\mathbb{Z}$ are required to satisfy the equations of motion and m,n must be relative primes to avoid collisions. □

Corollary 4.2. *The Gerono lemniscata choreography can accommodate any number of odd bodies greater than 3.*

Proof. For the Gerono lemniscate $m=2$, then $2\pm 1\neq\beta n$, for $n>3$, the equations of motion are thus satisfied for all $n>3$. The number of loops and bodies $m=2,n$ are relative primes for any n odd. □

An example of 4 loops with 11 bodies is depicted in Figure 4.1, that is a case illustrated in [11, Fig.4b] for a numerical solution of the Newtonian potential. Bodies are located at $\mathbf{r}_k(\omega t)=\mathbf{r}\left(\omega t+\frac{2\pi}{11}(k-1)\right)$. A k_y factor of $\frac{1}{8}$ gives chains similar to those numerically reported, although the end loops seem to be somewhat less prominent. In Figure 4.1 lower row, a chain with 9 loops and 7 bodies is depicted. For $m\phi=\pm\beta\pi$, $\beta\in\mathbb{Z}$, the parametric curve (4.1) crosses the abscissas axis. The corresponding x values are $\cos\left(\frac{\beta\pi}{m}\right)$; thus the zeros of the trajectory get closer to each other further away from the origin. These trajectories will be presented in a more encompassing framework, where folia, limax, lemniscatae and other curves generated by harmonic functions, will be treated in a unified way.

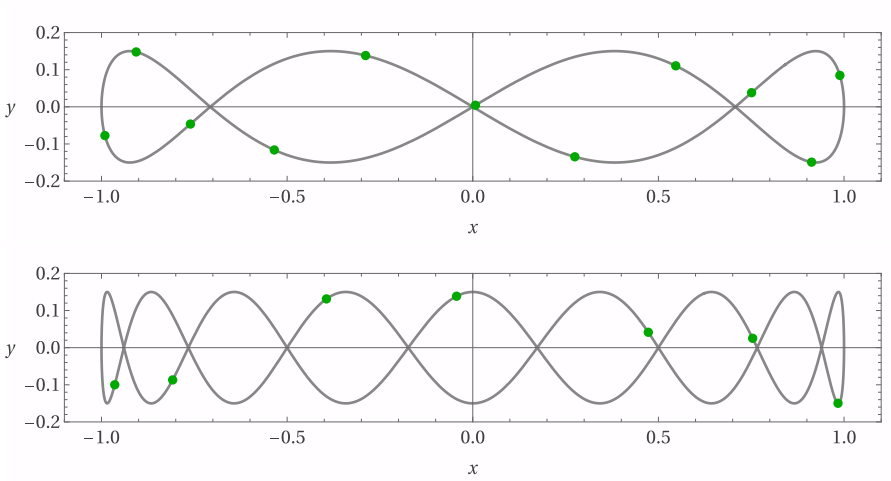

Figure 4.1: Harmonic chains, 4 loops with 11 bodies in upper row and 9 loops with 7 bodies in lower row.

5. Conclusion

Five bodies in a Gerono type lemniscata orbit have been shown to satisfy choreographic motion under a combination of an attractive and a repulsive linear potential. The trigonometric functions parametrization provides a simple description of the bodies positions as well as their velocities and accelerations. The motion shares some common properties with the Bernoulli lemniscata parametrized by the more complicated elliptic functions. For example, the kinetic and potential energies are separately conserved, and most notably, the angular momentum is zero in both trajectories. The generalization to describe orbits with an arbitrary number of loops has been outlined. A pattern seems to emerge, where the analytic choreographies with harmonic attractive and repulsive potential, generate orbits that exhibit the same overall form of the curves obtained numerically for the Newtonian and other inverse potentials.

Article Information

Acknowledgements: The author acknowledges support by SECIHTI, project CF-2023-I-1864.

Artificial Intelligence Statement: Artificial intelligence was not used at any stage in this article.

Conflict of Interest Disclosure: No potential conflict of interest was declared by the author.

Plagiarism Statement: This article was scanned by the plagiarism program.

References

[1] C. Moore, *Braids in classical dynamics*, Phys. Rev. Lett., **70** (1993), 3675-3679. https://doi.org/10.1103/PhysRevLett.70.3675

[2] A. Chenciner, R. Montgomery, *A remarkable periodic solution of the three-body problem in the case of equal masses*, Ann. of Math., **152**(3) (2000), 881-901.

[3] C. Simó, *New Families of Solutions in N-Body Problems*, European Congress of Mathematics, (2001), 101-115.

[4] T. Fujiwara, H. Fukuda, H. Ozaki, *Choreographic three bodies on the lemniscate*, J. Phys. A Math. Gen., **36** (2003), Article ID 2791. https://doi.org/10.1088/0305-4470/36/11/310

[5] J. C. Lopez Vieyra, *Five-body choreography on the algebraic lemniscate is a potential motion*, Phys. Lett. A, **383**(15) (2019), 1711-1715. https://doi.org/10.1016/j.physleta.2019.03.004

[6] I. Popescu, L. Luca, S. S. Ghimisi. *Mechanisms that generate Gerono's lemniscate*, IOP Conference Series: Materials Science and Engineering, **514** (2019), Article ID 012035. https://doi.org/10.1088/1757-899X/514/1/012035

[7] M. Fernández-Guasti, *The components exponential function in scator hypercomplex space: Planetary elliptical motion and three body choreographies*, In P. Debnath, H. M. Srivastava, K. Chakraborty, P. Kumam (Eds.), *Advances in Number Theory and Applied Analysis*, World Scientific, Singapore, 2023, pp. 195-230. https://doi.org/10.1142/13314

[8] M. Fernandez-Guasti, *Analytic four-body limaçon choreography*, Celestial Mech. Dynam. Astronom., **137**(4) (2025), 1-12. https://doi.org/10.1007/s10569-024-10235-x

[9] M. Fernandez-Guasti, *Trifolium rose analytic four-body choreography*, J. Appl. Math., 2025. Under review.

[10] T. Fujiwara, H. Fukuda, H. Ozaki, *N-body choreography on the lemniscate*, Developments and Applications of Dynamical Systems Theory, 1369 (2004), 163-177.

[11] A. Chenciner, J. Gerver, R. Montgomery, C. Simó, *Simple Choreographic Motions of N Bodies: A Preliminary Study*, In P. Newton, P. Holmes, A. Weinstein (Eds.), *Geometry, Mechanics, and Dynamics*, Springer-Verlag, NY, 2002. https://link.springer.com/chapter/10.1007/0-387-21791-6_9

[12] G. Yu, *Simple choreographies of the planar Newtonian N-Body problem*, Arch. Ration. Mech. Anal., **225** (2017), 901-935. https://doi.org/10.1007/s00205-017-1116-1

J. Math. Sci. Model., 8(4) (2025) 201-217 https://doi.org/10.33187/jmsm.1731496

Journal of Mathematical Sciences and Modelling

ISSN (Online) 2636-8692
https://dergipark.org.tr/en/pub/jmsm

Research Article

A Mathematical Model of Substance Abuse–Driven Criminality: Exploring the Dynamics of Addiction and Crime

Robert Kajambeu[1] **and Farai Nyabadza**[1,2]*

[1]*Mathematics and Applied Mathematics, University of Johannesburg, South Africa*
[2]*Institute of Research and Professional Training, Emirates Aviation University, Dubai International Academic City, UAE*

Article Info

Keywords: *Drug abuse criminogenic growth number, Narcocriminality, Rehabilitation, Relapse rate, Sensitivity analysis, Simulations*
2020 AMS: *34A30, 92F05, 34L30*
Received: *01 July 2025*
Accepted: *14 December 2025*
Available online: *15 December 2025*

Abstract

Drug abuse and crime are deeply interconnected, forming a vicious cycle that exacerbates public health and criminal justice challenges. In South Africa's Gauteng province, substance abuse remains a major socioeconomic burden with far-reaching consequences. This study develops a seven-compartment deterministic model using ordinary differential equations to analyze the dynamics between drug abuse and criminal activity. The model incorporates homogeneous population mixing and accounts for removal rates associated with drug-related crime and rehabilitation. Analytical results indicate two equilibrium states: a narcocriminality-free equilibrium and a persistent (endemic) equilibrium. This study establishes that the narcocriminality-free equilibrium is globally asymptotically stable when the drug abuse criminogenic growth number (DGN, $\mathcal{D}_0 < 1$), while the endemic equilibrium exists when $\mathcal{D}_0 > 1$. Sensitivity analysis identifies the initiation rate as the most influential parameter on $\mathcal{D}_0$, showing that $\mathcal{D}_0$ increases with the progression rates α (light drug users) and ρ (heavy drug users). Conversely, $\mathcal{D}_0$ shows a decrease with higher incarceration rates (ϵ, γ_1) and rehabilitation rates (γ_2). These findings have important policy implications related to early intervention strategies targeting the drug-crime cycle, and enhancing rehabilitation programs and incarceration efficacy to reduce drug-driven criminality.

Drug abuse criminogenic growth number, Narcocriminality, Rehabilitation, Relapse rate, Sensitivity analysis, Simulations

1. Introduction

Drug abuse, defined as the excessive consumption of addictive substances through unsafe quantities or harmful methods [1], constitutes a major public health challenge with profound societal repercussions. Extensive research has established drug abuse as a key driver of adverse outcomes, including heightened criminal activity, diminished workforce productivity, unemployment, family destabilization, and political instability [2]. Moreover, substance abuse is strongly correlated with the onset of chronic diseases, preventable injuries, and premature mortality [2–4]. The complex interplay between drug abuse and criminal behaviour has therefore emerged as a global concern, increasingly recognized as a pathological condition requiring medical and social intervention. In South Africa, the rapid expansion of the illicit drug market—particularly among youth populations—has exacerbated the incidence of substance use disorders, accompanied by severe social and health-related comorbidities, with criminal activity representing one of the most critical consequences [5].

Recent empirical evidence underscores the gravity of this crisis. During the 2022/2023 reporting period, South African law enforcement documented approximately 162,100 drug-related offences, reflecting an increase of 21,800 cases compared to the preceding year [6]. Gauteng Province has been disproportionately affected, with escalating drug-related criminality exerting significant social and economic strain. In response, mathematical biology has increasingly been employed to investigate the dynamics of drug abuse and its criminological consequences. Several modelling frameworks have been proposed to capture the epidemiological characteristics of substance abuse and associated behaviours [7–11]. Parallel advances in crime modelling include the work of [12], who developed an epidemiological-inspired

Email addresses: robertk@uj.ac.za, fnyabadza@uj.ac.za
Cite as: R. Kajambeu, F. Nyabadza, *A mathematical model of substance abuse–driven criminality: Exploring the dynamics of addiction and crime*, J. Math. Sci. Model., 8(4) (2025), 201-217.

framework for criminal behaviour in developing countries, highlighting unemployment as a primary determinant. Similarly, [13] employed deterministic approaches to examine the syndemic relationship between illicit drug use and crime dynamics in South Africa's Western Cape province.

Age-structured modelling has further enriched this field. For instance, [14] demonstrated that children are generally less susceptible to criminal involvement and developed a model distinguishing between criminal and non-criminal populations in a naïve society. Their framework incorporated law enforcement as a regulatory mechanism under homogeneous mixing assumptions, subdividing the criminal population into three categories. The analysis revealed that effective law enforcement suppresses criminal activity, whereas inadequate enforcement fosters its persistence. In a related study, [15] constructed a nonlinear dynamical system to simulate interactions between criminal and non-criminal populations, drawing analogies from predator–prey, epidemic, and harvesting models. Their stability analysis showed that harvesting and conversion rates critically determine long-term system behaviour, with low rates favouring persistence of criminal populations and high rates driving eventual extinction. Likewise, [16] employed a predator–prey framework with a Holling type II functional response to investigate the role of law enforcement. Their findings indicated that insufficient enforcement allows crime to persist, whereas enforcement above a critical threshold can stabilize the system at a crime-free equilibrium.

Mathematical modelling has thus proven indispensable in elucidating epidemiological, biological, and behavioural phenomena [17–19]. Importantly, the initiation of individuals into drug abuse and criminal activity exhibits transmission-like dynamics analogous to infectious diseases [20]. Building on this analogy, the present study develops a mathematical framework to investigate the recruitment of drug addicts into criminal activities, incorporating correctional and rehabilitation services as control measures. Specifically, we construct a drug-agnostic model that captures the progression of both light and heavy drug users into criminal behaviour, with a focus on Gauteng Province, South Africa. The model integrates incarceration and rehabilitation as intervention strategies aimed at curbing the escalating prevalence of drug-related criminality.

A distinctive contribution of this study lies in its dual-pathway rehabilitation framework. We examine two concurrent intervention modalities: (1) institutional rehabilitation within correctional facilities, and (2) community-based psychosocial rehabilitation delivered through specialized centres. While prior studies have largely considered these approaches in isolation [21, 22], our deterministic model incorporates both simultaneously, enabling comparative evaluation of their effectiveness. The objectives of this framework are threefold: first, to provide evidence-based insights for policy formulation targeting substance abuse and crime reduction; second, to elucidate the substance abuse–crime nexus for public education and community engagement; and third, to generate predictive scenarios that inform strategic decision-making regarding resource allocation and intervention planning by law enforcement agencies, public health authorities, and policymakers. This dual-pathway approach offers novel perspectives for optimizing intervention strategies in urban contexts analogous to Gauteng Province.

The remainder of the paper is organized as follows: Section 2 presents the model formulation and underlying assumptions. Section 3 provides the analytical results, including the narcocriminality-free and endemic equilibria and their stability properties. Section 4 reports numerical simulations, and Section 5 concludes with key findings and policy implications.

2. Formulation of the Model

The model divides a population of size $N(t)$ into seven mutually exclusive compartments: $S(t)$, susceptible individuals who do not use drugs, are not involved in crime, and may be vulnerable to initiating drug use; $U_1(t)$, light drug users, referring to individuals who have started using drugs but have not yet progressed to heavy use or criminal activity; $U_2(t)$, heavy drug users defined as individuals who have progressed to a more severe stage of drug use. They are more likely to engage in risky behaviour, suffer from health complications, or get involved in crime; $H(t)$, individuals undergoing rehabilitation; $C(t)$ referring to individuals engaged in criminal activity, often as a result of drug use. This includes both light and heavy users who have progressed into the crime compartment; $J(t)$ is defined as criminals who have been arrested and are currently in jail or prison; and $R(t)$ refers to recovered individuals who cease drug use after rehabilitation or incarceration. The individuals may relapse into heavy drug use. The population dynamics follow the conservation law

$$N(t) = S(t) + U_1(t) + U_2(t) + H(t) + C(t) + J(t) + R(t).$$

Susceptible individuals enter the population through Λ either through immigration or by reaching the age at which drug initiation typically occurs, with attrition occurring through natural mortality (rate μ) or transition to drug use governed by the force of initiation

$$\lambda = \beta(U_1 + \eta_1 U_2 + \eta_2 C)S,$$

where β represents the initiation parameter, and $0 < \eta_{1,2} < 1$ quantify the relative influence of heavy users and criminals compared to light users. Drug use progression follows a hierarchical structure: susceptible individuals become light users, then may advance to heavy use at a rate τ [23], with both user categories potentially engaging in criminal activities at rates α (light users) and ρ (heavy users).

Heavy users face elevated risks including drug-induced mortality (rate δ), rehabilitation enrollment (rate γ_2), and incarceration (rate γ_1). The rehabilitation subsystem incorporates recovery to susceptibility (rates θ for rehabilitated individuals and σ for incarcerated individuals), relapse to heavy use (rate κ), and program dropout (rate ϑ), leading to reversion to heavy use. All compartments experience baseline mortality (rate μ), with heavy users subject to additional substance-related mortality δ. This structure captures the core transitions between behavioural states while accounting for both social influences and intervention effects on drug abuse dynamics.

To construct the model, several fundamental assumptions are considered. First, the population is assumed to be homogeneously mixed, meaning individuals within each compartment are indistinguishable and have equal probabilities of interaction [24]. The model further assumes a unidirectional progression in drug use: individuals who become heavy drug users do not revert to light use, reflecting the chronic and escalating nature of addiction [25]. Social dynamics are incorporated by allowing the criminal population to influence susceptible individuals toward engaging in criminal behaviour [26]. Entry into correctional services is restricted to those who have advanced to heavy

drug use, underscoring the threshold of severity required for institutional intervention [27]. Additionally, the model posits that the transition from susceptibility to criminal activity occurs exclusively through prior drug use, thereby establishing a direct drug-crime pathway [26]. Finally, the potential for relapse or dropout is acknowledged: individuals who have passed through correctional services or rehabilitation centers may return to heavy drug use following release or discontinuation of treatment [27].
We assume that all parameters are constant and nonnegative. A transmission diagram is shown in Figure 2.1 based on the assumptions and definitions of variables and parameters. We obtain the following systems of nonlinear ordinary differential equations from Figure 2.1.

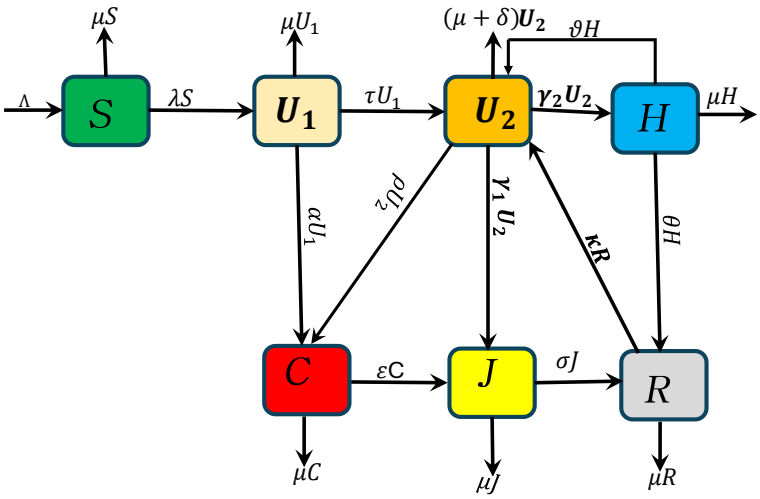

Figure 2.1: Schematic representation of the narcocriminality model incorporating incarceration and rehabilitation pathways.

$$\left.\begin{aligned}
\frac{dS}{dt} &= \Lambda - (\lambda + \mu)S,\\
\frac{dU_1}{dt} &= \lambda S - Q_1 U_1,\\
\frac{dU_2}{dt} &= \tau U_1 + \kappa R + \vartheta H - Q_2 U_2,\\
\frac{dH}{dt} &= \gamma_2 U_2 - Q_3 H,\\
\frac{dC}{dt} &= \alpha U_1 + \rho U_2 - Q_4 C,\\
\frac{dJ}{dt} &= \gamma_1 U_2 + \varepsilon C - Q_5 J,\\
\frac{dR}{dt} &= \sigma J + \theta H - Q_6 R,
\end{aligned}\right\} \tag{2.1}$$

where,

$$Q_1 = \mu + \alpha + \tau,\ Q_2 = \mu + \rho + \gamma_1 + \gamma_2 + \delta,\ Q_3 = \mu + \theta + \vartheta,\ Q_4 = \mu + \varepsilon,\ Q_5 = \mu + \sigma \text{ and } Q_6 = \mu + \kappa.$$

We assume all parameters to be nonnegative, with the model's initial conditions specified as follows:

$$S(0) > 0,\ U_2(0) > 0,\ C(0) > 0,\ U_1(0) > 0, H(0) > 0,\ J(0) > 0,\ R(0) > 0.$$

3. Mathematical Model Analysis

We present a comprehensive exploration of the narcocriminality model to establish its mathematical well-posedness and key dynamical properties. To demonstrate that the model is well-posed, we first show that all solutions of the system defined in (2.1) are nonnegative for all $t \geq 0$. With positive initial conditions, the solutions are bounded within the nonnegative domain $t \geq 0$ and remain bounded within the feasible region Ω. The analysis includes positivity of solutions, boundedness of solutions, existence of solutions, equilibrium points, drug abuse criminogenic growth number, and global stability.

3.1. Positivity, boundedness, and existence of solutions

To demonstrate the biological feasibility of the model, we need to prove that the systems of equations (2.1) are positive and bounded for all $t > 0$.

Theorem 3.1. *For the given initial conditions in (2.1) the solutions of the model system in (2.1) remain positive for all $t > 0$ in Ω.*

Proof. We can express the model equation $S(t)$ as:

$$\frac{dS}{dt} = \Lambda - (\lambda + \mu)S > 0, \tag{3.1}$$

Without compromising generality, and after removing the positive term Λ from the right-hand side,we express equation (3.1) as:

$$\frac{dS}{dt} \geq -(\lambda + \mu)S.$$

After integrating, we obtain the solution of the differential inequality after integration can be written as:

$$S(t) = S(0)e^{-(\mu(t)+\int_0^t \lambda(\tau)d\tau))}.$$

Given that the solution components involve exponential terms, which do not take negative terms, it follows that $S(t) \geq 0$.
The second equation of the system (2.1) yields

$$\frac{dU_1}{dt} \geq -Q_1 U_1,$$

from which we obtain the following,

$$U_1(t) \geq U_1(0)e^{-Q_0(t)}.$$

Since exponential functions are always non-negative, irrespective of whether the exponent is positive or negative, it follows that $U_1(t) \geq 0$.

Similarly,

$$U_2(t) \geq U_2(0)e^{-Q_0(t)} \geq 0.$$

and

$$H(t) \geq 0,\ C(t) \geq 0,\ J(t) \text{ and } R(t) \geq 0$$

from the remaining equations. Therefore, we conclude that the model variable $S(t)$, $U_1(t)$, $U_2(t)$, $H(t)$, $C(t)$, $J(t)$ and $R(t)$ representing population sizes of different classes are positive and will remain in $\mathbb{R}_+^7$ for all t. □

Theorem 3.2. *All positive solutions of the system in (2.1) remain bounded for all $t > 0$.*

Proof. We know that each population component is bounded if the total population is bounded. Therefore, it suffices to show that the total population $N(t)$, is bound for all t. We can also show that all feasible solutions are uniformly bounded in a proper subset $\Omega \in \mathbb{R}_t^7$ where the feasible region Ω is given by

$$\Omega = \left\{(S,\ U_1,\ U_2,\ H,\ C,\ J \text{ and } R) \in \mathbb{R}_t^7 : N(t) \leq \frac{\Lambda}{\mu}\right\}.$$

The derivative of the population function with respect to time t is given by

$$\frac{dN}{dt} = \Lambda - \mu N(t) - \delta H \leq \Lambda - \mu N(t).$$

We proceed to solve the differential inequality by applying [28] with an appropriate integrating factor, so that

$$N(t) \leq \frac{\Lambda}{\mu} + \left(N_0 - \frac{\Lambda}{\mu}\right)e^{-\mu t}.$$

for $t \geq 0$. If $N_0 \leq \frac{\Lambda}{\mu}$, the solution of the differential equation is monotone increasing and bounded by $\frac{\Lambda}{\mu}$.
Otherwise, if $N_0 > \frac{\Lambda}{\mu}$, the solutions are monotone decreasing and bounded below by $\frac{\Lambda}{\mu}$. Therefore, the phase space becomes

$$\Omega = \left\{S,\ U_1,\ U_2,\ H,\ C,\ J,\ R : N \leq \max\left(N_0,\ \frac{\Lambda}{\mu}\right)\right\}.$$

However, in either case, at a limiting equilibrium

$$\lim_{x\to\infty} N = \frac{\Lambda}{\mu}.$$

Given that all phase space variables have been shown to remain nonnegative, the solution trajectory of the model equation (2.1) does not go through the boundary of Ω forward in time. This condition holds for all phase variables, implying that the phase space is both positively invariant and attracting. □

3.2. Model analysis

At the steady state of model (2.1), it satisfies the following equations;

$$\begin{aligned}
&\Lambda - (\lambda + \mu)S^* = 0,\\
&\lambda S^* - Q_1 U_1^* = 0,\\
&\tau U_1^* + \kappa R^* + \vartheta H - Q_2 U_2^* = 0,\\
&\gamma_2 U_2^* - Q_3 H^* = 0,\\
&\alpha U_1^* + \rho U_2^* - Q_4 C^* = 0,\\
&\gamma_1 U_2^* + \varepsilon C^* - Q_5 J^* = 0,\\
&\sigma J^* + \theta H^* - Q_6 R^* 32 = 0.
\end{aligned} \tag{3.2}$$

From equations in (3.2) after algebraic manipulations, we have:

$$
\begin{aligned}
R^* =& \Psi_2 U_1^*, \text{ where} \Psi_2 = \frac{(\alpha\varepsilon\sigma Q_2 + \varepsilon\sigma(\rho\tau - \alpha\vartheta\Psi_1) + \tau Q_4(\sigma\gamma_1 + \theta Q_5\Psi_1))}{Q_2Q_4Q_5Q_6(\phi_1 - 1)}.\\
J^* =& \Psi_4 U_1^*, \text{ where } \Psi_4 = \frac{(\varepsilon\rho\tau + \alpha\varepsilon Q_2 + \tau\gamma_1 Q_4 - \alpha\varepsilon\vartheta\Psi_1 + \varepsilon\kappa\rho\Psi_2 + \kappa\gamma_1\Psi_2 Q_4)}{Q_4Q_5(Q_2 - \vartheta\Psi_1)} \text{ and}\\
\phi_1 =& \frac{\varepsilon\kappa\rho\sigma}{Q_2Q_4Q_5Q_6} + \frac{\kappa\sigma\gamma_1}{Q_2Q_5Q_6} + \frac{\theta\kappa\gamma_2}{Q_2Q_3Q_6} + \frac{\vartheta\gamma_2}{Q_2Q_3}.\\
C^* =& \Psi_5 U_1^*, \text{ where } \Psi_5 = \frac{\rho\tau + \alpha Q_2 - \alpha\vartheta\Psi_1 + \kappa\rho\Psi_2}{Q_4(Q_2 - \vartheta\Psi_1)},\\
H^* =& \Psi_6 U_1^*, \text{ where } \Psi_6 = \frac{(\alpha\varepsilon\kappa\sigma + \tau Q_4Q_5Q_6)\Psi_1}{Q_2Q_4Q_5Q_6(\phi_1 - 1)},\\
U_2^* =& \Psi_7 U_1^*, \text{ where } \Psi_7 = \frac{\alpha\varepsilon\kappa\sigma + \tau Q_4Q_5Q_6}{Q_2Q_4Q_5Q_6(\phi_1 - 1)}.
\end{aligned}
$$

Using the second equation of the system (3.2), we obtain

$$
U_1^*\left[\frac{\xi_2 S}{S^* + \xi_1 U_1^*} - Q_1\right] = 0, \text{ where } \xi_1 = 1 + \Psi_2 + \Psi_4 + \Psi_5 + \Psi_6 + \Psi_7. \text{ and } \xi_2 = \beta(1 + \eta_2\Psi_5 + \eta_1\Psi_7).
$$

We thus have $U_1^* = 0$, giving us the 'narcocriminality-free' equilibrium point,

$$
E_0 = \left(\frac{\Lambda}{\mu}, 0, 0, 0, 0, 0\right).
$$

3.3. Drug abuse criminogenic growth number (DGN)

We introduce a novel metric termed the Drug Abuse Criminogenic Growth Number (DGN), denoted by $\mathcal{D}_0$, which quantitatively integrates the concepts of drug abuse prevalence and its criminogenic potential within a population. This metric characterizes both:

- The temporal increase in substance abuse rates
- The associated rise in criminal activity attributable to drug use

Mathematically, $\mathcal{D}_0$ is analogous to the basic reproduction number in epidemiological models [29, 30], where it represents the expected number of new drug users generated by a single drug user in a completely susceptible population. The drug abuse criminogenic growth number thus quantifies the potential spread of drug abuse and associated criminal activity within a population. In this context, "susceptibility" refers to individuals within a community vulnerable to both:

- Initiation of drug use
- Engagement in drug-related criminal behaviour

If $\mathcal{D}_0 < 1$, then on average, each initiated individual, whether a light drug user, heavy drug user, or criminal, results in fewer than one new initiation. This condition implies that the contribution of each individual is insufficient to sustain or expand the cycle of drug use and associated criminal activities. Conversely, when $\mathcal{D}_0 > 1$, each initiated individual generates more than one new initiate on average, thereby not only maintaining the spread of drug use but also exacerbating the proliferation of drug-related criminal behaviour within the population. We compute $\mathcal{D}_0$ using the next-generation matrix method [31]. This drug abuse criminogenic growth number determines the local stability of the narcocriminality-free equilibrium point. Following the matrix approach, we derive the matrices for new initiation terms and transfer terms between compartments as follows:

$$
\mathcal{F} = \begin{pmatrix} \beta(U_1 + \eta_1 U_2 + \eta_2 C)S \\ 0 \\ 0 \\ 0 \\ 0 \\ 0 \end{pmatrix} \text{ and } \mathcal{V} = \begin{pmatrix} Q_1 U_1 \\ -\tau U_1 - \kappa R - \vartheta H + Q_2 U_2 \\ -\gamma_2 U_2 + Q_3 H \\ -\alpha U_1 - \rho U_2 + Q_4 C \\ -\gamma_1 U_2 - \varepsilon C + Q_5 J \\ -\sigma J - \theta H + Q_6 R \end{pmatrix}
$$

where $\mathcal{F}$ denotes the rate at which new initiations occur in compartments U_1, U_2, C, H, J and R and ν capture the transitions among these compartments. We then define matrices F and V to the Jacobian matrices for $\mathcal{F}$ and $\mathcal{V}$ respectively evaluated at the drug-free equilibrium,

$$
F = \begin{pmatrix} \frac{\beta\Lambda}{\mu} & \frac{\beta\eta_1\Lambda}{\mu} & 0 & \frac{\beta\eta_2\Lambda}{\mu} & 0 & 0 \\ 0 & 0 & 0 & 0 & 0 & 0 \\ 0 & 0 & 0 & 0 & 0 & 0 \\ 0 & 0 & 0 & 0 & 0 & 0 \\ 0 & 0 & 0 & 0 & 0 & 0 \\ 0 & 0 & 0 & 0 & 0 & 0 \end{pmatrix} \text{ and } V = \begin{pmatrix} Q_1 & 0 & 0 & 0 & 0 & 0 \\ -\tau & Q_2 & -\vartheta & 0 & 0 & -\kappa \\ 0 & -\gamma_2 & Q_3 & 0 & 0 & 0 \\ -\alpha & -\rho & 0 & Q_4 & 0 & 0 \\ 0 & -\gamma_1 & 0 & -\varepsilon & Q_5 & 0 \\ 0 & 0 & -\theta & 0 & -\sigma & Q_6 \end{pmatrix}.
$$

The drug abuse criminogenic growth number is given as $\mathcal{D}_0 = \rho(FV^{-1})$, where F and V represent the matrix of initiation rates and the transitions between compartments, respectively. The inverse of matrix V is given as V^{-1}. This follows that $\mathcal{D}_0$ is the maximum eigenvalue of the next generation matrix FV^{-1} is such that:

$$\nu(FV^{-1}) = \mathcal{D}_0 = \mathcal{D}_{0U_1} + \mathcal{D}_{0U_2} + \mathcal{D}_{0C},$$

where

$$\mathcal{D}_{0U_1} = \frac{\beta\Lambda}{Q_1\mu}, \quad \mathcal{D}_{0U_2} = \frac{\beta\eta_1\Lambda}{Q_2\mu\,(1-\phi_1)}\left(\frac{\alpha\varepsilon\sigma\kappa}{Q_1Q_4Q_5Q_6} + \frac{\tau}{Q_1}\right) \text{ and } \mathcal{D}_{0C} = \frac{\beta\eta_2\Lambda}{Q_4\mu\,(1-\phi_1)}\left(\frac{\alpha}{Q_1}\,(1-\phi_2) + \frac{\rho\tau}{Q_1Q_2}\right),$$

with

$$\phi_1 = \frac{\gamma_2\vartheta}{Q_2Q_3} + \frac{\gamma_2\theta\kappa}{Q_2Q_3Q_6} + \frac{\gamma_1\kappa\sigma}{Q_2Q_5Q_6} + \frac{\epsilon\kappa\rho\sigma}{Q_2Q_4Q_5Q_6} \quad \text{and} \quad \phi_2 = \frac{\vartheta\gamma_2}{Q_2Q_3} + \frac{\gamma_2\theta\kappa}{Q_2Q_3Q_6} + \frac{\gamma_1\kappa\sigma}{Q_2Q_5Q_6}.$$

The growth number $\mathcal{D}_0$ comprises three components representing contributions from light drug users,$\mathcal{D}_{0U_1}$, heavy drug users, $\mathcal{D}_{0U_2}$ and criminals, $\mathcal{D}_{0C}$. Each component measures the expected number of new individuals (light users, heavy users, or criminals) initiated into drug abuse and subsequent criminal activities within the population.

Following [31], we have the following result:

Theorem 3.3. *The drug-free equilibrium E_0 of system (2.1) is locally asymptotically stable whenever $\mathcal{D}_0 < 1$ and unstable otherwise.*

3.4. The narcocriminality persistent equilibrium point

After some tedious algebraic manipulations, we obtain

$$S^* = \frac{\Lambda Q_1\xi_1(\mathcal{D}_0 - 1)}{(\xi_2 - Q_1)(\mu\xi_1 + Q_1(\mathcal{D}_0 - 1)}$$

and

$$U_1^* = \frac{\Lambda(\mathcal{D}_0 - 1)}{\mu\xi_1 + Q_1(\mathcal{D}_0 - 1)}, \text{ where } \mathcal{D}_0 = \frac{\xi_2}{Q_1}.$$

The model's narcocriminality persistent equilibrium point is given by

$$E_1 = (S^*,\ U_1^*,\ U_2^*,\ H^*,\ C^*,\ J^*,\ R^*),$$

where

$$\left.\begin{array}{llll} S^* = \frac{\Lambda Q_1\xi_1(\mathcal{D}_0-1)}{(\xi_2-Q_1)(\mu\xi+Q_1(\mathcal{D}_0-1)}, & U_1^* = \frac{\Lambda(\mathcal{D}_0-1)}{\mu\xi_1+Q_1(\mathcal{D}_0-1)}, & U_2^* = \frac{\Psi_7\Lambda(\mathcal{D}_0-1)}{\mu\xi_1+Q_1(\mathcal{D}_0-1)}, & H^* = \frac{\Psi_6\Lambda(\mathcal{D}_0-1)}{\mu\xi_1+Q_1(\mathcal{D}_0-1)}, \\ C^* = \frac{\Psi_5\Lambda(\mathcal{D}_0-1)}{(\mu\xi_1+Q_1(\mathcal{D}_0-1))}, & J^* = \frac{\Psi_4\Lambda(\mathcal{D}_0-1)}{\mu\xi_1+Q_1(\mathcal{D}_0-1)}, & R^* = \frac{\Psi_2\Lambda(\mathcal{D}_0-1)}{\mu\xi_1+Q_1(\mathcal{D}_0-1)}. & \end{array}\right\} \tag{3.3}$$

We thus have the following result on the existence of the endemic equilibrium;

Theorem 3.4.
The persistent narcocriminality equilibrium point E_1 of system (2.1) exists iff $\mathcal{D}_0 > 1$.

3.5. Global stability of the narcocriminality equilibrium

In this section, we analyse the global stability of the model described in equation (2.1). A narcocriminality-free equilibrium (NFE) exists when the basic reproduction number satisfies $\mathcal{D}_0 < 1$. This condition implies that introducing a small number of drug users or criminals into the population will not lead to a persistent increase in either group. Consequently, under appropriate conditions and effective intervention strategies, both drug use and criminal activity can be eradicated from the population.

Theorem 3.5. *The narcocriminality-free equilibrium is globally asymptotically stable (GAS) whenever $\mathcal{D}_0 < 1$.*

Proof. Consider a Lyapunov function

$$V = U_1 + \bar{w_1}U_2 + \bar{w_2}H + \bar{w_3}C + \bar{w_4}J + \bar{w_5}R,$$

where $\bar{w_1}, \bar{w_2}, \bar{w_3}, \bar{w_4}$ and $\bar{w_5}$ are positive integers to be evaluated. We note that $S \leq \frac{\Lambda}{\mu}$. The time derivative of the Lyapunov function is given by:

$$\begin{aligned}\frac{dV}{dt} =\leq{}& (\beta - Q_1 + \bar{w_1}\tau + \bar{w_3}\alpha)\,U_1 + (\beta\eta_1 - \bar{w_1}Q_2 + \bar{w_3}\rho + \bar{w_4}\gamma_1 + \bar{w_2}\gamma_2)\,U_2 + (\bar{w_1}\vartheta - \bar{w_2}Q_3 + \bar{w_5}\theta)\,H \\ &+ (\beta\eta_2 - \bar{w_3}Q_4 + \bar{w_4}\varepsilon)\,C + (\bar{w_5}\sigma - \bar{w_4}Q_5)\,J + (\bar{w_1}\kappa - \bar{w_5}Q_6)\,R.\end{aligned}$$

We now equate the coefficients of U_1, U_2, H, C, J and R to zero so that

$$
\begin{aligned}
0 =& \beta\eta_1 - \bar{w_1}Q_2 + \bar{w_3}\rho + \bar{w_4}\gamma_1 + \bar{w_2}\gamma_2,\\
0 =& \bar{w_1}\vartheta - \bar{w_2}Q_3 + \bar{w_5}\theta,\\
0 =& \beta\eta_2 - \bar{w_3}Q_4 + \bar{w_4}\varepsilon,\\
0 =& \bar{w_5}\sigma - \bar{w_4}Q_5,\\
0 =& \bar{w_1}\kappa - \bar{w_5}Q_6.
\end{aligned}
$$

The solution of the coefficients is given by

$$
\begin{aligned}
\bar{w}_1 =& \frac{Q_3Q_5Q_6\beta\left(Q_4\eta_1 + \eta_2\rho\right)}{Q_2Q_3Q_4Q_5Q_6 - Q_4Q_5\gamma_2\left(Q_6\vartheta + \theta\kappa\right) - Q_3\kappa\left(Q_4\gamma_1 + \varepsilon\rho\right)\sigma},\\
\bar{w}_2 =& -\frac{Q_5\beta(Q_6\vartheta + \theta\kappa)(Q_4\eta_1 + \eta_2\rho)}{-Q_2Q_3Q_4Q_5Q_6 + Q_4Q_5\gamma_2}(Q_6\vartheta + \theta\kappa) + Q_3\kappa(Q_4\gamma_1 + \varepsilon\rho)\sigma,\\
\bar{w}_3 =& \frac{Q_5\beta\eta_2(Q_2Q_3Q_6 - \gamma_2(Q_6\vartheta + \theta\kappa)) + Q_3\beta(\varepsilon\eta_1 - \gamma_1\eta_2)\kappa\sigma}{Q_2Q_3Q_4Q_5Q_6 - Q_4Q_5\gamma_2(Q_6\vartheta + \theta\kappa) - Q_3\kappa(Q_4\gamma_1 + \varepsilon\rho)\sigma},\\
\bar{w}_4 =& -\frac{Q_3\beta\kappa(Q_4\eta_1 + \eta_2\rho)\sigma}{-Q_2Q_3Q_4Q_5Q_6 + Q_4Q_5\gamma_2(Q_6\vartheta + \theta\kappa) + Q_3\kappa(Q_4\gamma_1 + \varepsilon\rho)\sigma},\\
\bar{w}_5 =& \frac{Q_3Q_5\beta\kappa(Q_4\eta_1 + \eta_2\rho)}{Q_2Q_3Q_4Q_5Q_6 - Q_4Q_5\gamma_2(Q_6\vartheta + \theta\kappa) - Q_3\kappa(Q_4\gamma_1 + \varepsilon\rho)\sigma}.
\end{aligned}
$$

Substituting the coefficients into the time derivative of the Lyapunov function gives,

$$
\begin{aligned}
\frac{dV}{dt} \leq& Q_1Q_2Q_3Q_4Q_5Q_6\left(1-\phi_1\right)\frac{\beta}{Q_1} + \frac{\beta\eta_1}{Q_1Q_2\left(1-\phi_1\right)}\left(\frac{\alpha\varepsilon\kappa\sigma}{Q_4Q_5Q_6} + \frac{\tau}{Q_1}\right) + \frac{\beta\eta_2}{Q_4\left(1-\phi_1\right)}\left(\frac{\alpha}{Q_1}\left(1-\phi_2\right) + \frac{\rho\tau}{Q_1Q_2}\right)U_1,\\
\leq& Q_1Q_2Q_3Q_5Q_6\left(1-\phi_1\right)\left(\mathcal{D}_0 - 1\right)U_1.
\end{aligned}
$$

From the inequality above, it follows that when $\mathcal{D}_0 < 1$, we have $\frac{dV}{dt} < 0$. By applying LaSalle's Invariance Principle [32], the solution trajectories approach the narcocriminality free equilibrium E_0. This establishes the global asymptotic stability of E_0. □

3.6. Global stability of the endemic equilibrium

Theorem 3.6.
If $\mathcal{D}_0 > 1$, then the endemic equilibrium E^* is globally asymptotically stable in the region $\mathbb{R}^7_+$.

Proof. We construct a Lyapunov function such that

$$
\begin{aligned}
\mathcal{V} =& \left(S - S^* - S^*\ln S\right) + a\left(U_1 - U_1^* - U_1^*\ln U_1\right) + b\left(U_2 - U_2^* - U_2^*\ln U_2\right)\\
&+ c\left(H - H^* - H^*\ln H\right) + d\left(C - C^* - C^*\ln C\right) + e\left(J - J^* - J^*\ln J\right)\\
&+ f\left(R - R^* - R^*\ln R\right),
\end{aligned}
$$

where a, b, c, d, e and f are constants to be determined. At the endemic equilibrium, the partial derivatives with respect to each variable are given by:
The derivative of $\mathcal{V}$ is given by

$$
\begin{aligned}
\frac{\partial\mathcal{V}}{\partial S} =& \left(1 - \frac{S^*}{S}\right), \frac{\partial\mathcal{V}}{\partial U_1} = a\left(1 - \frac{U_1^*}{U_1}\right), \frac{\partial\mathcal{V}}{\partial U_2} = b\left(1 - \frac{U_2^*}{U_2}\right), \frac{\partial\mathcal{V}}{\partial H} = c\left(1 - \frac{H^*}{H}\right),\\
\frac{\partial\mathcal{V}}{\partial C} =& d\left(1 - \frac{C^*}{C}\right), \frac{\partial\mathcal{V}}{\partial J} = e\left(1 - \frac{J^*}{J}\right), \frac{\partial\mathcal{V}}{\partial R} = f\left(1 - \frac{R^*}{R}\right).
\end{aligned}
$$

The endemic equilibrium point is a critical point of $\partial\mathcal{V}$. The second-order derivatives are:

$$
\frac{\partial^2\mathcal{V}}{\partial S^2} = \frac{S^*}{S^2}, \frac{\partial^2\mathcal{V}}{\partial U_1^2} = a\frac{U_1^*}{U_1^2}, \frac{\partial^2\mathcal{V}}{\partial U_2^2} = b\frac{U_2^*}{U_2^2}, \frac{\partial^2\mathcal{V}}{\partial H^2} = c\frac{H^*}{H^2}, \frac{\partial^2\mathcal{V}}{\partial C^2} = d\frac{C^*}{C^2}, \frac{\partial^2\mathcal{V}}{\partial J^2} = e\frac{J^*}{J^2}, \frac{\partial^2\mathcal{V}}{\partial R^2} = f\frac{R^*}{R^2}.
$$

The second derivatives of $\mathcal{V}$ are nonnegative at any point of $\mathbb{R}^7_t$; this implies that the Lyapunov function $\mathcal{V}$ exhibits upward concavity, with the endemic equilibrium located at its minimum. We now show that $\frac{\partial\mathcal{V}}{\partial t} \leq 0$. The time derivative of $\mathcal{V}$ is given by:

$$
\dot{\mathcal{V}} = \left(1 - \frac{S^*}{S}\right)\dot{S} + a\left(1 - \frac{U_1^*}{U_1}\right)\dot{U}_1 + b\left(1 - \frac{U_2^*}{U_2}\right)\dot{U}_2 + c\left(1 - \frac{H^*}{H}\right)\dot{H} + d\left(1 - \frac{C^*}{C}\right)\dot{C} + e\left(1 - \frac{J^*}{J}\right)\dot{J} + f\left(1 - \frac{R^*}{R}\right)\dot{R}.
$$

At the equilibrium of the system (2.1) we have

$$
\begin{aligned}
\Lambda =& \frac{\beta(U_1 + \eta_1U_2 + \eta_2C)S^*}{U_1}, Q_1 = \frac{\beta(U_1 + \eta_1U_2 + \eta_2C)S^*}{U_1}, \quad Q_2 = \frac{\tau U_1^* + \kappa R^* + \vartheta H^*}{U_2^*},\\
Q_3 =& \frac{\gamma_2U_2^*}{H^*}Q_4 = \frac{\alpha U_1^* + \rho U_2^*}{C^*}, \quad Q_5 = \frac{\gamma_1U_2^* + \varepsilon C^*}{J^*}, Q_6 = \frac{\sigma J^* + \theta H^*}{R^*}.
\end{aligned}
$$

We then substitute the derivatives of state variables for the expressions to get

$$\begin{aligned}\dot{\mathcal{V}} =& \left(1-\frac{S^*}{S}\right)\left(\beta\left(U_1^*+\eta_1U_2^*+\eta_2C^*\right)S^*+\mu S^*-\beta\left(U_1+\eta_1U_2+\eta_2C\right)S-\mu S\right)\\ &+a\left(1-\frac{U_1^*}{U_1}\right)\left(\beta(U_1+\eta_1U_2+\eta_2C)S-\beta(U_1+\eta_1U_2+\eta_2C)S^*\frac{U_1}{U_1^*}\right)\\ &+b\left(1-\frac{U_2^*}{U_2}\right)\left(\tau U_1+\kappa R+\vartheta H-\left(\frac{\tau U_1^*+\kappa R^*+\vartheta H^*}{U_2^*}\right)U_2\right)\\ &+c\left(1-\frac{H^*}{H}\right)\left(\gamma_2U_2-\frac{\gamma_2U_2^*H}{H^*}\right)\\ &+d\left(1-\frac{C^*}{C}\right)\left(\alpha U_1+\rho U_2-\left(\frac{\alpha U_1^*+\rho U_2^*}{C^*}\right)C\right)\\ &+e\left(1-\frac{J^*}{J}\right)\left(\gamma_1U_2+\varepsilon C-\left(\frac{\gamma_1U_2^*+\varepsilon C^*}{J^*}\right)J\right)\\ &+f\left(1-\frac{R^*}{R}\right)\left(\sigma J+\theta H-\left(\frac{\sigma J^*+\theta H^*}{R^*}\right)R\right).\end{aligned}$$

We let $P_0=\beta U_1^*S^*$; $P_1=\beta\eta_1U_2^*S^*$ and $P_2=\beta\eta_2C^*S^*$,

and

$$\bar{U}=\frac{S}{S^*},\ \bar{V}=\frac{U_1}{U_1^*},\ \bar{W}=\frac{H}{H^*},\ \bar{X}=\frac{C}{C^*},\ \bar{Y}=\frac{J}{J^*},\ \bar{T}=\frac{U_2}{U_2^*},\ \bar{Z}=\frac{R}{R^*}.$$

The derivatives of $\mathcal{V}$ with $a=1$ reduces to

$$\mathcal{V}_{\mathcal{F}}=\left(\frac{-\mu}{S}\right)(S-S^*)+P_0\left(4-\frac{\bar{T}}{\bar{U}}-\frac{\bar{V}\bar{U}}{\bar{X}}-\frac{\bar{X}}{\bar{T}}-\frac{1}{\bar{V}}\right)+f_1-f_2, \tag{3.4}$$

where,

$$\begin{aligned}f_1 =&P_1\left(4-\frac{\bar{W}}{\bar{U}}-\frac{\bar{T}\bar{U}}{\bar{X}}-\frac{\bar{X}}{\bar{W}}-\frac{1}{\bar{T}}\right)+P_2\left(4-\frac{\bar{T}}{\bar{U}}-\frac{\bar{X}\bar{U}}{\bar{Z}}-\frac{\bar{Z}}{\bar{T}}-\frac{1}{\bar{X}}\right)+P_3\left(4-\frac{\bar{T}}{\bar{U}}-\frac{\bar{V}\bar{U}}{\bar{X}}-\frac{\bar{X}}{\bar{V}}-\frac{1}{\bar{T}}\right)\\ &+P_4\left(4-\frac{\bar{T}}{\bar{V}}-\frac{\bar{V}}{\bar{T}\bar{U}}-\frac{\bar{U}}{\bar{W}}-\bar{W}\right)+P_5\left(4-\frac{\bar{V}}{\bar{X}\bar{U}}-\frac{\bar{U}}{\bar{V}}-\frac{\bar{X}}{\bar{W}}-\bar{W}\right)+bP_6\left(4-\frac{\bar{V}}{\bar{T}}-\frac{\bar{T}}{\bar{X}}-\frac{\bar{X}}{\bar{W}}-\frac{\bar{W}}{\bar{V}}\right)\\ &+bP_7\left(4-\frac{\bar{Z}}{\bar{T}}-\frac{\bar{T}}{\bar{X}}-\frac{\bar{X}}{\bar{Y}}-\frac{\bar{Y}}{\bar{Z}}\right)+bP_8\left(4-\frac{\bar{W}}{\bar{T}}-\frac{\bar{T}}{\bar{Y}}-\frac{\bar{Y}}{\bar{Z}}-\frac{\bar{Z}}{\bar{W}}\right)+cP_9\left(4-\frac{\bar{T}}{\bar{W}}-\frac{\bar{W}}{\bar{Z}}-\frac{\bar{Z}}{\bar{Y}}-\frac{\bar{Y}}{\bar{T}}\right)\\ &+dP_{10}\left(4-\frac{\bar{V}}{\bar{X}}-\frac{\bar{X}}{\bar{Y}}--\frac{\bar{Y}}{\bar{Z}}-\frac{\bar{Z}}{\bar{V}}\right)+dP_{11}\left(4-\frac{\bar{T}}{\bar{X}}-\frac{\bar{X}}{\bar{Y}}-\frac{\bar{Y}}{\bar{Z}}-\frac{\bar{Z}}{\bar{T}}\right)+eP_{12}\left(4-\frac{\bar{T}}{\bar{Y}}-\frac{\bar{Y}}{\bar{Z}}-\frac{\bar{Z}}{\bar{W}}-\frac{\bar{W}}{\bar{T}}\right)\\ &+eP_{13}\left(4-\frac{\bar{X}}{\bar{Y}}-\frac{\bar{Y}}{\bar{W}}-\frac{\bar{W}}{\bar{Z}}-\frac{\bar{Z}}{\bar{X}}\right)+fP_{14}\left(4-\frac{\bar{Y}}{\bar{Z}}-\frac{\bar{Z}}{\bar{X}}-\frac{\bar{X}}{\bar{W}}-\frac{\bar{W}}{\bar{Y}}\right)+fP_{15}\left(4-\frac{\bar{W}}{\bar{Z}}-\frac{\bar{Z}}{\bar{X}}-\frac{\bar{X}}{\bar{Y}}-\frac{\bar{Y}}{\bar{W}}\right)\end{aligned}$$

and

$$\begin{aligned}f_2 =&\left(1-\frac{1}{\bar{U}}-\bar{V}\bar{U}+\bar{V}\right)+P_1\left(1-\frac{1}{\bar{U}}-\bar{T}\bar{U}+\bar{T}\right)+P_2\left(1-\frac{\bar{X}}{\bar{U}}-\frac{1}{\bar{U}}+\bar{X}\right)+P_3\left(1-\frac{1}{\bar{U}}-\frac{1}{\bar{V}}+\frac{1}{\bar{V}\bar{U}}\right)\\ &+P_4\left(1-\frac{1}{\bar{V}}-\frac{\bar{V}}{\bar{T}\bar{U}}+\frac{1}{\bar{T}\bar{U}}\right)+P_5\left(1-\frac{\bar{V}}{\bar{X}\bar{U}}-\frac{1}{\bar{V}}+\frac{1}{\bar{X}\bar{U}}\right)+P_6\left(1-\frac{\bar{V}}{\bar{T}}-\bar{T}+\bar{V}\right)+P_7\left(1-\frac{\bar{Z}}{\bar{T}}-\bar{T}+\bar{Z}\right)\\ &+P_8\left(1-\frac{\bar{W}}{\bar{T}}-\bar{T}+\bar{W}\right)+P_9\left(1-\frac{\bar{T}}{\bar{W}}-\bar{W}+\bar{T}\right)+P_{10}\left(1-\frac{\bar{V}}{\bar{X}}-\bar{X}+\bar{V}\right)+P_{11}\left(1-\frac{\bar{T}}{\bar{X}}-\bar{X}+\bar{T}\right)\\ &+P_{12}\left(1-\frac{\bar{T}}{\bar{Y}}-\bar{Y}+\bar{T}\right)+P_{13}\left(1-\frac{\bar{X}}{\bar{Y}}-\bar{Y}+\bar{X}\right)+P_{14}\left(1-\frac{\bar{Y}}{\bar{Z}}-\bar{Z}+\bar{Y}\right)+P_{15}\left(1-\frac{\bar{W}}{\bar{Z}}-\bar{Z}+\bar{W}\right).\end{aligned}$$

To the inequality of property, $\left(4-\frac{\bar{W}}{\bar{U}}-\frac{\bar{T}\bar{U}}{\bar{X}}-\frac{\bar{X}}{\bar{W}}-\frac{1}{\bar{T}}\right)\leq\left(1-\frac{1}{\bar{U}}-\bar{V}\bar{U}+\bar{V}\right)$
$\Longrightarrow f_1\leq f_2$, equality holds$\Longleftrightarrow\bar{V}=\bar{T}=\bar{U}=1$. In order to prove that $\dot{\mathcal{V}}_{\mathcal{F}}\leq 0$
since the first term

$$-\left(\frac{\mu}{S}\right)(S-S^*)^2.$$

Our only task is to prove that the remaining terms are all negative. To prove this, we need to apply the arithmetic mean geometric mean inequality [33]

$$n\sqrt[n]{a_1a_2a_3...a_n}\leq a_1+a_2+...+a_n,$$

where $i\in 1,2,3,...,n$ with $n\geq 0$. We apply the arithmetic mean-geometric mean inequality on the first term of f_1. We consider,

$$\left(4-\frac{\bar{W}}{\bar{U}}-\frac{\bar{T}\bar{U}}{\bar{X}}-\frac{\bar{X}}{\bar{W}}-\frac{1}{\bar{T}}\right).$$

By applying the arithmetic mean-geometric mean inequality,

$$4 \cdot \sqrt[4]{\frac{\bar{W}}{\bar{U}} \cdot \frac{\bar{T}\bar{U}}{\bar{X}} \cdot \frac{\bar{X}}{\bar{W}} \cdot \frac{1}{\bar{T}}} \leq \left(\bar{V} + \frac{1}{\bar{U}} + \bar{V}\bar{U}\right) 4 \leq \left((\bar{V} + \frac{1}{\bar{U}} + \bar{V}\bar{U}\right) - 4 \geq \left((\bar{V} - \frac{1}{\bar{U}} - \bar{V}\bar{U}\right).$$

Similarly, we prove that all other terms of $\dot{\mathcal{V}}$ in equation (3.4) are non-positive. Therefore, $\dot{\mathcal{V}}$ is shown to be positive definite at the endemic equilibrium point and $\frac{\partial \mathcal{V}_{\mathcal{F}}}{\partial t} \leq 0$ with $\frac{\partial \mathcal{V}}{\partial t} = 0$ if and only if $S = S^*, U_1 = U_1^*, U_2 = U_2^*, H = H^*, C = C^*, J = J^*$ and $R = R^*$ for $\bar{U} = \bar{V} = \bar{W} = \bar{X} = \bar{T} = \bar{Z} = 1$. The unique invariant set within $\Omega \subset \mathbb{R}_+^7$ is the singleton comprising the endemic equilibrium. Consequently, every solution trajectory that intersects $\mathbb{R}_t^7$ asymptotically approaches the endemic equilibrium.
Consequently, the largest invariant set satisfying $\dot{\mathcal{V}} = 0$ consists solely of the endemic equilibrium. By applying LaSalle's Invariance Principle [34], it follows that the endemic equilibrium is globally asymptotically stable within the specified invariant region $\Omega \subset \mathbb{R}_+^7$. □

4. Numerical Simulations

4.1. Parameter estimation

This section provides the theoretical results of our model obtained through numerical simulation of the system (2.1). In this paper, MATLAB will be used to carry out the numerical simulations. It is crucial to recognize that drug use and crime patterns vary significantly from region to region in South Africa. According to Statistics South Africa, the total population of Gauteng in 2022 was 15 099 422 [6].

At $t = 0$, the state variables are set as $S = 15419976$, $U_1 = 3000$, $U_2 = 1950$, $H = 1800$, $C = 2000$, $J = 860$ and $R = 3850$ with reasonable assumptions. Table 4.1 presents the estimated parameter values used in carrying out numerical simulations of the narcocriminality model. Many parameters are known to lie within some limits, and only a few are known exactly, and it is apparent then to estimate the others [9]. In our model, we identified a few parameters from the literature and estimated the remaining ones.

Parameter	Description	Baseline	Range of Values	References
Λ	Recruitment rate	34000	(34500, 35700)	Estimated
μ	Natural mortality rate	0.0083	(0.007885, 0.008715)	[8]
α	Progression rate from light users to criminals	0.0016735	(0.0159, 0.0176)	Estimated
τ	Progression rate from light users to heavy users	0.01	(0.0095, 0.0105)	Estimated
κ	Relapse rate	0.05	(0.0475, 0.053)	Estimated
ϑ	Dropout rate from rehabilitation	0.02	(0.019, 0.021)	[9]
ρ	Progression rate from heavy users to criminals	0.11	(0.1045, 0.1155)	[8]
γ_1	Incarceration rate of heavy drug users	0.00013	(0.000124, 0.000137)	Estimated
γ_2	Rehabilitation rate	0.3856	(0.366, 0.405)	Estimated
δ	Death rate due to drug use	0.9	(0.855, 0.9944)	Estimated
θ	Recovery rate from rehabilitation	0.947	(0.8997, 0.9944)	Estimated
ε	Incarceration rate of criminals	0.8234349	(0.7823, 0.865)	Estimated
σ	Recovery rate from jail	0.99857	(0.9986, 1)	Estimated
β	Initiation rate of drug use	0.00000002	(0.000000019-8, 0.000000021)	Estimated
η_1	Interaction rate between susceptible individuals and light drug users	0.6	(0.57, 0.63)	[23]
η_2	Rate at which heavy drug users are recruited into criminality due to association with criminals	0.8	(0.76, 0.81)	[23]

Table 4.1: Parameter values used in the narcocriminality model. Ranges indicate values used for sensitivity analysis.

4.2. Sensitivity analysis

Through sensitivity analysis, we quantify the relative influence of parameter variations on the system's state variables [35]. Our analysis focuses specifically on understanding how each parameter affects the drug abuse criminogenic growth number ($\mathcal{D}_0$) [12]. The primary focus is to determine how each parameter influences the drug abuse criminogenic growth number, with the broader aim of informing effective intervention strategies to address drug-related crime in Gauteng Province. We computed the sensitivity indices of $\mathcal{D}_0$ using Latin Hypercube Sampling (LHS) coupled with Partial Rank Correlation Coefficient (PRCC) analysis, conducting 1000 simulations per run following the methodology established by [36]. This stratified sampling approach ensures comprehensive coverage of each parameter's range while minimizing clustering, thereby enhancing the reliability of our sensitivity estimates.

The resulting sensitivity indices reveal crucial relationships between model parameters and $\mathcal{D}_0$. Parameters exhibiting positive indices demonstrate a direct correlation with $\mathcal{D}_0$, meaning their increase would exacerbate the drug crime epidemic. Conversely, parameters with negative indices show an inverse relationship, suggesting their enhancement could help mitigate the problem. As shown in Figure 4.2, the transmission rate β (estimated at 0.579) emerges as the most sensitive parameter, displaying perfect positive correlation with $\mathcal{D}_0$ - a 1% increase in β leads to a corresponding 1% increase in $\mathcal{D}_0$. This strong relationship underscores β's pivotal role in driving narcocriminality dynamics through its direct influence on drug abuser populations. Equally significant is the natural mortality rate μ, which shows a substantial negative correlation (sensitivity index: -0.7418) with $\mathcal{D}_0$, indicating that increased population turnover may help reduce the drug crime burden. These findings provide critical insights for prioritizing intervention strategies, highlighting which parameters most significantly

influence $\mathcal{D}_0$ and therefore offering the most promising targets for effective crime reduction measures. If we increase μ, say, by 1%, this has the effect of reducing the drug abuse criminogenic growth number. Some other parameters in our model are less influential to $\mathcal{D}_0$, and these are $\rho, \kappa, \eta_1, \eta_2, \kappa, \vartheta, \rho, \gamma_1, \gamma_2, \delta, \theta, \varepsilon$, and σ. Figure 4.1 below shows the plot of partial rank correlation coefficients, also showing the effects of the parameters on $\mathcal{D}_0$.

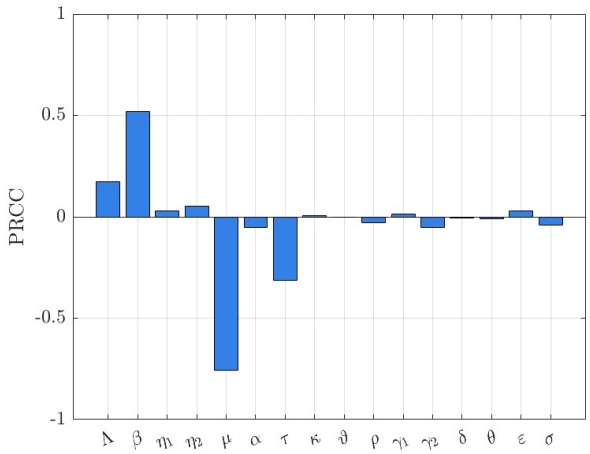

Figure 4.1: The PRCC analysis illustrates how variations in the parameters (within the ranges specified in Table 4.1) influence the value of $\mathcal{D}$, Parameters with positive PRCC values contribute to an increase in $\mathcal{D}$, as their values rise, while those with negative PRCC values lead to a decrease in $\mathcal{D}$, when increased.

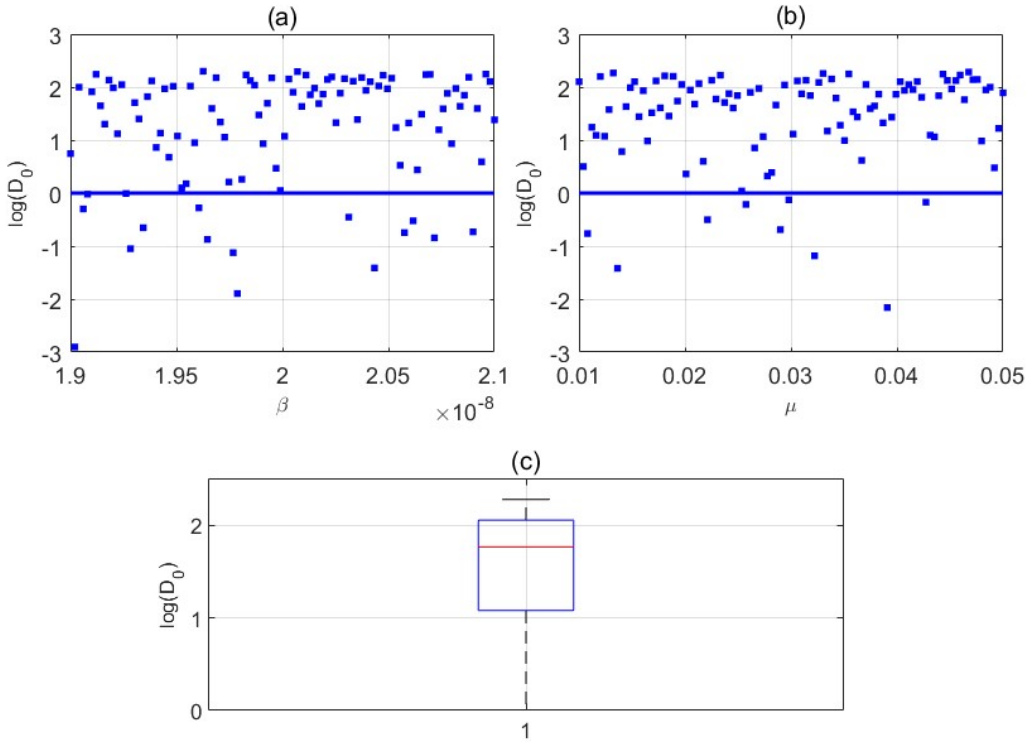

Figure 4.2: Scatter plots showing the three parameters with the greatest PRCC magnitude in the narcocriminality model, 1000 simulations per run were used.

The scatter plots in Figure 4.2 illustrates the effects of varying β, η_2 and μ on the drug abuse criminogenic growth number $\mathcal{D}_0$.The scatter plots indicates that the drug abuse criminogenic growth number $\mathcal{D}_0$ is most sensitive to variations in the initiation parameter β, the natural death rate μ and the interaction rate η_2 between the heavy drug users and the criminals. An increase in β, the transmission parameter, leads to a rise in $\mathcal{D}_0$, meaning that if β increases by 1% , $\mathcal{D}_0$ also increases by 1%. The natural death rate μ shows an inverse relationship with the drug abuse criminogenic growth number. A decrease in μ results in a corresponding decrease in $\mathcal{D}_0$, and an increase in μ results in a decrease in the drug abuse criminogenic growth number, as shown in the diagram Figure 4.1.

4.3. Model validation

To assess the reliability of the proposed model, we validated its simulated outputs against empirical data obtained from the South African Police Service (SAPS). The validation dataset consists of annual reports on drug-related crimes spanning the years 2010 to 2024, extracted from the official SAPS crime statistics portal, [37]. Model predictions were compared with the observed temporal trends, focusing on both the direction and magnitude of variation across the years. Goodness-of-fit metrics, including the root mean square error (RMSE) and mean absolute percentage error (MAPE), were computed to quantify the level of agreement. Residual analyses were further conducted to identify periods of under- or overestimation. Where notable discrepancies were detected—such as sharper-than-expected declines in certain years—the model structure was revisited to account for possible external influences, including policy changes, enforcement intensity, or resource allocation. This validation process enhances the model's credibility and provides a quantitative foundation for forecasting and scenario evaluation in the context of drug-related crime dynamics in South Africa. The data from the Gauteng province is obtained from [**?**] for the years 2014 to 2023. To determine the data for the remaining years, we then used the average percentage of Gauteng data compared to national data.

Year	Drug-related crimes in SA	Drug-related crimes in Gauteng
2010	150 561	34 253
2011	176 218	40 090
2012	206 721	47 029
2013	260 596	59 286
2014	266 902	70 264
2015	259 165	55 442
2016	292 689	62 837
2017	323 547	69 285
2018	232 657	55 639
2019	170 510	43 275
2020	121 359	28 034
2021	140 326	29 578
2022	162 122	34 963
2023	172 999	38 093
2024	186 586	42 448

Table 4.2: Reported drug-related crimes in South Africa and Gauteng Province (2010–2024).

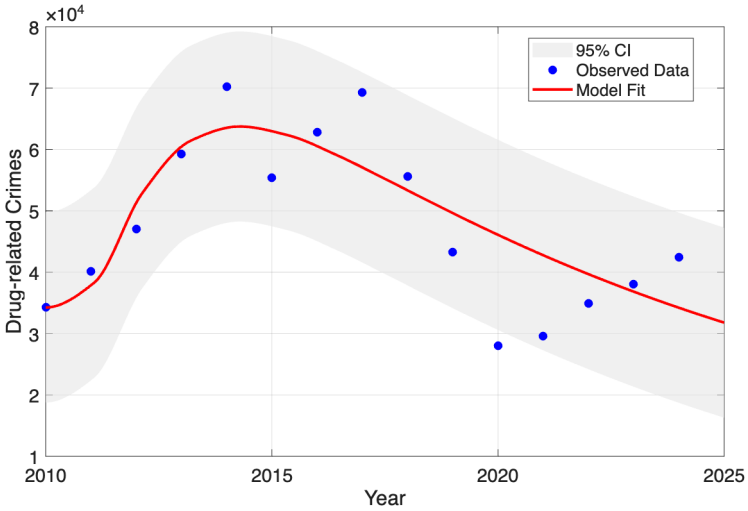

Figure 4.3: Comparison between the simulated model outputs and the empirical SAPS data on drug-related crimes in South Africa (2010–2024). The model demonstrates a strong alignment with observed trends, accurately capturing both the rise in reported cases between 2010 and 2017 and the subsequent decline following 2018. Minor deviations observed in 2020–2021 correspond to pandemic-related enforcement fluctuations. The overall fit indicates the model's robustness in replicating temporal patterns of drug-related crime dynamics.

4.4. Influence of light and heavy user criminal progression rates on narcocriminality epidemic

This section presents numerical results demonstrating the impact of key parameters on the dynamics of the narcocriminality epidemic. The parameter α captures the transition of individuals from light drug use to criminal involvement. We considered varying values of $\alpha = \{0.016735, 0.026735, 0.036735, 0.046735\}$, as illustrated in Figure 4.4(a). The findings reveal that a higher progression rate α results in more criminals, thus intensifying the incidence of criminal activities in Gauteng Province.

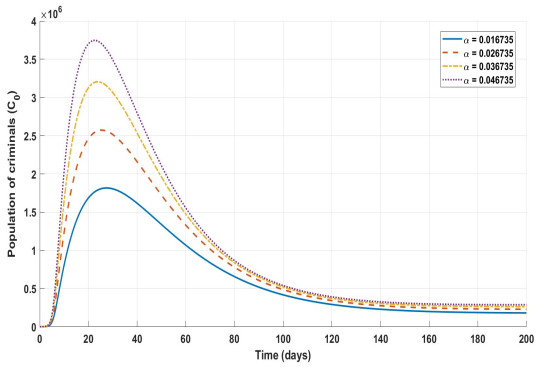

(a) Effects of the progression rate α on Criminals (C)

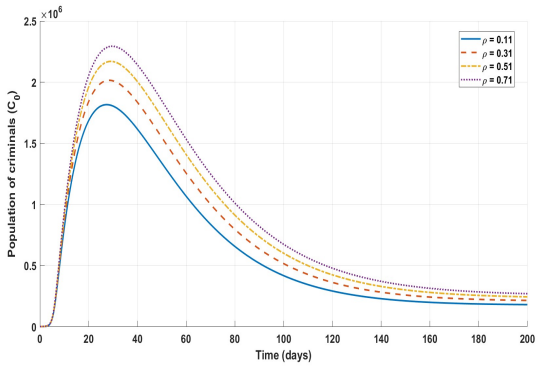

(b) Effects of the progression rate ρ on Criminals (C).

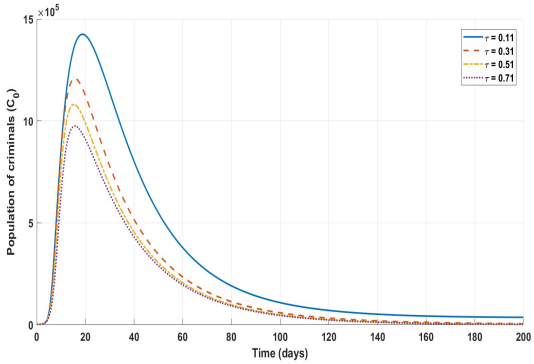

(c) Effects of the progression rate τ on Criminals (C).

Figure 4.4: The impact of key parameters in the narcocriminality epidemics model.

Figure 4.4(b) illustrates the impact of varying the progression rate ρ. Specifically, we considered values of $\rho = 0.11, 0.31, 0.51, 0.71$. The results show that as ρ increases, representing the rate at which heavy drug users transition into the criminal population, criminality rises. In contrast, lower values of ρ result in reduced criminality. This trend is evident in the plot displayed in Figure 4.4(b). We therefore conclude that higher values of ρ contribute to a greater prevalence of criminality within the epidemic dynamics.

Figure 4.4(c) illustrates the effect of varying the progression rate τ, which governs the transition from light to heavy drug use, on crime levels. We explored values of $\tau = \{0.11, 0.31, 0.51, 0.71\}$. The results indicate that increasing τ leads to a rise in the number of heavy drug users, which in turn contributes to higher rates of criminal activity. In summary, a higher progression rate τ amplifies the prevalence of the epidemic through its impact on criminality.

4.5. Impact of parameters on the drug abuse criminogenic growth number

The parameters $\alpha, \rho, \gamma_1, \gamma_2$ and ε have a significant impact on the Drug Abuse Criminogenic Growth Number (DGN). The progression rates α and ρ to crime increases $\mathcal{D}_0$ as they expand the criminal population. Contrary, the incarceration rates γ_1 ε and the rehabilitation rate γ_2 reduces $\mathcal{D}_0$ by removing individuals from the population of light drug users, heavy drug users and criminals. Plots in Figures (4.5a, 4.5b, 4.5c, 4.5d and 4.5e) displays the relationship between the parameters and $\mathcal{D}_0$.
Figure 4.5a and Figure 4.5e show that increasing the progression rates α and ρ results in an increasing exponential function towards the drug abuse criminogenic growth number (DGN) in the narcocriminality model. If we increase the rate of incarceration γ_1, this also results in the reduction of $\mathcal{D}_0$. This means that correctional services gradually control the prevalence of the epidemic. Figure 4.5d shows a decreasing function of $\mathcal{D}_0$ plotted as a function of the rehabilitation rate γ_2. This is as a result of the heavy drug users who progress to the rehabilitation centres, thereby reducing the drug abuse criminogenic growth. We also observe that the incarceration parameter ε from the crime compartment to the jail compartment exhibits a decreasing trend when plotted against the drug abuse criminogenic growth number, as shown in Figure 4.5b. In this case, the drug abuse criminogenic growth number decreases as a result of the psycho-social support that they receive while in jail. Some of the arrested will recover from drug abuse and criminal activities. This results in a reduction of the (DGN) in the narcocriminality model.

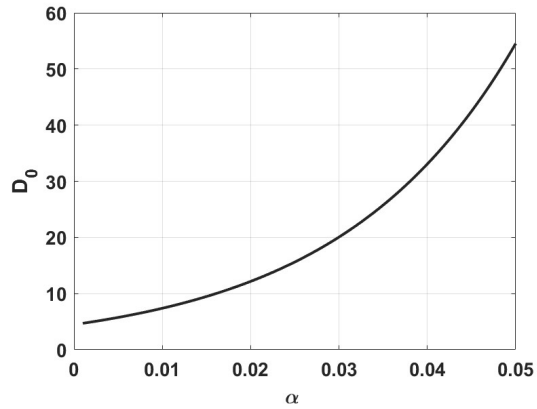

(a) The plot shows the progression rate α plotted as a function of the Drug abuse criminogenic growth number. As the number of light drug users progresses to the criminal population, $\mathcal{D}_0$ increases.

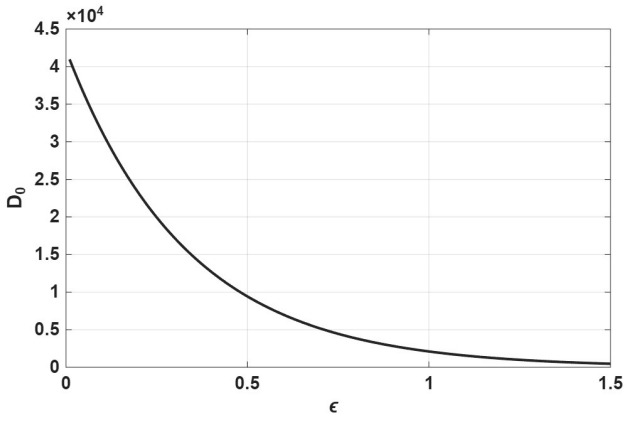

(b) The plot shows the incarceration rate ϵ plotted as a function of the drug abuse criminogenic growth number $\mathcal{D}_0$. The plot shows that as criminals get incarcerated, this has an effect of reducing the drug abuse criminogenic growth number.

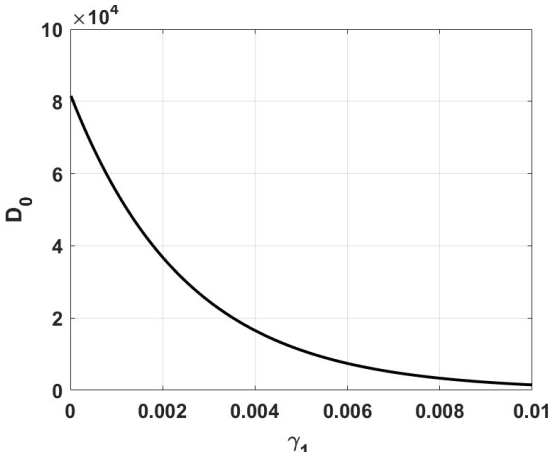

(c) The plot shows the incarceration rate γ_1 plotted as a function of the drug abuse criminogenic growth number $\mathcal{D}_0$. The plot shows that as heavy drug users get incarcerated, this reduces the number of heavy drug users. This has an effect of reducing the drug abuse criminogenic growth number.

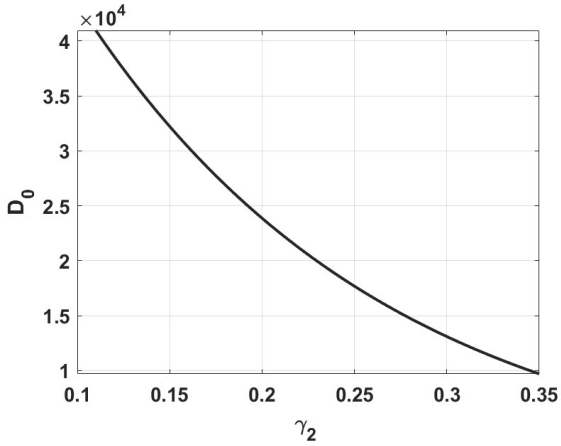

(d) The plot shows the rehabilitation rate γ_2 plotted as a function of the drug abuse criminogenic growth number $\mathcal{D}_0$. The plot shows a decreasing exponential function towards the drug abuse criminogenic growth number. As the number of heavy drug users increases in rehabilitation centres, this has an effect of reducing $\mathcal{D}_0$.

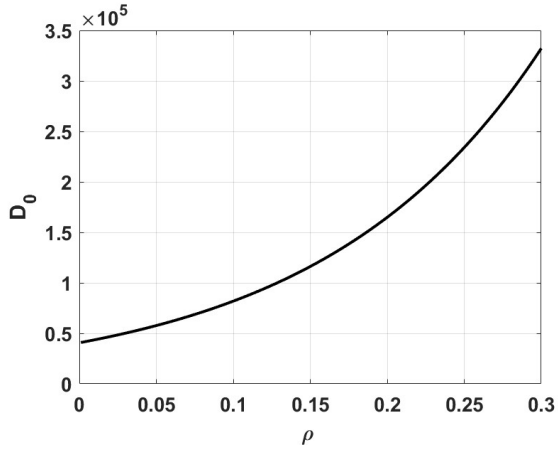

(e) The plot shows the progression rate ρ plotted as a function of the drug abuse criminogenic growth number $\mathcal{D}_0$. The plot shows that as the number of heavy drug users increases, the drug criminogenic number also increases exponentially.

Figure 4.5: Effects of key parameters on the drug abuse criminogenic growth number $\mathcal{D}_0$.

4.6. Comparison of the effects of the key parameters on drug-related crime transitions

Figure 4.6 compares how reducing key transition rates affects drug crime dynamics. In each figure, the shaded regions show the decrease in individuals progressing into crime or jail. Heavy drug users (a), criminals (b), and light drug users (c) all exhibit lower peaks and faster declines when these transitions are limited, demonstrating that mitigating progression into crime-related compartments significantly lowers the population levels in crime-related compartments. The description of each subfigure is given under the subfigure.

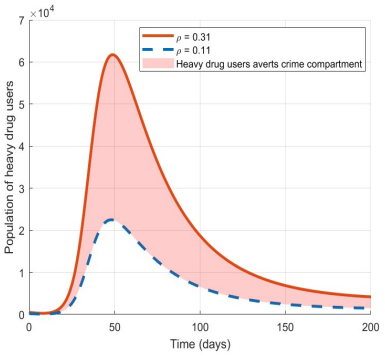

(a) The trajectory of heavy drug users who avoided progressing to criminal behaviour because of other factors is shown by the shaded region.

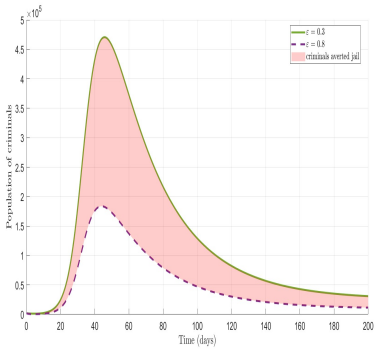

(b) The trajectory of criminals who avoided progressing to the jail compartment because of other factors is shown by the shaded region.

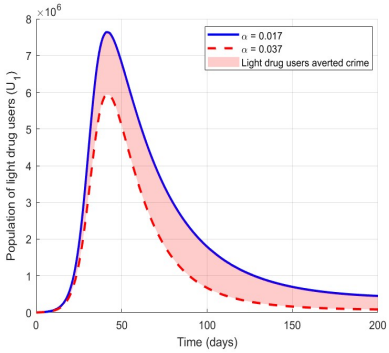

(c) The trajectory of light drug users who avoided progressing to criminal behaviour because of other factors is shown by a shaded region

Figure 4.6: Comparison of the effects of key parameters on drug-crime transitions.

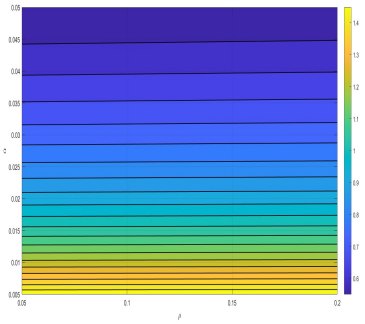

(a)

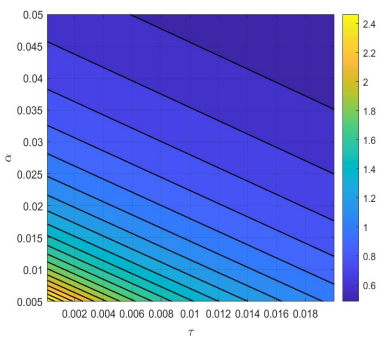

(b)

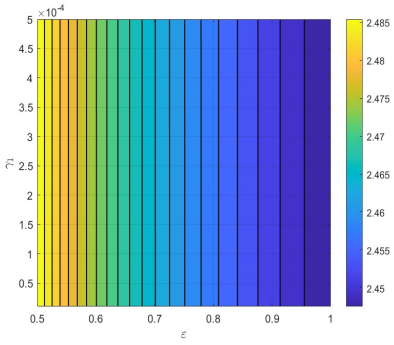

(c)

Figure 4.7: (a) present contour plot for the drug abuse criminogenic growth number $\mathcal{D}_0$ plotted as a function of the rates α and ρ, (b) is the contour plot for the drug abuse criminogenic growth number $\mathcal{D}_0$ plotted as a function of the rates ε and γ_1, and (c) presents the contour plots for the drug abuse criminogenic growth number $\mathcal{D}_0$ plotted as a function of the rates τ and α.

Figures 4.7(a), 4.7(b) and 4.7(c) presents contour plots for the drug abuse criminogenic growth number (DGN) plotted as a function of (a)Progression rate from light drug users to criminals, α (b) Progression rate from heavy drug users to criminals, ρ (c) Incarceration rate of criminals, ε (d) Incarceration rate of heavy drug users, γ_1 (e) Progression rate from light drug users to heavy drug users, τ. As shown, on Figure 4.7, if we increase ρ, the criminals increase as heavy drug users progress to the crime compartment. This results in an increase in $\mathcal{D}_0$. If the progression rate of light drug users α is increased, we also see an increase in $\mathcal{D}_0$ because the number of criminals increases.

Figure 4.7(c) presents the drug abuse criminogenic growth number plotted as a function of α and τ. If we increase the progression rate from light drug users τ to heavy drug users, this leads to an increase in the population of heavy drug users. The heavy drug users also progress to the criminal compartment by ρ. Therefore, increasing τ also increases (DGN).

In Figure 4.7(b), we see that as we increase the incarceration rate ε, this leads to a decline in the number of criminals. This reduces the number of drug abuse criminogenic factors. It is also shown through the contour plots that, as we increase the other incarceration rate from the heavy drug users γ_1, this also decreases the population of heavy drug users, thereby contributing to a reduction in $\mathcal{D}_0$.

Figure 4.6 present the trajectory of heavy drug users who avoid progressing to criminal behaviour because of other factors, and also the number of criminals who avoid getting into jail by parameters ρ and ε, respectively. Some heavy drug users might avoid the criminal compartment and rather join the rehabilitation compartment.

4.7. Impact of incarceration parameters on drug abuse criminogenic growth number $\mathcal{D}_\prime$.

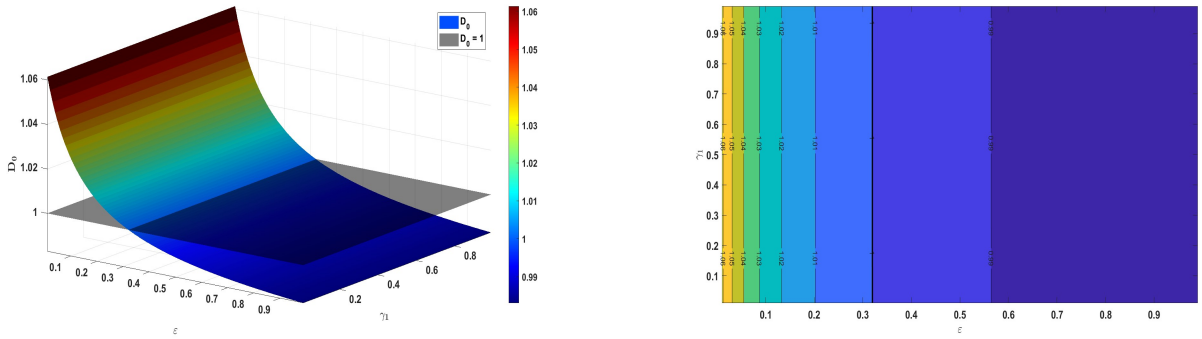

(a) Surface plot showing the impact of γ_1 and ε on $\mathcal{D}_\prime$.

(b) Contour plot showing the impact of γ_1 and ε on $\mathcal{D}_\prime$.

Figure 4.8: The impact of incarceration parameters on the Drug Criminogenic Growth Number $\mathcal{D}_\prime$.

Figures 4.8(a) and 4.8(b) show the surface plot and the contour plot illustrating the impact of incarceration parameters on the $\mathcal{D}_\prime$. Increasing either parameter reduces the persistence of the narcocriminality burden by removing high-risk individuals from the cycle of drug abuse and crime. Consequently, both serve as effective control measures for reducing the drug abuse criminogenic growth number $\mathcal{D}_\prime$, and when sufficiently large, $\mathcal{D}_\prime$ will ultimately be less than a unit, indicating the epidemic will die out. The threshold $\mathcal{D}_\prime = \infty$ serves as a key indicator of stability and guides the design of control strategies.

4.8. Relapse effects on the threshold behaviour of the drug abuse criminogenic growth number $\mathcal{D}_\prime$

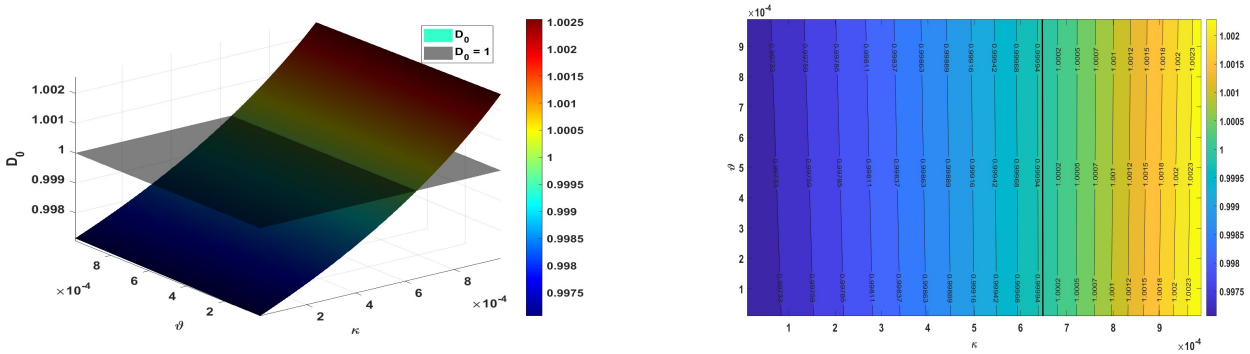

(a) Surface plot showing the relapse effects of ϑ and κ on $\mathcal{D}_\prime$.

(b) Contour plot showing the effects of the relapse effects ϑ and κ on $\mathcal{D}_\prime$ on $\mathcal{D}_\prime$.

Figure 4.9: The relapse effects on the threshold behaviour of $\mathcal{D}_\prime$.

Figure 4.9 presents both the surface and contour plots illustrating the impact of the relapse rates on the drug abuse criminogenic growth number, $\mathcal{D}_\prime$. The plots demonstrate that an increase in the relapse rates leads to a corresponding rise in $\mathcal{D}_\prime$,indicating the continued persistence of the narcocriminality burden in the population. Conversely, lower relapse rates result in $\mathcal{D}_\prime < \infty$, suggesting that the pandemic will

eventually die out. The bold black contour represents the critical threshold where $\mathcal{D}_\prime = \infty$. As the system approaches this threshold, it becomes increasingly unstable, and even slight changes in relapse behaviour may determine whether the epidemic is eliminated or persists.

4.9. Critical role of progression parameters α and ρ in sustaining criminal dynamics

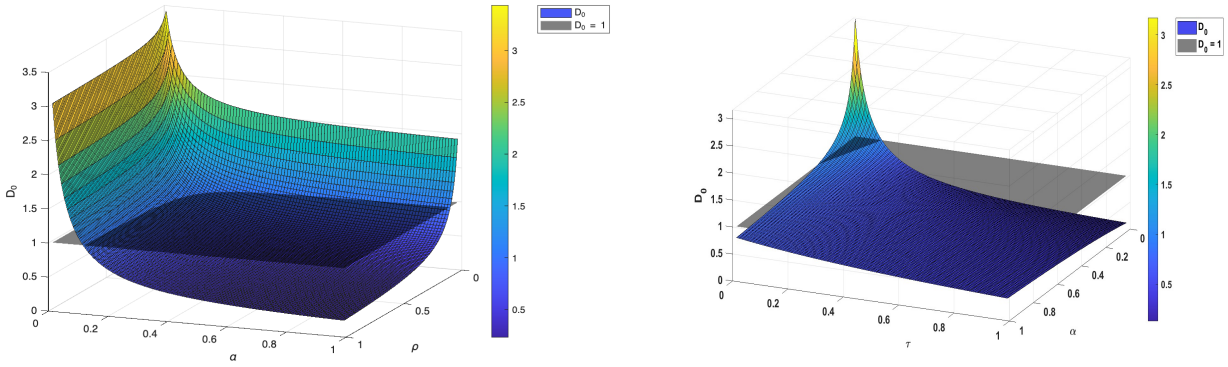

(a) Surface plot showing the combined effects of the progression rates on the Drug Criminogenic Growth Number.

(b) The surface plot show the combined effects of α ρ on the Drug Criminogenic Growth Number $\mathcal{D}_\prime$.

Figure 4.10: The surface plots show the combined effects of the progression rates α and τ on the Drug Abuse Criminogenic Growth Number (DGN).

The combined influence of progression rates α and ρ significantly amplifies criminality within the population. These parameters represent the pathways through which both light and heavy drug users are funnelled into crime. Simulation results show that increasing either parameter leads to a higher criminal population and a larger drug abuse criminogenic growth number $\mathcal{D}_\prime$,reinforcing the persistence of the narcocriminality epidemic. This highlights the importance of early intervention strategies that aim to interrupt the drug-to-crime transition at multiple stages of drug use. The surface plot in Figure 4.10(a) shows the combined effects of both parameters in raising criminality.

Figure 4.10(b) displays the combined effects of α and τ. The effects of these two parameters play an important role in capturing the dynamics of the narcocriminality epidemic. Increasing τ results in an increase in the heavy drug user population, which is more likely to engage in criminal behaviour. Simultaneously, an increase in α accelerates the direct transition of light drug users into the criminal compartment. When both parameters are increased, the number of heavy drug users increases. This amplifies the prevalence of criminal activities.

5. Conclusion

The study presents a deterministic compartmental model to explore the complex relationship between substance abuse and crime in Gauteng province, South Africa. By incorporating seven distinct population compartments, susceptible individuals, light and heavy drug users, criminals, incarcerated individuals, those undergoing rehabilitation, and recovered individuals, the model successfully captures the dynamic interplay between drug abuse and criminal behaviour. Inclusion of rehabilitation and incarceration as control measures provides a comprehensive framework for evaluating the effectiveness of the intervention. The model demonstrates that the narcocriminality-free equilibrium stabilizes when $\mathcal{D}_0 < 1$, while the endemic equilibrium persists when $\mathcal{D}_0 > 1$. The key parameters β, α, and ρ were identified as the most sensitive to $\mathcal{D}_0$, suggesting that the targeted interventions should focus on reducing the rates of initiation and progression. The effectiveness of rehabilitation and incarceration in controlling the system was demonstrated.

Key insights reveal that the narcocriminality-free equilibrium is globally asymptotically stable when the Drug Abuse Criminogenic Growth Number (DGN, $\mathcal{D}_0 < 1$), while the persistent narcocriminality equilibrium becomes asymptotically stable when $\mathcal{D}_0 > 1$, indicating the continued presence of drug-associated criminal behaviour. Sensitivity analysis identifies the initiation rate (β) and progression rates (α and ρ) as the most influential parameters affecting $\mathcal{D}_0$, highlighting the importance of prevention programs targeting drug use initiation and the transition to criminal activities. Numerical simulations demonstrate how rehabilitation (γ_2) and incarceration rates (ε and γ_1) can reduce heavy drug use and criminal prevalence, with visualizations through contour and scatter plots reinforcing these findings. Robust statistical validation, utilizing Latin Hypercube Sampling (LHS) and Partial Rank Correlation Coefficients (PRCC), enhances the model's reliability.

Future research directions include incorporating stochastic elements for random fluctuations, adding spatial heterogeneity for regional variations, and validating the model with empirical data. The findings provide valuable insights for policymakers, emphasizing the need for prevention programs and law enforcement strategies. To enhance the practical application of the model, future work could incorporate real-world data validation, explore additional community-based interventions, and consider socioeconomic factors such as unemployment that may influence drug-related crime rates. This study establishes a strong theoretical foundation for addressing narcocriminality, offering actionable recommendations for both policymakers and researchers working to mitigate this complex social challenge.

Article Information

Acknowledgements: The authors would like to express their sincere thanks to the editor and the anonymous reviewers for their helpful comments and suggestions.

Author Contributions: Robert Kajambeu was the primary author of the manuscript. He developed the model, carried out the analysis, and drafted the paper. Farai Nyabadza supervised the research, provided guidance on the methodology and conceptualization, and contributed to

the model development through simulations and manuscript editing.

Artificial Intelligence Statement: Artificial intelligence tools were used only for language refinement and improving the clarity of the written text. No AI tools contributed to data analysis, modelling, simulations, or scientific interpretation. All analytical and computational work was carried out entirely by the authors.

Conflict of Interest Disclosure: No potential conflict of interest was declared by authors.

Plagiarism Statement: This article was scanned by the plagiarism program.

References

[1] T. O. Orwa, F. Nyabadza, *Mathematical modelling and analysis of alcohol-methamphetamine co-abuse in the Western Cape Province of South Africa*, Cogent Math. Stat., **6**(1) (2019), Article ID 1641175. https://doi.org/10.1080/25742558.2019.1641175

[2] J. Liebenberg, L. Du Toit-Prinsloo, V. Steenkamp, G. Saayman, *Fatalities involving illicit drug use in Pretoria, South Africa, for the period 2003–2012*, S. Afr. Med. J., **106**(10) (2016), 1051–1055. https://doi.org/10.7196/SAMJ.2016.v106i10.11105

[3] E. R. Bos, D. T. Jamison, F. Bainga, R. G. A. Feacham, M. Makgoba, K. J. Hofman et al., *Disease and Mortality in Sub-Saharan Africa*, World Bank, Washington, DC, 2006.

[4] T. Jackson, A. Radunskaya, *Applications of Dynamical Systems in Biology and Medicine*, Vol. 158, Springer, New York, 2015.

[5] K. K. Nantomah, B. Seidu, C. S. Bornaa, *A mathematical model of drug-crime dynamics*, Asian J. Math. Appl. **2022** (2022), Article ID 14.

[6] Statista Research Department, *Number of Drug-Related Crimes in South Africa 2013/2014–2023/2024*, https://www.statista.com/statistics/1448515/number-of-drug-related-crimes-in-South-Africa/, Accessed: 12 December 2024.

[7] S. Ramlagan, K. Peltzer, G. Matseke, *Epidemiology of drug abuse treatment in South Africa*, S. Afr. J. Psychiatry, **16**(2) (2010), Article ID 172. https://doi.org/10.4102/sajpsychiatry.v16i2.172

[8] F. Nyabadza, J. B. H. Njagarah, R. J. Smith, *Modelling the dynamics of crystal meth ('tik') abuse in the presence of drug-supply chains in South Africa*, Bull. Math. Biol., **75** (2013), 24–48. https://doi.org/10.1007/s11538-012-9790-5

[9] A. S. Kalula, F. Nyabadza, *A theoretical model for substance abuse in the presence of treatment*, S. Afr. J. Sci., **108**(3/4) (2012), 1–12. http://dx.doi.org/10.4102/sajs.v108i3/4.654

[10] S. P. Gatyeni, *Modelling in-and out-patient rehabilitation for substance abuse in dynamic environments*, Ph.D. Thesis, University of Stellenbosch, 2015.

[11] M. Ma, S. Liu, H. Xiang, J. Li, *Dynamics of synthetic drugs transmission model with psychological addicts and general incidence rate*, Physica A, **491** (2018), 641–649. https://doi.org/10.1016/j.physa.2017.08.128

[12] B. Mataru, O. J. Abonyo, D. Malonza, *Mathematical model for crimes in developing countries with some control strategies*, J. Appl. Math., **2023**(1) (2023), Article ID 8699882. https://doi.org/10.1155/2023/8699882

[13] F. Nyabadza, L. A. Coetzee, *A systems dynamic model for drug abuse and drug-related crime in the Western Cape Province of South Africa*, Comput. Math. Methods Med., **2017**(1) (2017), Article ID 4074197. https://doi.org/10.1155/2017/4074197

[14] K. Manoj, A. Syed, *Modelling and prevention of crime using age-structure and law enforcement*, J. Math. Anal. Appl., **519**(2) (2023), Article ID 126849. https://doi.org/10.1016/j.jmaa.2022.126849

[15] A Kaur, M. Sadhwani, S. Abbas, *Law enforcement: the key to a crime-free society*, J. Math. Sociol., **46**(4) (2022), 342–359. https://doi.org/10.1080/0022250X.2021.1941002

[16] T. J. Prakash, B. Sarita, B. Kavita, A. Syed, *Dynamical analysis and effects of law enforcement in a social interaction model*, Physica A, **567** (2021), Article ID 125725. https://doi.org/10.1016/j.physa.2020.125725

[17] Fatmawati, H. Tasman, *A malaria model with controls on mass treatment and insecticide*, Appl. Math. Sci., **7**(68) (2013), 3379–3391. https://doi.org/10.12988/ams.2013.33180

[18] Fatmawati, H. Tasman, *An optimal treatment control of TB-HIV coinfection*, Int. J. Math. Math. Sci., **2016** (2016), Article ID 8261208. https://doi.org/10.1155/2016/8261208

[19] Fatmawati, H. Tasman, *An optimal control strategy to reduce the spread of malaria resistance*, Math. Biosci., **262** (2015), 73–79. https://doi.org/10.1016/j.mbs.2014.12.005

[20] F. Nyabadza, S. D. Hove-Musekwa, *From heroin epidemics to methamphetamine epidemics: Modelling substance abuse in a South African province*, Math. Biosci., **225**(2) (2010), 132–140. https://doi.org/10.1016/j.mbs.2010.03.002

[21] M. Gossop, J. Marsden, D. Stewart, T. Kidd, *The national treatment outcome research study (NTORS): 4–5 year follow-up results*, Addiction, **98**(3) (2003), 291–303. https://doi.org/10.1046/j.1360-0443.2003.00296.x

[22] S. Belenko, M. Hiller, L. Hamilton, *Treating substance use disorders in the criminal justice system*, Curr. Psychiatry Rep., **15**(11) (2013), Article ID 414. https://doi.org/10.1007/s11920-013-0414-z

[23] T. L. Gasebonno, *Modelling substance abuse in Botswana in presence of multiple amelioration stages and outpatient rehabilitation, optimal control and fractional-order dynamics*, M.Sc. Thesis, Botswana International University of Science and Technology, 2020.

[24] B. J. Bassingthwaighte, E. Butterworth, B. Jardine, G. M. Raymond, *Compartmental modeling in the analysis of biological systems*, In *Computational Toxicology: Volume I*, Springer, New York, 2012, pp. 391–438. https://doi.org/10.1007/978-1-62703-050-2_17

[25] T. Decorte, *Drug users' perceptions of 'controlled' and 'uncontrolled' use*, Int. J. Drug Policy, **12**(4) (2001), 297–320. https://doi.org/10.1016/S0955-3959(01)00095-0

[26] S. Abbas, J. P. Tripathi, A. A. Neha, *Dynamical analysis of a model of social behavior: Criminal vs non-criminal population*, Chaos Solitons Fractals, **98** (2017), 121–129. https://doi.org/10.1016/j.chaos.2017.03.027

[27] A. Galassi, E. Mpofu, J. Athanasou, *Therapeutic community treatment of an inmate population with substance use disorders: Post-release trends in re-arrest, re-incarceration, and drug misuse relapse*, Int. J. Environ. Res. Public Health, **12**(6) (2015), 7059–7072. https://doi.org/10.3390/ijerph120607059

[28] G. Birkhoff, G. C. Rota, *Ordinary Differential Equations*, Blaisdell Publishing Co., Waltham, 1969.

[29] O. Diekmann, J. A. P. Heesterbeek, J. A. J. Metz, *On the definition and the computation of the basic reproduction ratio R_0 in models for infectious diseases in heterogeneous populations*, J. Math. Biol., **28** (1990), 365–382. https://doi.org/10.1007/BF00178324

[30] R. M. Anderson, R. M. May, *Infectious Diseases of Humans: Dynamics and Control*, Oxford University Press, Oxford, 1991.

[31] P. Van den Driessche, J. Watmough, *Reproduction numbers and sub-threshold endemic equilibria for compartmental models of disease transmission*, Math. Biosci., **180**(1–2) (2002), 29–48. https://doi.org/10.1016/S0025-5564(02)00108-6

[32] C. Robinson, *Dynamical Systems: Stability, Symbolic Dynamics, and Chaos*, CRC Press, Boca Raton, 1998.

[33] D. I. Cartwright, M. J. Field, *A refinement of the arithmetic mean-geometric mean inequality*, Proc. Amer. Math. Soc., **71** (1978), 36–38. https://doi.org/10.1090/s0002-9939-1978-0476971-2

[34] J. P. LaSalle, *Stability theory for ordinary differential equations*, J. Differ. Equations, **4**(1) (1968), 57–65. https://dx.doi.org/10.1016/0022-0396(68)90048-X

[35] N. I. Hamdan, A. Kilicman, *Sensitivity analysis in a dengue fever transmission model: A fractional order system approach*, J. Phys.: Conf. Ser., **1366**(1) (2019), 012048. https://doi.org/10.1088/1742-6596/1366/1/012048

[36] R. L. Iman, W. J. Conover, *Small sample sensitivity analysis techniques for computer models, with an application to risk assessment*, Commun. Stat., Theory Methods, **9**(17) (1980), 1749–1842. https://doi.org/10.1080/03610928008827996

[37] South African Police Service (SAPS), *Annual Crime Statistics: Drug-Related Crime (2010–2024)*, Available at: https://www.saps.gov.za/, Accessed October 2024.